# Hybrid Integrated Circuit/Microfluidic Chips for the Control of Living Cells and Ultra-Small Biomimetic Containers

A Dissertation Presented

by

David Aaron Issadore

to

The School of Engineering and Applied Sciences

In partial fulfillment of the requirements

for the degree of

Doctor of Philosophy

in the subject of

Applied Physics

Harvard University

Cambridge, Massachusetts

May 2009

**David Aaron Issadore**　　　　　　　　**Adviser: Robert Westervelt**

**Hybrid Integrated Circuit/Microfluidic Chips for the Control of**

**Living Cells and Ultra-Small Biomimetic Containers**

**Abstract**

This thesis describes the development of a versatile platform for performing biology and chemistry experiments on a chip, using the integrated circuit (IC) technology of the commercial electronics industry. This work represents an important step towards miniaturizing the complex chemical and biological tasks used for diagnostics, research, and manufacturing into automated and inexpensive chips.

Hybrid IC / microfluidic chips are developed in this thesis to simultaneously control many individual living cells and small volumes of fluid. Taking inspiration from cellular biology, phospholipid bilayer vesicles are used to package pL volumes of fluid on the chips. The chips can be programmed to trap and position, deform, set the temperature of, electroporate, and electrofuse living cells and vesicles. The fast electronics and complex circuitry of ICs enable thousands of living cells and vesicles to be simultaneously controlled on the chip, allowing many parallel, well-controlled biological and chemical operations to be performed in parallel.

The hybrid chips consist of a microfluidic chamber built directly on top of a custom IC, that uses integrated electronics to create local electric and magnetic fields above the chip's surface. The chips operate in three distinct modes, controlled by setting the frequency of the electric field. Electric fields at kHz frequencies are used to induce electroporation and electrofusion, electric fields at MHz frequencies are used for dielectrophoresis (DEP) to trap and move objects, and electric fields at GHz frequencies are used for dielectric heating. In addition, magnetophoresis, using magnetic fields created with DC current on the chip, is used to deform and to position objects tagged with magnetic nanoparticles.

To demonstrate these functions two custom hybrid IC / microfluidic chips and a droplet based PDMS microfluidic device with external electronics are presented. The laboratory functions demonstrated on these chips provide important building blocks for a versatile lab-on-a-chip platform that can be built on the well-developed IC technology of the commercial electronics industry.

# Table of Contents

# Acknowledgements

First I would like to express my appreciation and gratitude for my adviser, Bob Westervelt. Bob's deep understanding of physics and his unique and often times unusual perspective on research, science, and technology have challenged me intellectually and helped me develop as a scientist. He has been a constant source of insightful ideas and thoughtful feedback and has given me the support and freedom that I needed to drive my own research. I am very grateful that I ended up in his lab. It seems that I was very lucky.

I would like to thank the Westervelt Lab folks that I have had the pleasure to work with and share space with over the last 5 years. First and foremost, I'd like to thank Tom Hunt. Tom helped me find direction in my research and kept me on track when my research was lacking focus. He also taught me the pleasures of road biking. I'd like to thank Keith Brown who joined the group two years after me. Keith has been great to work with, he provided me with the key feedback that I so often needed and his earnest enthusiasm and scientific rigor often improved my work. Also, he is an admirable Worms player. Jonathan, Ognjen, Lori, and Almalchi and the rest of the undergrads that have worked their way through the Westervelt lab have kept life interesting and were a pleasure to work with. Erin, Halvar, and Jesse are awesome people to share a lab with and I am grateful to them for keeping me somewhat knowledgeable about cold temperature physics. Alex, Nan, and Tina are new comers to the group and seem to be keeping the good traditions alive.

# Abbreviations and Symbols

| | |
|---|---|
| $a$ | Particle radius |
| $\vec{B}$ | Magnetic Field |
| $C$ | Capacitance |
| $C_{mem}$ | Specific membrane capacitance |
| $CM$ | Clausius Mosotti Factor |
| $\chi$ | Magnetic Susceptibility |
| CMOS | Complimentary Metal Oxide Silicon |
| $D$ | Diffusion Constant |
| DC | Direct current |
| DEP | Dielectrophoresis |
| $\Delta T$ | Change in Temperature |
| $\vec{E}$ | Electric Field |
| $\varepsilon$ | Relative Permittivity |
| $\varepsilon_o$ | Vacuum Permittivity |
| $\varepsilon'$ | Real Component of the Permittivity |
| $\varepsilon''$ | Imaginary Component of the Permittivity |
| $f$ | Frequency |
| $\vec{F}$ | Force |
| $g_m$ | Surface Conductivity |
| $GUI$ | Graphical User Interface |
| $HV$ | High Voltage |
| $\eta$ | Viscosity |
| I/O | Input / Output |
| IC | Integrated Circuit |
| $j$ | $\sqrt{-1}$ |
| kB | Boltzmann's Constant |
| $L$ | The length of a pixel |

| | |
|---|---|
| $L_D$ | Characteristic Length in the Heating Model for Drops |
| MOSIS | Metal Oxide Semiconductor Implementation Service |
| MUX | Multiplexer |
| $n$ | Concentration |
| NMR | Nuclear Magnetic Resonance |
| PBS | Phosphate Buffer Saline |
| $R$ | Resistance |
| $Re$ | Reynolds Number |
| RF | Radio Frequency |
| ROI | Region of Interest |
| SPICE | Simulation Program with Integrated Circuit Emphasis |
| SRAM | Static Random Access Memory |
| $\sigma$ | Conductivity |
| $T$ | Temperature |
| $\Delta T_{SS}$ | Steady State Change in Temperature |
| $\tau_{diff}$ | Characteristic Time for an Object to Diffuse a Half Pixel length L/2 |
| $\tau_{mem}$ | Characteristic Charging Time of a Vesicle or Cell's Membrane |
| $\tau_{move}$ | Characteristic Time to Move an Object a Pixel Length L |
| $\tau_{SS}$ | Characteristic Time to Reach Steady State Temperature |
| $\tau_{MW}$ | Dielectric Relaxation Time of a vesicle or cell |
| $\tau_W$ | Dielectric Relaxation Time of Water |
| $\mu_o$ | Vacuum Permeability |
| $V$ | Volume |
| $V$ | Voltage |
| $V_{TM}$ | Transmembrane Voltage |
| $\omega$ | Angular Frequency |

# List of Figures

## List of Tables

# Chapter 1. Introduction

*Lab-on-a-chip: A Technology that miniaturizes and integrates the complex chemical and biological tasks used for diagnostics, research, and manufacturing onto automated, portable, and inexpensive chips.*

## 1.1 Lab-on-a-Chip – Motivation

A major challenge of the 21st century is to better diagnose and treat infectious disease for the large portion of the world's population that is currently underserved. Diseases, such as HIV/AIDS, Tuberculosis, and Malaria, for which there exists interventions, continue to kill millions and infect millions more each year due, in part, to our inability to diagnose diseases effectively in poor countries. (Urdea *et al.*, 2006) The Bill and Melinda Gates Foundation and the National Institute of Health have declared the assessment of disease in poor countries a *Grand Challenge for Public Health*. These challenges read: (Varmus *et al.*, 2003)

1. *Develop technologies that permit quantitative assessment of population health statistics.*
2. *Develop technologies that permit quantitative assessment of individuals for multiple conditions or pathogens at point of care.*

With these goals in mind, researchers around the world are developing technology to measure biological and chemical markers for infectious disease in infrastructure-poor parts of the world. (Ahn *et al.*, 2004, Chin *et al.*, 2007, and Martinez *et al.*, 2008) The laboratories that perform the chemical and biological tests to diagnose disease

in the world's wealthier nations require resources that are not readily found elsewhere, such as centrally located air conditioned buildings, clean water, electricity, access to expensive reagents, and well-trained technicians. (Chin *et al.*, 2007)  As such, technology to assess disease in poor countries faces challenges not ordinarily found in a modern laboratory space.

Lab-on-a-chip technology offers a powerful tool to bring existing medical and environmental tests from the laboratory into the field and the clinic. (Figeys *et al.*, 2000, Petra *et al.*, 2006, Chin *et al.*, 2007)  At the forefront of this technology are the micro-fabricated pipes, valves, pumps, and mixers of microfluidics that are leading to integrated lab-on-a-chip devices. (Whitesides *et al.*, 2001 and Stone *et al.,* 2004)  In addition to the potential for low-cost medicine, the miniaturization of the handling of liquid and biological samples has enabled advances in fields such as drug discovery, genetic sequencing and synthesis, cell sorting, and single cell gene expression studies. (Tabeling *et al.*, 2005, Yager *et al.*, 2006, and Martinez *et al.*, 2008)  These integrated microfluidic devices are leading a paradigm shift in fluid handling that is analogous to what integrated circuits did for electronics half of a century ago. (Lee *et al.*, 2007)  However, a lab-on-a-chip that can perform the complex, multi-step experiments that are currently performed in laboratories, akin to a microprocessor for fluids, remains a challenge. (Lee *et al.*, 2007)

The potential impact of a lab-on-a-chip microprocessor could be enormous.  Imagine a device the size of an iPod that cost less than $100 and can perform numerous complex biological and chemical tests on small samples of bodily fluids, drinking

water, or air.  Such a device would make medical and environmental testing **inexpensive**, **portable** and **automated.**  Testing could be performed in the field, at home, or at a clinic by a non-expert.  The results of tests would be **quantitative** and **consistent** such that relevant data could be collected for both personal and public health statistics. (Chin *et al.*, 2007)  And, the device could easily be connected to the Internet such that relevant data could be shared.  Such a device could fundamentally change the way that people interact with the chemical and biological information of their surroundings and of their own bodies.

In addition to its applications in the developing world, lab-on-a-chip devices have a big role to play in the future of health care in The United States.  Currently, 15.2% of the United State's GDP is spent on healthcare and that fraction is expected to grow to 19.5% by 2020. (U.S. Department of Health and Human Services, 2007)  This amount of spending is believed to be unsustainable, especially as the population grows and ages. (Keehan *et al.,* 2008)  Lab-on-a-chip devices can be used to lower the price of medical diagnostics and monitoring, enabling diseases to be detected in their earlier stages where treatment is easier and far less expensive. (Tudos *et al.*, 2001)

In this thesis a lab-on-a-chip platform is developed that can control single cells and very small volumes of fluid to perform simultaneous, programmable experiments on a chip.  In contrast to technology that attempts to make lab-on-a-chip devices ultra-low cost by being low tech, (Martinez *et al.*, 2008) the chips described in this thesis

use cutting-edge technology. The chips remain inexpensive, however, by using the integrated circuit (IC) technology of the commercial electronics industry.

## 1.2 Hybrid IC / Microfluidic Chips - Concept

Integrated circuits are central to many of the technological wonders of the 21st century. Built on a slab of crystalline silicon no bigger than a square centimeter in area (roughly the size of a quarter) an IC contains 100s of millions of transistors and a maze of wires that connect the transistors into complex circuits to perform billions of operations per second. The transistors and wires of ICs are fabricated with nano-lithography (as opposed to one at a time), which allow ICs to be complex, small, fast, and also, inexpensive. (Lee, 1998) Integrated circuits are ubiquitous in today's technology. They are the microprocessors in computers, the radio frequency (RF) circuits in cell phones, the film in digital cameras, and the microcontrollers in heart patients' pace makers. Integrated circuits, having been invented only 50 years ago, have profoundly changed the way humans use, store, and communicate information. In Fig. 1.1a the original IC is shown, built by Jack Kilby in 1958, it contains only a single transistor. (Kilby, 1976) In Fig. 1.1b a modern Pentium quad-core IC, that can be found in today's laptops is shown, it contains 820 million transistors. (Intel)

In a spirit analogous to the miniaturization of electronics that lead to today's ICs, modern researchers are miniaturizing the fluid-handling tools of biology and chemistry laboratories into small, inexpensive chips to perform automated experiments. A growing library of microfluidic elements for lab-on-a-chip systems have been developed in recent years for tasks such as the mixing of reagents,

detecting and counting cells, sorting cells, genetic analysis, and protein detection. (Whitesides *et al.*, 2001, Stone *et al.*, 2004, Tabeling, 2005, and Yager *et al.*, 2006) In Fig. 1.1c a typical two-channel glass microfluidic chip used to controllably mix two substances together from Micronit Corp. is shown.  Figure 1.1d shows an example of one of the more complex microfluidic chips built today, from the Quake Group at Stanford, that consists of hundreds of pneumatically controlled gates and valves and is used to perform genetic analysis on microbes in the human mouth. (Marcy *et al.*, 2007)

The complexity, small feature size, and low cost of ICs can be applied to biological and chemical applications by combining ICs with microfluidics to form hybrid IC / microfluidic chips.  Complimentary-metal-oxide-semiconductor (CMOS) optical sensors have been coupled with microfluidics to make a "microscope on a chip" that achieves enhanced resolution and sensitivity by bringing microscopic objects directly to the optical sensors.  (Eltoukhy, *et al.*, 2006 and Cui *et al.*, 2008)   Electrical sensor arrays have been built on IC/ microfluidic chips to stimulate and measure large arrays of individual neural and cardiac cells. (DeBusscherre *et al.*, 2001 and Eversmann *et al.*, 2003)  And, hybrid IC / microfluidic chips have been used to trap and move dielectric (Gascyone *et al.*, 2004 and Hunt *et al.*, 2008) and magnetic objects (Lee *et al.*, 2006) along programmable paths for chemistry and biology experiments on a chip.  Figure 1.1e shows a hybrid IC / microfluidic chip that traps and moves objects along arbitrary paths with DEP using a large array of pixels.  The theoretical framework for how DEP is used to transport cells and vesicles on a chip is detailed in Chapter 2 of this thesis.
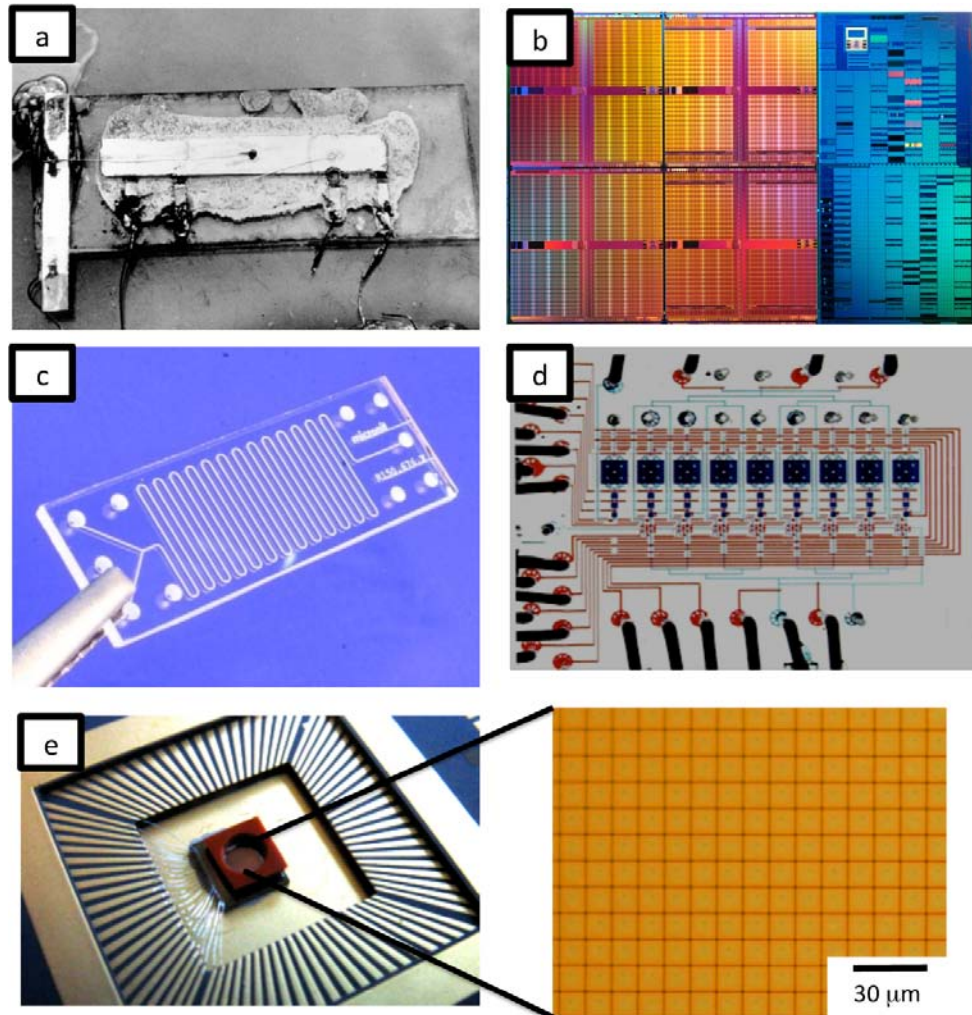
**Figure 1.1** (a) The original IC built by Jack Kilby at National Instruments in 1958 (Kilby, 1976) (b) a micrograph of the Intel quad-core processor, which has 820 million transistos (Intel Corp.), (c) a two channel glass microfluidic chip (Micronit Corp.), (d) an example of a complex microfluidic device that consists of hundreds of pneumatically controlled gates and valves and is used to perform genetic analysis on microbes in the human mouth, (Marcy *et al.*, 2007) (e) a photograph of an IC / microfluidic chip, the 'DEP Chip,' and a micrograph of the array of pixels that are used to trap and move objects with dielectrophoresis (DEP). (Chapter 3)

## 1.3 Overview of Thesis

This thesis describes the development of a versatile lab-on-a-chip platform using hybrid IC / microfluidic chips. The chips perform a wide range of functions on living cells and pL biomimetic containers for biology and chemistry experiments on a chip.

Previous work has been done developing programmable lab-on-a-chip platforms to control small volumes of fluid and cells. Pneumatic control has been used to create reconfigurable microfluidic components such as valves, latches, pumps, and multiplexers. (Unger *et al.*, 2000) Recently, similar structures have been developed that replace the cumbersome pneumatic lines with electronically activated components that are made of shape memory alloys (SMAs) and which can be built on top of commercial printed circuit boards (PCBs). (Vyawahare *et al.*, 2008) Droplets have been trapped, moved, mixed, and separated using both electrowetting (Lee *et al.*, 2002 and Pollack *et al.*, 2002) and dielectrophoresis (DEP) (Vykoukal *et al.*, 2001 and Peter *et al.*, 2004) with electronics that are external to the fluidic system. Hybrid integrated circuit (IC) / microfluidic chips have been developed that harness the mature technology of ICs to make general purpose, programmable fluid-handling systems. (Lee *et al.,* 2007, Gascyone *et al.,* 2004, Hunt *et al.*, 2008) The highly localized electric and magnetic fields that can be created by ICs have been used to trap and move small volumes of water suspended in oil (Hunt *et al.*, 2008), living single cells suspended in water (Gascyone *et al.*, 2004, Hunt *et al.*, 2008), and magnetically tagged biological objects suspend in water (Lee *et al.,* 2007) along programmable paths. Figure 1.2 shows a hybrid IC / microfluidic chip

7

simultaneously position thousands of yeast cells with DEP to spell "Lab on a Chip".

The chip shown in Fig. 1.2 is described in full detail in Chapter 3 of this thesis.
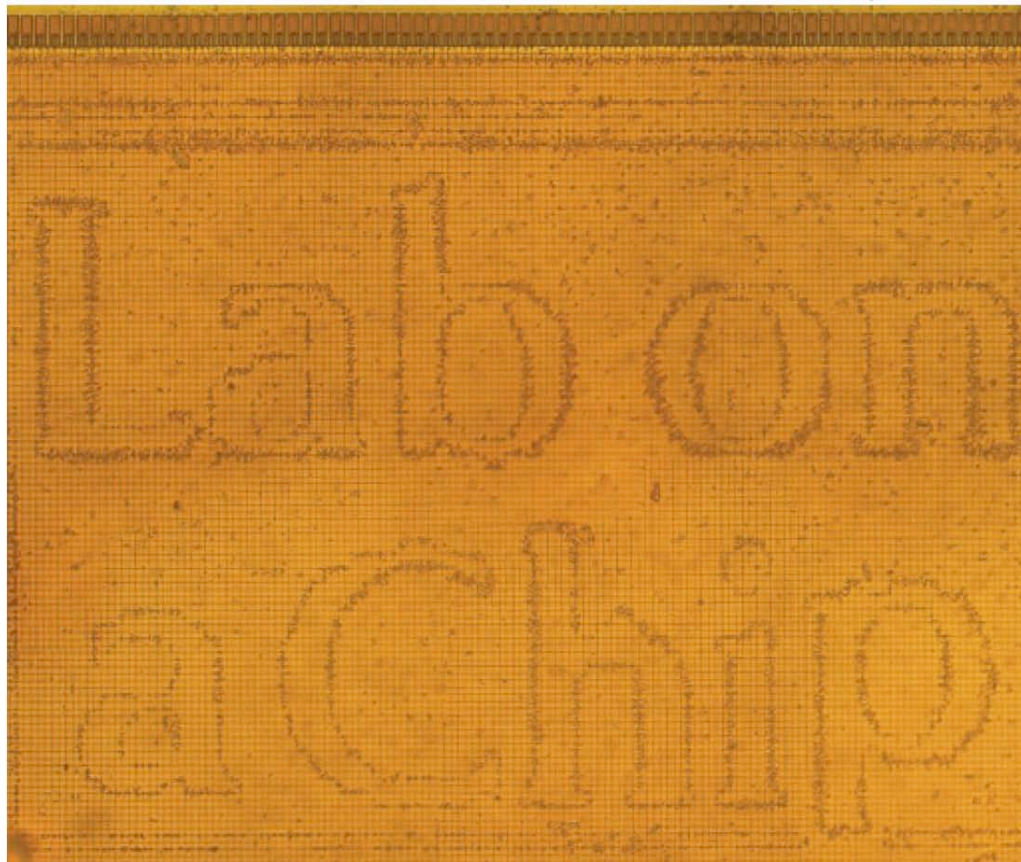
**Figure 1.2** The cover of Lab on a Chip featuring our hybrid IC / microfluidic chip simultaneously positioning thousands of yeast cells with DEP to spell "Lab on a Chip."

There are several key functions that are necessary to perform experiments on a chip that are analogous to typical laboratory processes. Any working medical or research laboratory has basic equipment: test tubes to keeps samples separate, pipettes to move samples around the laboratory, mixers to bring samples and reagents together, and heaters to control the temperature of experiments. In this thesis basic laboratory functions, as well as several functions that are not possible in a macro-scale laboratory, are performed on IC / microfluidic chips using electric and magnetic fields created above the IC's surface. In Table 1.1 the functions performed on hybrid IC / microfluidic chips in this thesis are listed.

Reagents and samples are kept separated, such that they can be transported around the 'laboratory' and mixed at the proper time in an experiment, by packaging them in pL containers as is demonstrated in Chapter 4. Inspiration is taken from cellular biology and phospholipid bilayer vesicles are used to package pL volumes of fluid on the chip. Vesicles are commonly used in cells for packaging quantities of substances for intercellular transport, to store enzymes, and as a reaction chamber. (Alberts *et al.,* 2007) Unilamellar vesicles made with electroformation provide robust pL containers that are impermeable and stable for a wide range of salinity, pH, and other environmental conditions. (Chiu *et al.,* 1999)

Vesicles and cells are transported across the 'laboratory' using DEP with electric fields at MHz frequencies above the chip's surface, as is demonstrated in Chapters 3, 4, and 5. The small feature-size of ICs allows micrometer-sized vesicles and individual living cells to be independently transported. The fast electronics and

complex circuitry of ICs allow thousands of living cells and vesicles to be simultaneously trapped and moved on the chip, allowing many parallel, well-controlled biological and chemical operations to be performed in parallel. The theoretical framework for DEP is introduced in Chapter 2.

Vesicles and cells are controllably permeabilized, fused, and released using kHz frequency electric fields above the chip's surface, as is demonstrated in Chapter 4. The vesicles can be triggered to release their contents locally into the solution and mix their contents with other vesicles using electric fields created by the chip. Electric fields at kHz frequencies induce voltages across the vesicle's membrane inducing electroporation or electrofusion.  Electroporation can also be performed on living cells, inducing the cells to take-up substances from the solution.  The complex circuitry of the chip allows specific vesicles or cells to be targeted for electroporation or electrofusion without harming surrounding cells or vesicles.  The chip can time-multiplex the kHz frequency electric fields with the MHz frequency electric fields used for DEP, such that objects remain trapped in place, as they are electroporated or electrofused.  The theoretical framework for electroporation and electrofusion is explained in Chapter 2.

A hybrid chip that can simultaneously perform DEP and magnetophoresis is demonstrated in Chapter 5.  Magnetophoresis, using magnetic fields created on the chip, provides a complimentary method to DEP for transporting substances across the 'laboratory.'  The ability to trap and move magnetic objects along programmed

paths is a useful tool to control the position of objects that cannot be trapped with DEP, but which can be tagged with magnetic particles. (Lee *et al.,* 2007)

The mechanical environment of individual cells and vesicles can be defined using the chip, a functionality that is not possible with macro-scale laboratory tools, as is demonstrated in Chapters 4 and 5. In-vitro experiments often suffer for not controlling the mechanical environment of cells, an aspect that plays an important role in-vivo. (Seifritz, 1924, Curtis *et al.*, 1964 and Wang *et al.*, 1994) Several DEP pixels can be patterned underneath a single vesicle or cell to control its mechanical environment by changing the shape of the DEP trap, as is demonstrated in Chapter 4 with unilamellar vesicles. Magnetic fields, created with DC current, are used to trap and move magnetically permeable objects such as iron oxide nanoparticles. These particles can be implanted into vesicles or living cells to apply local forces selectively to the location of the nanometer sized particles. This technique is demonstrated by controllably deforming vesicles implanted with iron oxide nanoparticles with magnetic fields created by the chip in Chapter 5.

The temperature of small compartments of fluid can be locally and rapidly controlled using dielectric heating with electric fields at GHz frequencies, as is demonstrated in Chapter 6. Electric fields with a frequency $f$ = 3 GHz are used to heat thermally isolated pL drops with dielectric heating. Changes in temperature $\Delta T = 0° – 30°C$ are achieved in a characteristic time $\tau_s$ = 15 ms.

**Table 1.1** A list of the functionalities demonstrated on the hybrid IC / microfluidic chips in this thesis.

| Action | Method | Field | Frequency | Details | Chapter |
|---|---|---|---|---|---|
| Contain | Unilamellar Vesicles | | | $a \approx 5\ \mu m$<br>$V \approx 0.5\ pL$ | 4 and 5 |
| Trap and Move | Dielectrophoresis | Electric | 1-10 MHz | Living Cells and Vesicles | 3, 4, and 5 |
| | Magnetophoresis | Magnetic | DC | Iron oxide nanoparticles | 5 |
| Deform | Dielectrophoresis | Electric | 1-10 MHz | Pattern several pixels underneath a vesicle | 4 |
| | Magnetophoresis | Magnetic | DC | Iron oxide nanoparticles embedded in vesicles | 5 |
| Release | Electroporation | Electric | 0.1-10 kHz | Trigger the release of chemicals into and out of vesicles | 4 |
| Permeabilize | Electroporation | Electric | 0.1-10 kHz | Trigger the passage of objects across a living cell's membrane | 4 |
| Mix | Electrofusion | Electric | 0.1-10 kHz | Fuse two vesicles together | 4 |
| Control Temperature | Dielectric Heating | Electric | 1-3 GHz | $\Delta T = 0° - 30°C$ in 15 ms | 6 |

Three devices are described in this thesis and are shown in Fig. 1.3. In Chapter 3 a custom IC / microfluidic chip that consists of 128 x 256 (32,768) 11 x 11 $\mu m^2$ pixels, each of which can be individually driven with 5 V peak-to-peak radio frequency (RF) voltages with frequencies from DC to 11 MHz, (Hunt, *et al.,* 2007) is developed into a lab-on-a-chip platform. This chip is called The DEP Chip (Fabutron 1.0) and a micrograph of it is shown in Fig. 1.3a.

In Chapter 5 a second custom IC / microfluidic chip is presented that can trap and move objects with both DEP and magnetic forces. The chips consists of 60 x 61 (3,660) 30 x 38 $\mu m^2$ pixels, each of which can be driven with a 50V peak-to-peak RF voltage with frequencies from DC to 10 MHz. Underneath the DEP pixel array, there is a magnetic grid that consists of 60 horizontal wires and 60 vertical wires running across the chip, each of which can be sourced with 120 mA to create local magnetic fields. This chip is called The HV-DEP / Magnetic Chip (Fabutron 2.0) and a micrograph of it is shown in Fig. 1.3b.

In Chapter 6 A PDMS based microfluidic device, fabricated with soft-lithography, is used to demonstrate rapid and local dielectric heating of drops. The device consists of an integrated flow-focusing drop maker, drop splitters, and metal line electrodes to locally deliver microwave power. This chip is called The Microwave Heater and a photograph of it is shown in Fig. 1.3c.
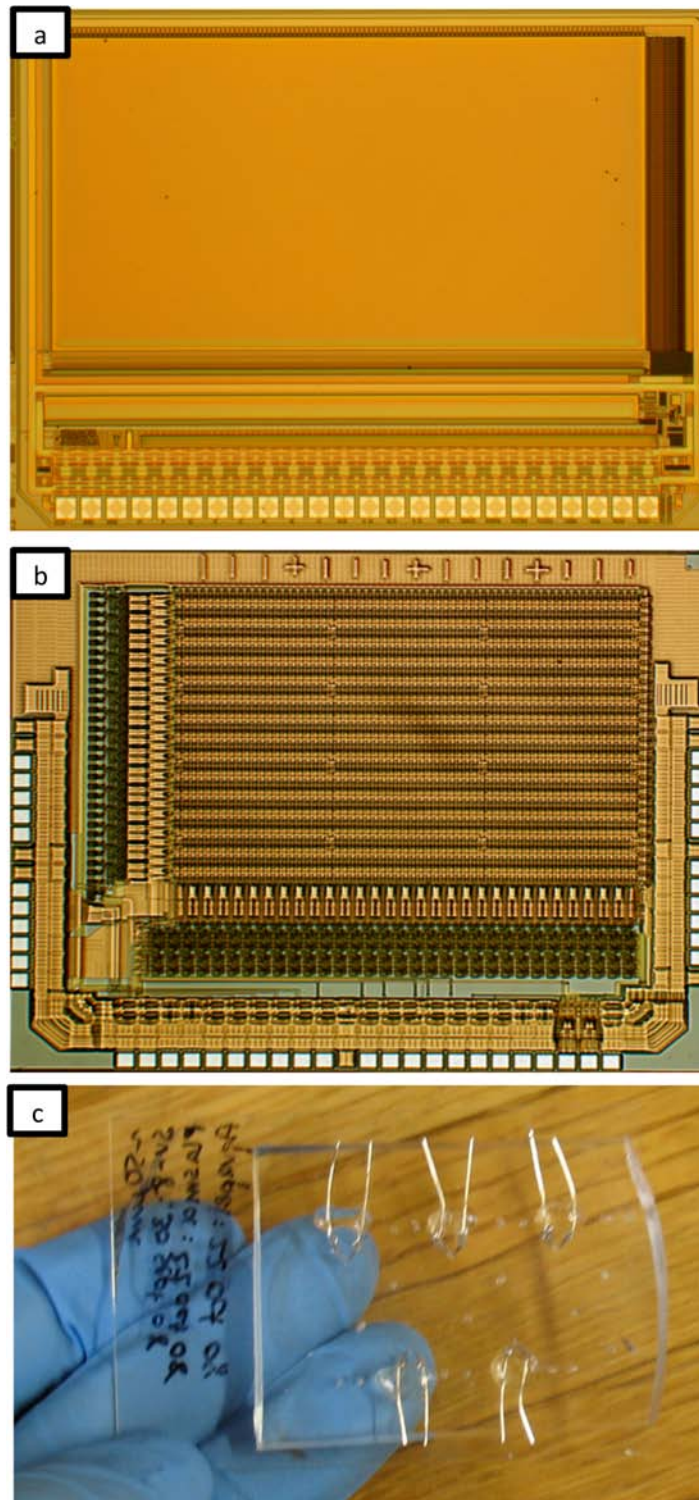
**Figure 1.2** (a) A micrograph of the DEP Chip (Fabutron 1.0), (b) a micrograph of the HV-DEP / Magnetic Chip (Fabutron 2.0), (c) a photograph of the PDMS microfluidic device (Microwave Heater) used to demonstrate microwave dielectric heating of drops.

# Chapter 2. Theory: Dielectric and Magnetic Control of Microscopic Objects

## 2.1 Overview

This chapter describes how electric and magnetic fields are used to control microscopic objects on hybrid integrated circuit (IC)/ microfluidic chips. Electric fields at kHz frequencies and below are used to induce electroporation and electrofusion. Electric fields at MHz frequencies are used for dielectrophoresis (DEP). Electric fields at GHz frequencies are used for dielectric heating. And, magnetic fields created with DC electrical currents are used to trap and move objects with magnetophoresis.

The frequency dependence of the dielectric properties of vesicles, cells, and solutions enable the dielectric phenomenon used in this thesis to be independently accessed with electric fields at different frequencies. The frequency dependence of DEP, electroporation, and dielectric heating is shown in Fig. 2.1. The strength of each of these effects is plotted in unitless values that are described in detail later in this chapter. At the MHz frequencies where DEP works best, both heating and electroporation is minimal, enabling vesicles and cells to be trapped and moved without damage. At the GHz frequencies where heating works best, both electroporation and DEP are minimal, enabling cells and vesicles to be heated without inadvertent trapping or damage. At the kHz frequencies where electroporation and electrofusion work best, heating is minimal and the DEP force is

negative, enabling vesicles and cells to be permeabilized and fused without

significant heating or inadvertent trapping.
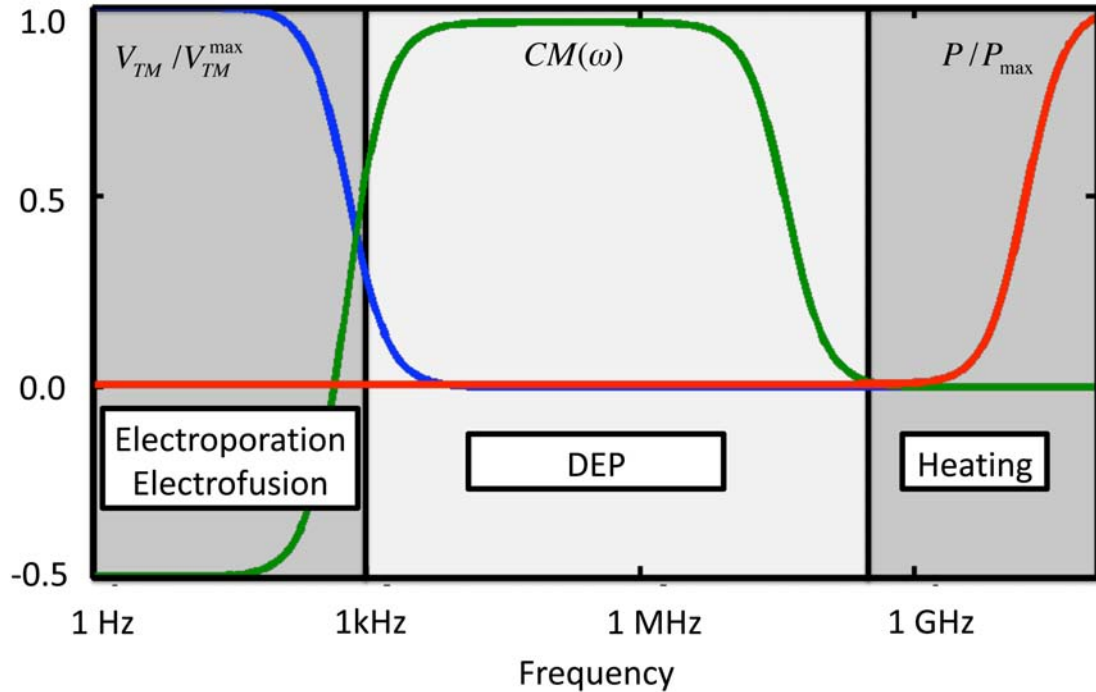


**Figure 2.1.** A semi-log plot of the efficacy of heating P/P$_{max}$ (red), dielectrophoresis CM($\omega$) (green), and electroporation $V_{TM}/V_{TM}^{max}$ (blue) *versus* the frequency $f$ of the applied electric field. The three frequency domains that are used for electroporation, DEP, and dielectric heating are labeled.

In this chapter the various dielectric and magnetic phenomenon that are used to control living cells and vesicles on our chips are explained.  In Section 2.1 water's unique dielectric properties, which play an important role in our ability to control objects with electric fields, are introduced.  In Section 2.2 dielectrophoresis, the force that is used to trap and move objects with electric fields, is introduced.  In Section 2.3 a geometric lumped-circuit model is developed to describe the dielectric properties of cells and vesicles.  In Section 2.4 this lumped-circuit model is used to explain the induced voltage that forms across the membranes of cells and vesicles, which is utilized in this thesis for electroporation and electrofusion.  In Section 2.5 dielectric heating with microwave frequency electric fields is introduced.  And finally, in Section 2.6 magnetophoresis is introduced as a method to compliment DEP for trapping and moving  objects, utilizing magnetic dipoles instead of electric permittivity.

## 2.1 The Dielectric Properties of Water and Solutions

To understand the dielectric properties of cells and vesicles it is necessary to first understand the dielectric properties of their most important ingredient, water.  Water is the primary constituent of cells and is the most commonly used solvent in chemical and biochemical experiments.  The DC dielectric constant of water $\varepsilon_s = 78\varepsilon_0$ (at T = 25°C) is very large compared to that of most other organic and inorganic solvents $\varepsilon_s < 10\varepsilon_0$, due to its permanent molecular dipole moment.  Water will typically dominate the dielectric properties of any object that is made of it. (Murrell *et al.*, 1994)

The dielectric response of water varies with the frequency of the applied electric field. (Grant, *et al.*, 1978) The permittivity is described by both the magnitude and the phase of the polarization relative to the applied field and can be represented as a complex function $\varepsilon(\omega) = \varepsilon'(\omega) + j\varepsilon''(\omega)$, with a real component $\varepsilon'$ and an imaginary component $\varepsilon''$. Figure 2.2a shows a plot of the real $\varepsilon'$ and imaginary $\varepsilon''$ components of the permittivity of water plotted versus frequency. The real component of the permittivity of water $\varepsilon'$ has a constant value of $\varepsilon_s = 78\varepsilon_0$ until a corner frequency defined by the dielectric relaxation of water $1/(2\pi*\tau_W) \approx 18$ GHz, at which point the permittivity monotonically drops. The imaginary component $\varepsilon''$ approaches zero everywhere, except at a resonant frequency defined by the dielectric relaxation time of water $\tau_W$. The permittivity of water can be described by an equation with a Debye form: (A. Stogryn, 1971)

$$\varepsilon_W = \varepsilon_\infty + \frac{\varepsilon_s - \varepsilon_\infty}{1 - j\omega\tau_W} \qquad\qquad \textbf{2.1}$$

where $\varepsilon_s = 78.4\varepsilon_0$ is the low frequency dielectric constant of water , $\varepsilon_\infty = 1.78\varepsilon_0$ is the optical dielectric constant, and $\tau_w = 9.55$ ps is the dielectric relaxation time at T = 25°C. The dielectric relaxation time $\tau_w$ can be understood as the characteristic time that it takes for water molecules to realign themselves to an instantaneous applied electric field.

The dielectric response of water depends on the concentration of ions in the solution. Dissolved ions change the conductivity of the solution $\sigma$ by acting as free

charge carriers.  The effect of ions in the solution can be incorporated into the permittivity of the solution: (A. Stogryn, 1971)

$$\varepsilon_W = \varepsilon_\infty + \frac{\varepsilon_s - \varepsilon_\infty}{1 - j\omega\tau_W} + j\frac{\sigma}{\varepsilon_o\omega} \qquad\qquad \textbf{2.2}$$

Figure 2.2b shows a plot of the imaginary component of the permittivity $\varepsilon''$ plotted versus frequency on a log-log scale for solutions with several different conductivities $\sigma$.  For solutions with a finite conductivity, the imaginary component of the permittivity $\varepsilon''$ decreases with increasing frequency until a characteristic frequency $1/\tau_I$.  The critical frequency $1/\tau_1$ is defined by the dielectric relaxation time $\tau_I = \varepsilon_s/\sigma$ that arises from conductivity of the solution $\sigma$ and the low frequency dielectric constant of the system $\varepsilon_s$.  As the conductivity of the solution $\sigma$ is increased, the characteristic frequency $1/\tau_I$ is pushed to higher values, as can be seen in Fig. 2.1b.  For low frequencies $\omega < 1/\tau_1$ the imaginary component of the permittivity $\varepsilon'' = \sigma/\omega\varepsilon_0$ is a function of only the conductivity $\sigma$ and no other material properties of the solution.  In the limit of water having zero conductivity $\sigma = 0$ the imaginary component of the permittivity $\varepsilon''$ increases monotonically with frequency until the characteristic frequency of water $\tau_w$.  The real part of the dielectric constant is slightly reduced with the addition of electrolytes, as water bound to the ions have a smaller dielectric response than free water molecules. (A. Stogryn, 1971)
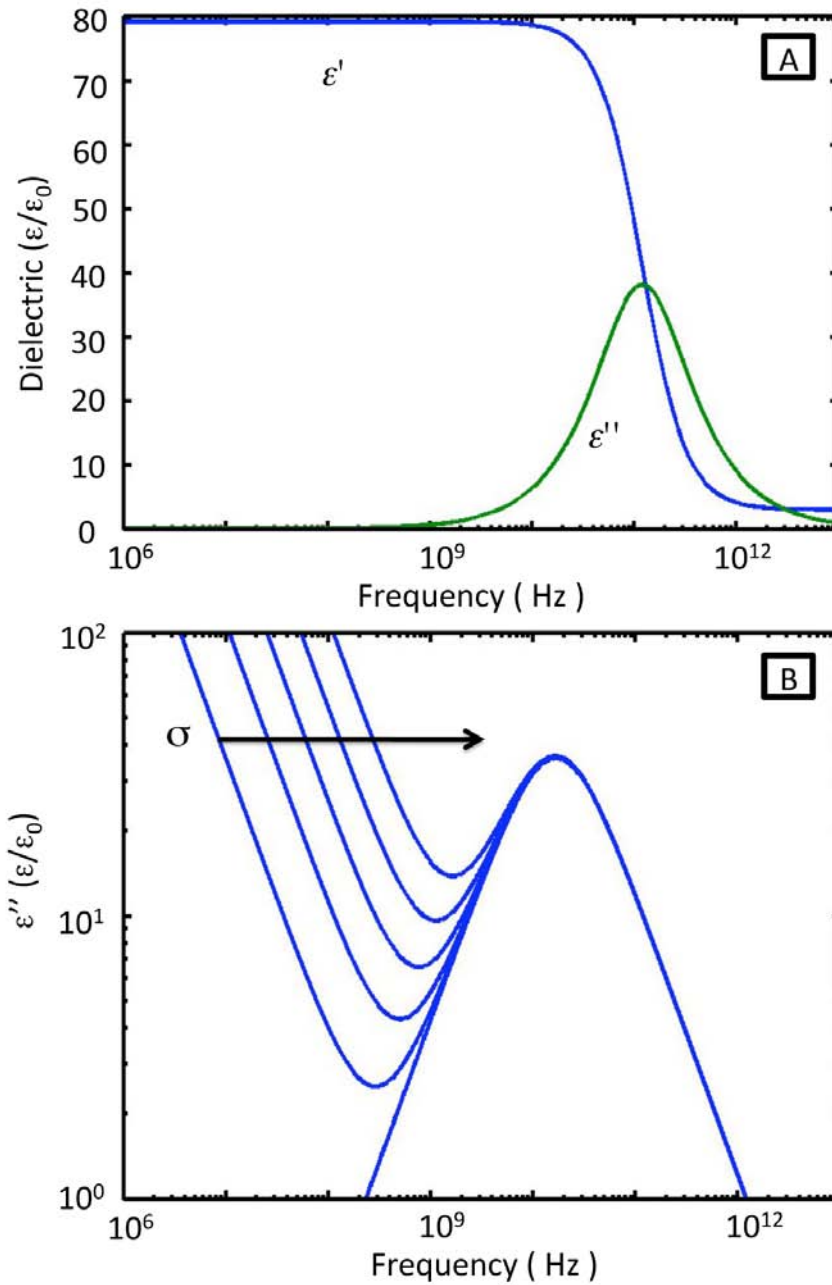
**Figure 2.2.** (a)The real ε' and imaginary parts ε''of the permittivity of water $ε_W$ plotted versus frequency, (b) the imaginary component ε'' of the permittivity of solutions of water plotted versus frequency for various conductivities σ. The conductivity σ increases going from left to right (as is shown with the black arrow) with values of 0 S/m, 0.03 S/m, 0.06 S/m, 0.14 S/m, 0.3 S/m, 0.62 S/m.

## 2.2 Dielectrophoresis

Dielectrophoresis is the induced motion of a dielectric object in a non-uniform electric field. Any object with a permittivity that is different than the surrounding medium can be controlled with DEP. The DEP force on a spherical object is: (Jones, 1995)

$$\vec{F}_{DEP} = 2\pi\varepsilon_m a^3 CM(\omega)\nabla\vec{E}_{RMS}^2$$

**2.3**

where $a$ is the radius of the particle, $\varepsilon_m$ is the dielectric constant of the medium, and $CM(\omega)$ is the Clausius-Mosotti factor, a relation between the frequency dependent complex permittivity of the particle and the medium.

$$CM(\omega) = \mathrm{Re}\left[\frac{\varepsilon_p - \varepsilon_m}{\varepsilon_p + 2\varepsilon_m}\right]$$

**2.4**

where $\varepsilon_p$ is the complex dielectric constant of the particle. When $CM(\omega) < 0$, the medium is more polarizable than the particle and the particle is pushed away from the local maximum of the electric field and this is called negative DEP. Positive DEP occurs when the particle is more polarizable than the fluid $CM(\omega) > 0$ and the particle is pulled toward the maximum of the electric field. The Clausius-Mosotti factor $CM(\omega)$ varies between -0.5 and 1.

The motion of microscopic objects is opposed by the viscous drag of the solution on the particle. At micrometer length scales inertia is very small compared to viscous drag (the Reynolds number $Re \approx 10^{-3}$). The viscous drag on a sphere can be described with a Stokes Drag Force $F_{drag} = -6\pi\eta a\vec{v}$ where $\eta$ is the dynamic viscosity

of the medium, $a$ is the radius of the sphere, and $\vec{v}$ is the velocity of the sphere

relative to the medium. The combination of the expression for the DEP force on a

sphere, Eq. 2.3, with the Stoke's Drag force gives the velocity of a particle $\vec{v}_{DEP}$ moved

with DEP,

$$\vec{v}_{DEP} = \frac{\varepsilon_m a^2 CM(\omega) \nabla \vec{E}_{RMS}^2}{3\eta}.$$  **2.5**

The low Reynolds number of the system allows the acceleration of the particle to be

ignored because the system is sufficiently over-damped that the particle reaches its

terminal velocity at a rate that is effectively instantaneous.

## 2.3 Dielectric Models for Cells and Vesicles

The dielectric properties of cells and vesicles can be described with simple models.

The permittivity of cells and vesicles are set by the intrinsic properties of the

object's constituent materials and also the object's geometry. Both vesicles and cells

can be modeled as spheres of water wrapped in a thin, impermeable membrane, as

is shown in the model in Fig. 2.3a. (Jones, 1995) The solution inside the vesicle has a

permittivity that is defined by the real part of the permittivity $\varepsilon_c$ and a

conductivity $\sigma_c$. The thin shell surrounding the vesicle has a capacitance per unit

area $c_{mem}$ and a surface conductivity $g_m$.

From the model described above, a lumped-element circuit model is developed to

describe vesicles and cells. The capacitance across the membrane is defined

$C = 2c_{mem}a$, where $a$ is the radius of the vesicle, and the surface conductivity is

assumed to be negligible. (Jones, 1995) The interior of the vesicle is defined by $R = 1/\sigma_c$ and $C = \varepsilon_c$ in parallel. By combining the lumped circuit elements assuming a spherical vesicle and an electric field in radial directions, as is shown in Fig. 2.3a, an effective permittivity for the object is arrived at

$$\varepsilon_{eff} = c_m a \left[ \frac{j\omega\tau_c + 1}{j\omega(\tau_m + \tau_c) + 1} \right].$$  **2.6**

where $\tau_m = c_m a/\sigma_c$ is the relaxation time of the charges that build up on the membrane and $\tau_c = \varepsilon_c/\sigma_c$ is the dielectric relaxation time of the solution inside the object. A similar model can be developed to understand the yeast cell, where a thin dielectric layer is added to the model to represent the cell wall that is not present in mammalian cells and vesicles. (Jones, 1995 and Hunt, 2007)

The DEP force on a vesicle or cell suspended in a solution can be calculated using the dielectric model developed above. The solution has a real permittivity $\varepsilon_s$ and conductivity $\sigma_s$. The effective permittivity for the vesicle or cell $\varepsilon_{eff}$ found in Eq. 2.6 is combined with the expression for the CM factor in Eq. 2.4:

$$CM(\omega) = \mathrm{Re}\left[ \frac{\omega^2(\tau_s\tau_m - \tau_c\tau_m') + j\omega(\tau_m' - \tau_s - \tau_m) - 1}{\omega^2(\tau_s\tau_m' + 2\tau_s\tau_m) - j\omega(\tau_m' + 2\tau_s + \tau_m) - 2} \right]$$  **2.7**

There are now two more characteristic times in the system, the dielectric relaxation time of the solution outside of the vesicle $\tau_s = \varepsilon_s/\sigma_s$ and the relaxation time of the charges on the outside of the vesicle building up on the membrane $\tau_m' = c_m a/\sigma_s$.

A vesicle can be trapped and moved with positive DEP at RF frequencies if the internal conductivity $\sigma_c$ is larger than the external conductivity $\sigma_s$.  In Fig. 2.3b the CM factor, Eq. 2.7, is plotted versus the interior conductivity $\sigma_c$ of a vesicle or cell suspended in a solution with $\sigma_s = 10^{-3}$ S/m, $\varepsilon_s' = \varepsilon_c'$, $a = 5$ μm, and $f = 1$ MHz.  If the conductivity inside the vesicle $\sigma_c > 10^{-3}$ S/m then the CM factor is positive and the vesicle experiences a positive DEP force.  The CM factor, and as a result the DEP force, plateaus to its maximum value above a conductivity $\sigma_c = 1$ S/m.

The DEP force on vesicles and cells depends on the frequency of the applied electric field.  In Fig. 2.3c the CM factor, Eq. 2.7, is plotted versus frequency for a vesicle with an interior conductivity greater than that of the solution $\sigma_c > \sigma_s$  The DEP force is negative at low frequencies, positive at intermediate frequencies, and negative at high frequencies.

The frequency response of CM($\omega$) can be understood heuristically by analyzing the lumped circuit model in Fig. 2.3a.  For frequencies slower than the interfacial charging time of the membrane  $\tau_{mem} = ac_{mem}(1/\sigma_c + 1/2\sigma_s)$, the DEP force is negative (CM < 0).  At these low frequencies the membrane has a high impedance and causes the vesicle to act like an insulating sphere, making it less polarizable than the medium.  At intermediate frequencies, above the charging time of the membrane $\tau_{mem}$ and below the interfacial dielectric relaxation time of the

vesicle $\tau_{mw} = (\varepsilon_p + 2\varepsilon_m)/(\sigma_c + 2\sigma_s)$, CM > 0 and the DEP force is positive.  At these

intermediate frequencies the membrane is transparent to the electric field and the

solution inside the vesicle acts like a conductor, making the vesicle more polarizable

than the medium.  At frequencies above the interfacial dielectric relaxation time $\tau_{mw}$

of the vesicle, the DEP force is negative (CM < 0).  At these high frequencies the

vesicle is transparent to the electric field, making the vesicle less polarizable than

the medium.
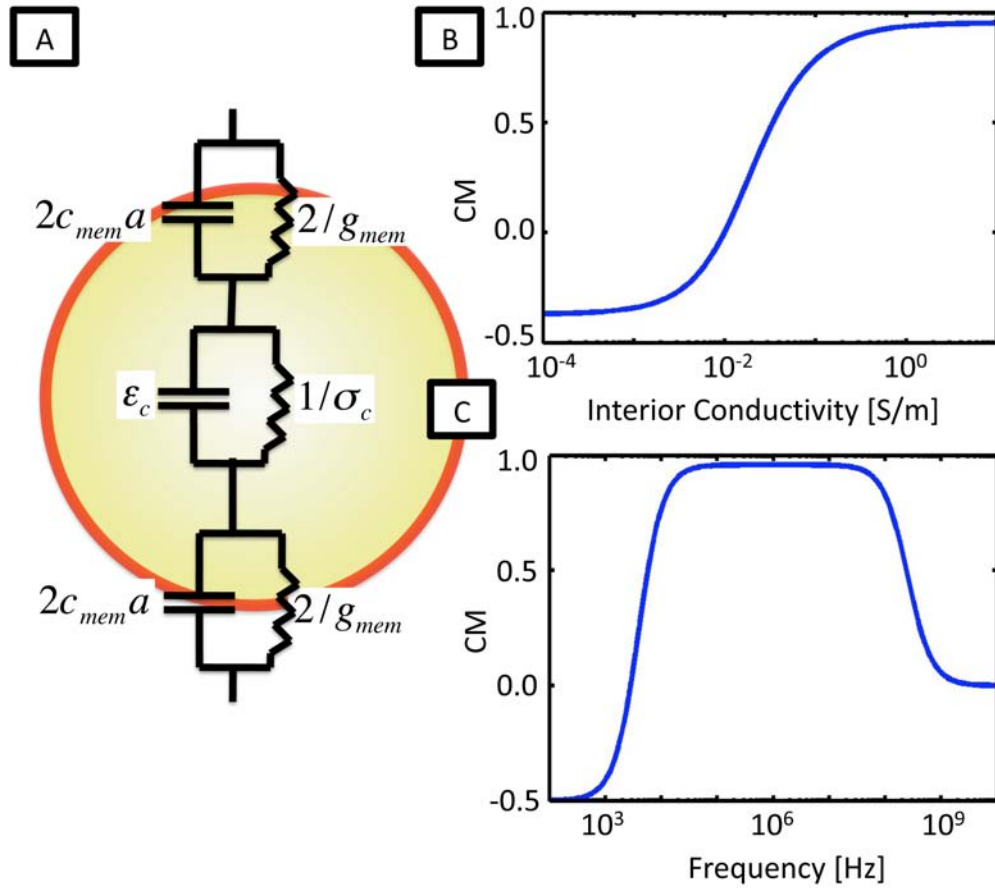
**Figure 2.3** (a) A lumped circuit model for a vesicle or a living cell with a radius a, that consists of an internal solution with a conductivity $\sigma_c$ and a dielectric constant $\varepsilon_c$, wrapped in a thin shell with a conductivity $g_{mem}$ and a capacitance per unit area $c_{mem}$, (b) the Clausius Mosotti factor CM plotted versus the internal conductivity of a vesicle suspended in a solution with an external conductivity $\sigma_s = 10^{-2}$ S/m in a field with a frequency $\omega = 1$ MHz, (c) CM of a vesicle with an internal conductivity $\sigma_c = 0.1$ S/m suspended in a solution with a conductivity $\sigma_s = 10^{-2}$ S/m factor plotted versus the frequency $\omega$ of the applied electric field.

## 2.4 Transmembrane Potential Difference and its Applications

In addition to the ability to trap and move objects with DEP, electric fields can be used to electroporate vesicles to release their contents, fuse two vesicles together, or permeabilize cell membranes, as is demonstrated in Chapter 4. These tasks are accomplished by using lower frequency electric fields (kHz frequencies compared to the MHz frequencies used for DEP) to induce voltages across the membranes of vesicles and cells. A large transmembrane voltage can cause pores to form in membranes (electroporation) or cause two vesicles to fuse together (electrofusion).

The electroporation of a vesicle or cell occurs when there is a large potential difference across the membrane of a cell or vesicle $V_{TM}$. In general, electroporation and electrofusion occur when the maximum transmembrane voltage $V_{TM}^{max}$ is greater than 1 V. (Sugar *et al.*, 1987) The maximum voltage $V_{TM}^{max}$ induced across the membrane of a spherical vesicle in an external electric field is: (Grosse *et al.*, 1992)

$$V_{TM}^{max} = \frac{3|\vec{E}|a}{2\sqrt{1 + (\omega\tau_{mem})^2}}$$

**2.8**

where $\tau_{mem} = ac_{mem}(1/\sigma_c + 1/2\sigma_s)$ is the interfacial charging time of the membrane, as is described in the previous section. A typical vesicle or cell has a capacitance per unit area $C_{mem} = 10^{-2}$ F/m². (Jones, 1995) For a vesicle with a radius $a$ = 5 μm with an internal conductivity $\sigma_c$ = 0.1 S/m suspended in a solution with a conductivity $\sigma_s$ = 10⁻² S/m, there is an interfacial charging time $\tau_{mem}$ = 20 μs. The transmembrane voltage $V_{TM}$ is plotted versus frequency in Fig. 2.4 for a vesicle or cell, as is described in section 2.3, in an electric field $|\vec{E}| = 3 \ V/\mu m$. At the frequencies $f \approx 1$ MHz used for

DEP the vesicle or cell will have an induced transmembrane voltage of $V_{TM} \approx 1$ mV. This small transmembrane voltage does not have a significant effect on the membrane of a vesicle or cell. (Olofsson *et al.,* 2003)  At frequencies slower than the interfacial membrane charging time $\tau_{mem}$, a transmembrane voltage on the order of $V_{TM} \approx 1$V forms.  This much larger transmembrane voltage $V_{TM}$ can trigger electroporation or electrofusion.

It has been shown in the literature that electric field pulses can trigger the fusion (electrofusion) between adhering vesicles or cells. (Sugar *et al.,* 1987 and Tresset *et al.,* 2007)  The model for electrofusion is a multi-step process that is illustrated in Fig. 2.4b.  Figure 2.4b (i) shows two vesicles that are trapped and moved together with DEP.  Figure 2.4b (ii) shows the vesicles brought into tight contact, partially squeezing out the water layer between the two vesicles with DEP.  Electric field pulses with a duration less than $\tau_{mem}$ are then applied to create pores (electroporation) in the transmembrane contact area, as is shown in Fig. 2.4b (iii).  If the pore density is large enough then pores can then nucleate into a stable hole in the contact area as is shown in Fig. 2.4b (iv). (Tresset *et al.,* 2007)  On our chip electric fields at MHz frequencies are used to hold vesicles in contact with DEP while time-multiplexed electric field pulses with frequencies less than the membrane charging time $\omega < 1/\tau_{mem}$ trigger the fusion, as is demonstrated in Chapter 4.

Induced voltages across a cell's membrane $V_{TM}$ can affect the cell's viability and physiological state.  In a living cell, ion pumps maintain a transmembrane voltage of $V_{TM} = 70$ mV across the cell membrane.  It is a general rule of thumb that as long as

the induced transmembrane voltage is much less than the normal physiological

transmembrane voltage $V_{TM} << 70$ mV, then it will have only a small effect on cell

physiology. (Olofsson *et al.,* 2003)  A cell trapped in a DEP trap with an electric field

strength $\left|\vec{E}\right| = 3V / \mu m$ and a frequency $f$ = 1MHz will have an induced

transmembrane voltage $V_{TM} \approx 1$ mV.  Therefore, a cell in a DEP trap should remain

healthy until the frequency of the applied electric field is purposely lowered to

induce electroporation or electrofusion.
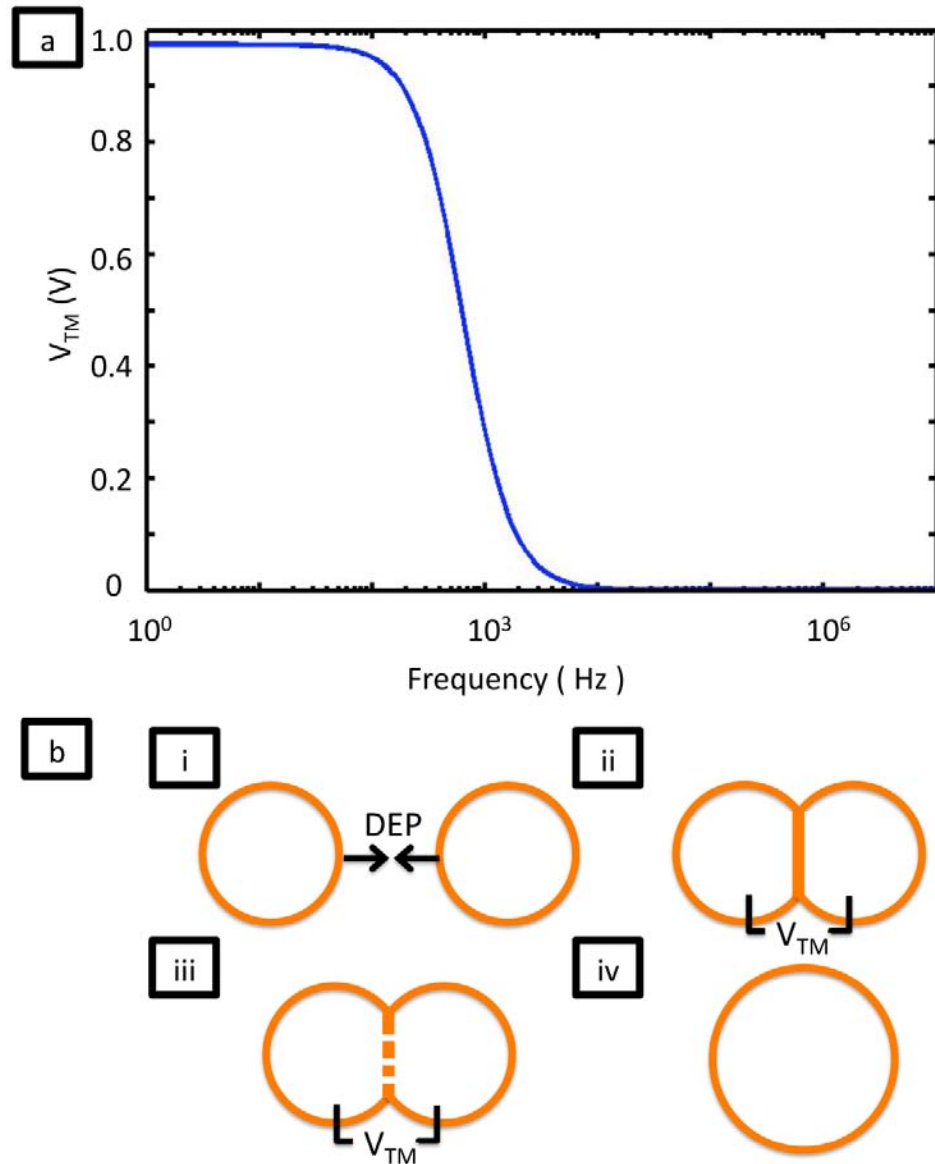
**Figure 2.4** (a) The transmembrane potential of a model of a vesicle or cell with an internal conductivity $\sigma_c = 0.1$ S/m, suspended in a solution with a conductivity $\sigma_s = 10^{-2}$ S/m, with a radius $a = 5$ μm and a capacitance of $C_{mem} = 10^{-2}$ F/m$^2$ is plotted versus the frequency $f$ of an applied electric field $\left| \vec{E} \right| = 3 \ V/\mu m$, (b) a step-by-step illustration of the fusion of two vesicles.

## 2.5 Dielectric Heating

Dielectric objects can be heated with time-varying electric fields.  Induced and intrinsic dipole moments within an object will attempt to align themselves with a time-varying electric field.  The energy associated with this alignment is viscously dissipated as heat into the surrounding solution.  The power density P absorbed by a dielectric material is given by the frequency of the applied electric field $f$, the imaginary component of the permittivity (the loss factor) $\varepsilon''$ of the material, the vacuum permittivity $\varepsilon_0$, and the electric field strength $|\vec{E}|$ with the expression (Bengtsson *et al.,* 1974):

$$P = \omega \varepsilon_o \varepsilon'' |\vec{E}|^2$$

**2.9**

The loss factor of the material depends on the frequency of the electric field and the characteristic time $\tau_W$ of the dielectric relaxation of the material, with the expression:

$$\varepsilon'' = \frac{(\varepsilon_s - \varepsilon_\infty)}{1 + (\omega\tau)^2} + \frac{\sigma}{\omega\varepsilon_o}$$

**2.10**

where $\varepsilon_s$ = 78.4$\varepsilon_0$  is the low frequency dielectric constant of water, $\varepsilon_\infty$ = 1.78$\varepsilon_0$ is the optical dielectric constant, $\tau_W$ = 9.55 ps is the characteristic relaxation time of water at T = 25°C (as is shown in Fig. 2.1), and $\sigma$ is the conductivity of the solution. (Murrell *et al.,* 1994)

The power that a material absorbs from a time-varying electric field depends on the frequency of the field.  In Fig. 2.5 the power density P [W/m$^3$] absorbed by water in

an electric field with a magnitude $\left|\vec{E}\right| = 10^5\ V/m$ is plotted versus frequency for

several solutions with different conductivities σ. For deionized water the power

density increases monotonically until it plateaus at $f$ = 18 GHz, the frequency

associated with the characteristic relaxation time of water $\tau_w$. For solutions with a

finite conductivity σ, the power density has a constant value $P = \varepsilon_o \left|\vec{E}\right|^2 \sigma$ at

frequencies below a critical frequency set by the dielectric relaxation time of the

solution $\tau_s = \varepsilon_s/\sigma_s$. At frequencies above the dielectric relaxation time of the

solution $\tau_s$ the power increases monotonically until it plateaus at $f$ = 18 GHz. For

biological solutions σ ≈ 0.5 S/m, the dielectric relaxation time of the solution is

$\tau_s$ ≈ 1.4 ns.

Due to water's large dielectric loss at GHz frequencies, microwave power is

absorbed much more strongly by water than polymers, glass, silicon, and most

objects that microfluidic devices could be constructed with. This allows microwave

power to be delivered to solutions without significantly heating the surrounding

microfluidic device. Effective heaters can be built that work at $f$ = 3.0 GHz, a

frequency very close to that of commercial microwave ovens (2.45 GHz), that is

below the frequency associated with the relaxation time of water but where water

still readily absorbs power (as is demonstrated in Chapter 6).
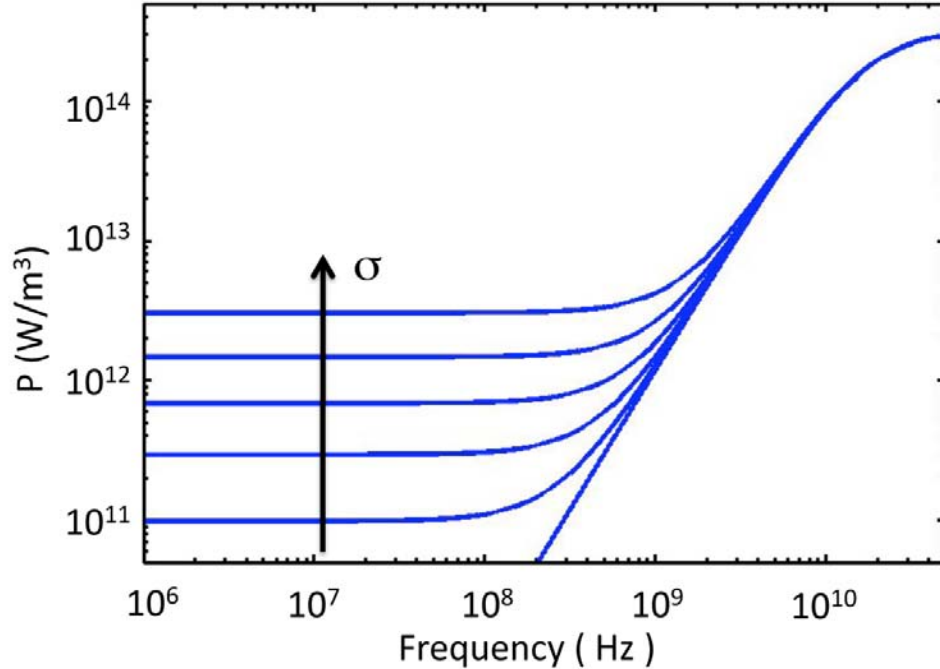
**Figure 2.5**. The power density P (W/m³) plotted versus the frequency f of the applied electric field. Several solutions with different conductivity σ are plotted, increasing going from the bottom to the top with values of 0 S/m, 0.03 S/m, 0.06 S/m, 0.14 S/m, 0.3 S/m, and 0.62 S/m.

## 2.6 Magnetophoresis

Magnetophoresis provide a technique to trap and move particles that compliments

DEP. Whereas almost all materials have some dielectric response, most objects are

completely transparent to magnetic fields. As such, magnetophoresis has the

benefit that forces can be applied specifically to magnetic particles while not

affecting the surrounding dielectric objects. This technique (as is demonstrated in

Chapter 5 of this thesis) is useful for applying local forces to microscopic objects.

A particle with a magnetic moment $\vec{m}$ in a magnetic field $\vec{B}$ experiences a force,

$$\vec{F}_{MAG} = \vec{m} \bullet \vec{B}.$$

**2.11**

For a paramagnetic particle with a magnetic susceptibility $\chi$, the moment

$\vec{m} = V\chi\vec{B}/\mu_o$ is proportional to the external magnetic field strength $\left|\vec{B}\right|$, the volume of

the particle $V$, and the vacuum permeability $\mu_0$. The force on a paramagnetic particle

is: (Lee *et al.*, 2004)

$$\vec{F}_{MAG} = \frac{-V\chi}{\mu_o}\nabla\vec{B}^2$$                    **2.12**

.

In the work presented in this thesis, superparamagnetic particles are used.

Superparamagnetism is a form of magnetism where very small ferromagnetic

particles behave like paramagnets. The particles are small enough that thermal

fluctuations cancel their net moment when there is no field applied, but an applied

field will cause the particles to align. As such, superparamagnetic particles may be

described with a high magnetic susceptibility $\chi$ at fields lower than their saturation

value. (Bean *et al.*, 1959 and Lee *et al.*, 2005)

# Chapter 3. Hybrid Integrated Circuit / Microfluidic Chips

In this chapter hybrid IC/ microfluidic chips and the experimental apparatus that surround them are presented.  Two hybrid chips are described in this thesis.  In this chapter the Dielectrophoresis (DEP) Chip (The Fabutron 1.0) is introduced. (Hunt *et al.,* 2008)  The High Voltage Dielectrophoresis / Magnetic Chip, (HV-DEP / Magnetic Chip, The Fabutron 2.0) which combines dielectric and magnetic trapping onto a single chip, is described in Chapter 5.  The details of the experimental apparatus surrounding both chips are presented in this chapter, including the fluidics, electronics, optics, thermal management, and computer control.

## 3.1 Overview

Hybrid IC / microfluidic chips combine the inexpensive complexity and small feature size of ICs with the biocompatible environment of microfluidics to perform programmable biological and chemical experiments on the micrometer scale. (Lee *et al.,* 2007)  In this chapter a chip is described that traps and moves individual microscopic objects along programmable paths with dielectrophoresis (DEP).  The DEP chip consist of a large array of micrometer-scale pixels that can be individually addressed with radio frequency (RF) voltages, creating electric fields above the chip's surface.  The chip can simultaneously and independently control the locations of thousands of dielectric objects such as living cells or pL drops of fluid, allowing thousands of biological and chemical experiments to be controlled in parallel.

**3.2 Dielectrophoresis Chip (Fabutron 1.0)**

The DEP Chip consists of a custom IC and a fluid cell that holds liquid directly on the chip's surface, as is shown in Fig. 1.1e. Electronic circuits integrated into the IC are used to create local electric fields above the chip's surface. These electric fields can be used to position objects with DEP or release, permeabilize, and fuse objects with electroporation and electrofusion. The complex circuitry and fast electronics of the DEP chip allow many living cells and vesicles to be controlled, allowing many parallel, well-controlled biological and chemical operations to be performed.

The DEP chip consists of an array of electrodes, each of which can be individually driven with a voltage, to create an electric field above the chip's surface as is shown in the inset in Fig. 1.1e. Specifically, the DEP chip consists of 128 x 256 (32,768) 11 x 11 $\mu m^2$ pixels, each of which can be individually driven with a 5V peak-to-peak radio frequency (RF) voltage with frequencies from DC to 11 MHz. Underneath each pixel is a static random access memory (SRAM) element. The state of the SRAM element determines whether the pixel is driven by the external RF voltage source (the pixel turned off) or by the logical inverse of the RF voltage (the pixel turned on). The RF voltage between the pixels creates an electric field above the chip's surface that is used to trap and move objects with DEP. The entire array of pixels can be updated hundreds of times in a second. The IC is designed using Cadence design software and is fabricated with a commercial 0.35 $\mu m$ process with 4 metal layers through MOSIS (process: TSMC35_P2). The detailed specifications of the DEP Chip are outlined in the appendix in the format of a data sheet. (Appendix A)

*3.2.1 Operating Principals*

The DEP Chip uses positive DEP to trap and move dielectric objects. By shifting the location of the pixels that are turned on, the location of local electric field maxima are moved around the array. In Fig. 3.1a quasi-static finite element simulations (Ansoft: Maxwell 11) are shown of the electric field magnitude $\left|\vec{E}\right|$ 5 µm above the chip's surface. Two pixels in the center of the array are set to 5 V and the rest of the pixels are set to 0 V. A dielectric object with a radius $a = 5$µm is schematically shown being pulled towards the maximum of the field. The simulations show that the object will experience a maximum field of $\left|\vec{E}\right| \approx 5 \; V/\mu m$. (Hunt, 2007)

The expected DEP force on an object above the chip's surface can be calculated by combining the electric field simulations shown in Fig. 3.1a with the dielectric models presented in Chapter 2. The force on a dielectric object with a radius $a = 5$ µm, described by the model in section 2.3, suspended in a solution with a conductivity $\sigma_s = 10^{-2}$ S/m, in an electric field with a frequency $f = 1$ MHz and an RMS magnitude shown in Fig. 3.1a, is plotted in Fig. 3.1b. The dielectric object is trapped at the interface of two pixels on the left that are turned on and two pixels on the right that are turned off. The magnitude of the trapping force is $F \sim 1$nN and the force is localized within two pixel lengths of the trap. A line is fit to the force curve at the location of the trap, and the effective spring constant is found to be $k = 520$ pN/µm.

*3.2.2 Characteristic Times*

The rate that the device can perform operations is limited by the time that it takes for microscopic objects suspended in solution above the chip's surface to react to the electric or magnetic fields, not the speed of the electronics. There are two important characteristic times that describe the microscopic objects suspended in solution on our chips: the time that it takes for a particle to diffuse away if a trap is turned off $\tau_{\text{diff}}$ and the time that it takes for a particle to move between traps when one pixel is turned off and the next is turned on $\tau_{\text{move}}$. A particle suspended in a solution takes a time $\tau_{\text{diff}} = L^2/16D$ to diffuse the distance of half of a pixel length $L/2$. The self-diffusion constant $D$ is defined by the Stokes-Einstein Equation $D = \text{kB}T/6\pi\eta a$, where $kBT$ is the thermal energy, $\eta$ is the viscosity of the solution, and $a$ is the radius of the particle. The time that it takes for an $a = 1$ μm particle suspended in water to diffuse $L/2 = 5$ μm is $\tau_{\text{diff}} \approx 1$ sec. The diffusion time $\tau_{\text{diff}}$ is longer for bigger particles.

The time that it takes for a particle to move from one pixel to the next $\tau_{\text{move}}$ is calculated using the relationship between the DEP force and velocity in Eq. 2.5 and the plot of the DEP force versus distance in Fig. 3.1b. The time that it takes for an $a = 1$ μm particle on the DEP chip to move from one pixel to the next is $\tau_{\text{move}} \approx 10$ ms. For larger particles the time that it takes to move particles between pixels $\tau_{\text{move}}$ increases. The IC operates at sub-ms time scales (as is described below) such that the IC can change its state many times in the time that it takes for a particle to react to the change in field.
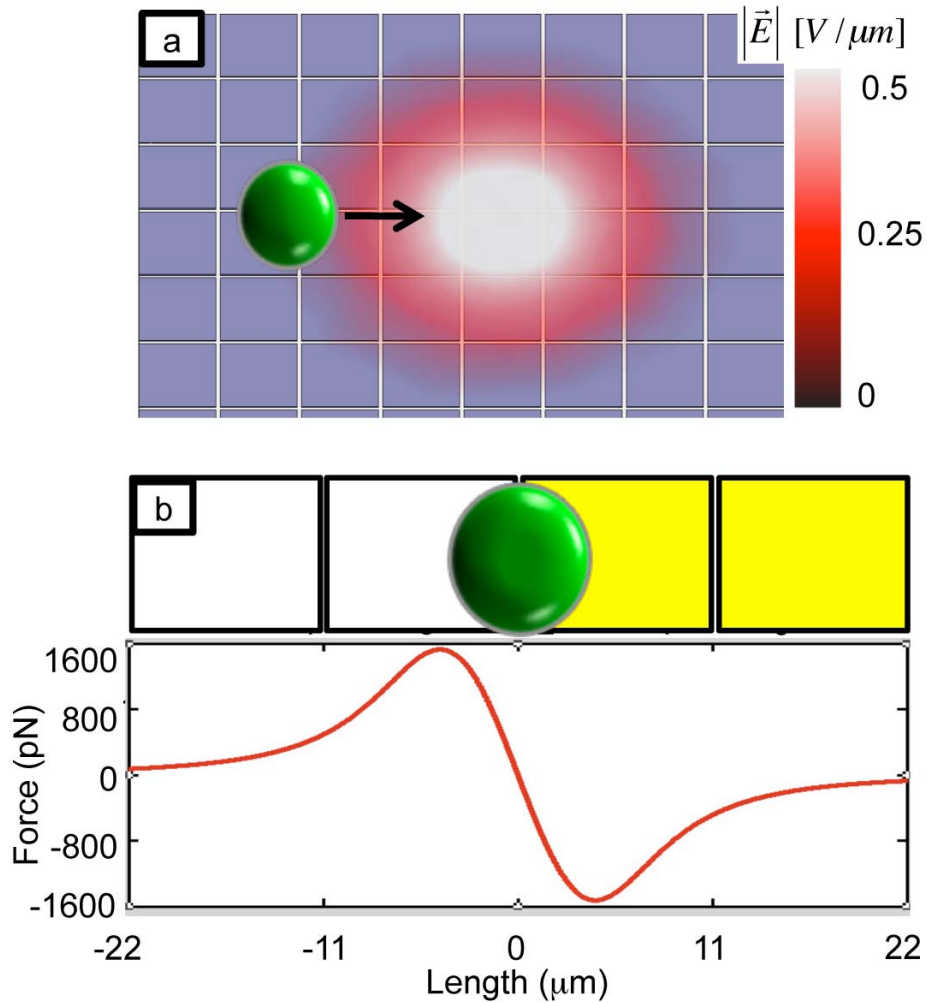
**Figure 3.1.** (a) A finite element simulation of the electric field strength 5 μm above the chip's surface, (b) a plot of the force on a dielectric object (as modeled in chapter 2.3) at the interface of two pixels on the left that are turned on (in yellow) and two pixels on the right that are turned off (in white).

*3.2.3 Integrated Circuit Design*

This section outlines the detailed description of the DEP chip given in Tom Hunt's Thesis. (Hunt, 2007 and Hunt *et al.,* 2008) The chip's 128 x 256 (32,768) pixels are addressed with logic and memory built into the IC, such that only 8 data lines (not including the two clocks and four control signals) are required to update the entire array. A schematic of the SRAM array and the logic and memory that surround it are shown in Fig. 3.2a. The SRAM memory is organized as 128 words x 256 bits. The bits of each word are read in and out of the chip with a sequentially loaded two-phase clocked shift register. Each word is addressed to a specific row in the array using a 7 bit row decoder. The row decoder takes 7 binary inputs and uses them to choose 1 of $2^7$ (128) rows of the SRAM array. A micrograph of the chip, showing a section of the array of DEP pixels surrounded by the control electronics, is shown in Fig. 3.2c.

A schematic of the circuit underneath each DEP pixel is shown in Fig. 3.2b. The SRAM memory elements underneath each pixel are addressed with a word-line and its value set with a bit-line. The SRAM element controls a multiplexer (MUX) that routes one of two signals, produced off of the chip, to the 11 x 11 $\mu m^2$ pixel above. Generally the two signals are RF voltages that are 180° out of phase, but can be set arbitrarily. The output of the MUX goes through a voltage-amplifier before driving the pixel. The voltage-amplifier is a two transistor inverter, appropriately sized to drive the capacitive load of the pixel. The voltage-amplifiers have an on-resistance of $R_{on} \approx 10$ kΩ, driving a pixel capacitance of less than $C_{load} \approx 50$ fF, which yields a

sub-ns RC time. The voltage on the pixel can have a peak-to-peak voltage of 5V and a bandwidth of DC – 11 MHz. The bandwidth could have been larger (DC – GHz) if greater care was taken in the design of the chip to buffer the RF lines throughout the circuit.

The chip's addressing architecture is a result of trade-offs between maximizing the refresh rate of the SRAM array, minimizing the size of the electronics needed underneath each pixel, and minimizing the number of input and output pins on the chip. The refresh rate of the chip is improved by allowing regions-of-interest (ROI) to be updated without updating the entire array. On the chip, words that are 256 bits in length are updated with random-access. For each pixel to be fully random-access would require two extra transistors underneath each pixel, increasing the pixel size and complexity of the circuit. The refresh rate is maximized by breaking the array into words with the smallest number of bits. In the limiting case, the chip would be as fast as it could be if each pixel had a wire to the outside-world. Conversely, the number of pins is minimized by increasing the size of each word. In the limiting case, the chip would have the minimum number of pins if the entire array was updated in serial with a shift register.

In our design, with a 128 word x 256 bit array, the shift register is updated at a maximum rate of 1 bit/0.1 μs making it take ~26 μs to update a single word on our chip and ~3.3 ms to update the entire array. Thus, the chip can refresh its entire state faster than the time $\tau_{move} > 10$ ms that it takes for the particles above the chip's surface to react to the fields. The update rate of the chip is currently limited

by the electronics surrounding the chip. With the current electronics the refresh rate of the chip is 400ms to update the entire array. The chip is interfaced to a computer and the interface is slower than the chip itself, as is explained in more detail below. A new generation of graduate students is currently designing a microcontroller interface to the chip that can refresh the chip at its maximum rate.

The design of the chip, using the Cadence software package, is hierarchical and incorporates digital and analog testing such that (if done correctly) the layout is guaranteed to meet design specifications and the design rules of the fabrication process. The chip design begins with breaking the chip into separable modules: the pixel, the shift register, the row decoder, a single SRAM element, etc... The individual modules are designed in terms of other modules, continuing downwards in the hierarchy until reaching the transistor-level. Each transistor corresponds to the layout of masks (doping and metal layers, vias, etc...). The modules are combined at the mask-layout level by manually placing the modules and manually connecting them with metal layers. The design software checks that the circuits at the mask-level matches the circuits at the module-level. The electrical testing begins at the bottom of the hierarchy at the module-level, using SPICE models for each element, to test the digital and analog (both time domain and frequency domain) response of the circuits. Once the layout for a module is drawn, additional unintended capacitances in the system are extracted from the layout and incorporated into the testing. The new layout can be modified based on the results of the testing, and this cycle can be repeated in iterations until the design specifications of the module are met. The modules are combined and the system is tested working from the bottom

of the hierarchy to the top, until the entire chip is laid out and fully tested.  For the

chips designed in this thesis, the design process takes about two months from start

to finish and results in a chip with N ≈ 300,000 transistors.
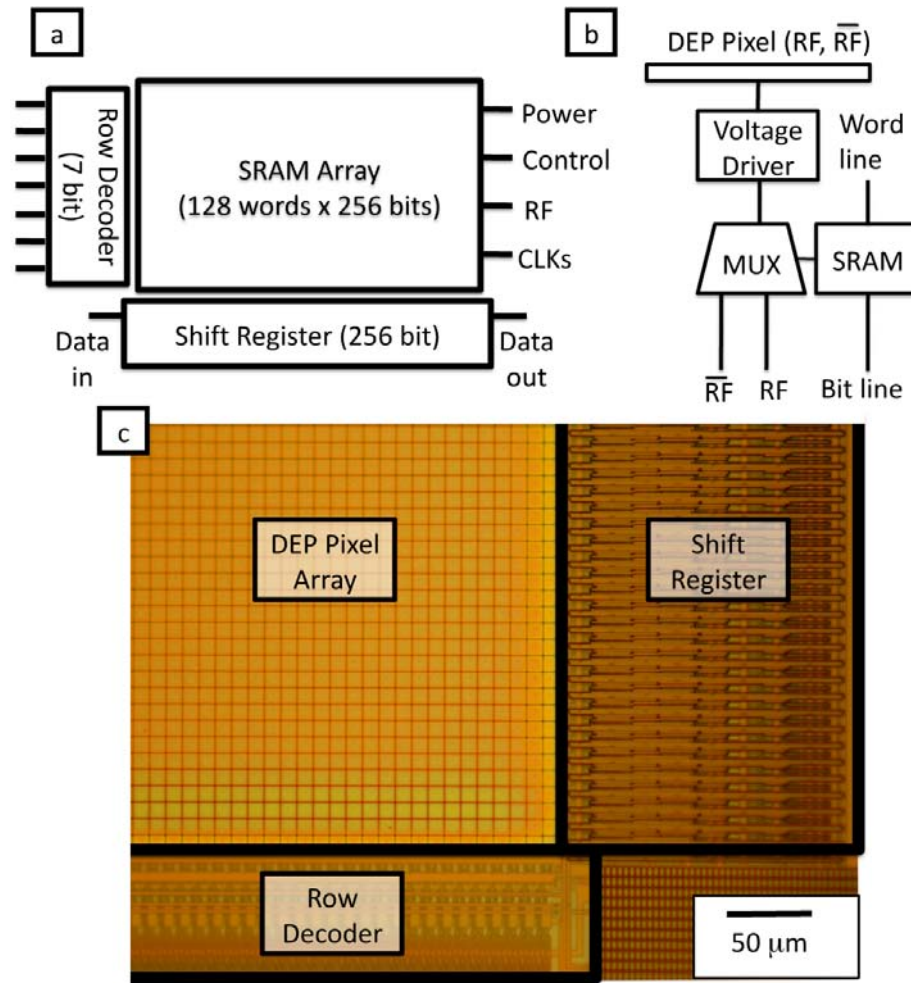
**Figure 3.2.** (a) A schematic of the architecture of the SRAM array and the logic and memory that are used to read and write to it on the DEP chip, (b) a schematic of the circuit underneath each DEP pixel, showing the SRAM memory element, a multiplexer (MUX) that directs either the RF signal or its logical inverse to a voltage driver that connects to the electrode, (c) a micrograph of a 250 x 200 $\mu m^2$ section showing a corner of the chip with a portion of the DEP array in the upper left corner, the row control circuits on the bottom, and the bit control circuits, including the shift register, on the right.

*3.2.4 Capabilities*

The DEP chip has been used to trap and move dielectric objects such as living cells, (Fig. 3.1a and Fig. 3.1c) drops of fluid immersed in oil, (Fig. 3.1b) and vesicles used as biomimetic containers(Chapter 6).  In addition to the ability to trap and move objects with DEP, electric fields can be used to electroporate vesicles to release their contents, fuse two vesicles together, or allow cells to take up substances from the solution. (Chapter 6)  These tasks are accomplished by using lower frequency electric fields (kHz frequencies compared to the MHz frequencies used for DEP) to induce voltages across the membranes of vesicles and cells, as is described in Chapter 2.  In addition to what has been demonstrated by our group, any application that could benefit from a programmable electric field controlled on the length scale of L = 10  μm with an RF bandwidth could be performed on the DEP chip, such as electro-optics (Lopez, 1970), electro-wetting (Pollack *et al,.* 2000), or electro-chemistry (Nyholm, 2005).
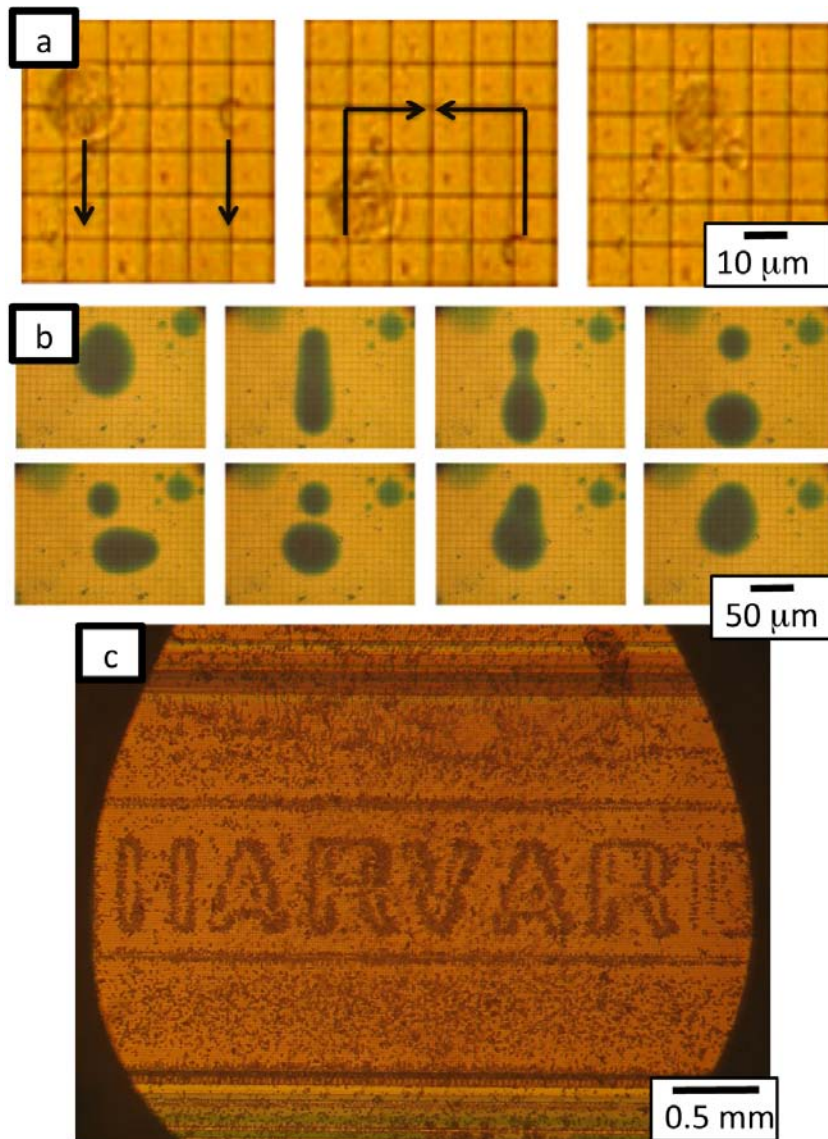
**Figure 3.3** (a) A time sequence of yeast and rat alveolar macrophages being trapped and moved with DEP. The black arrows indicate the direction that the cells are moved between frames. The cells move at a rate of ~50 μm/sec, (b) a time series of drops of colored water between a layer of fluorocarbon oil and hydrocarbon oil trapped, moved, split, and merged with the chip, (c) a micrograph of the entire chip being used to position thousands of yeast cells to spell "Harvard." (Hunt *et al.,* 2008)

## 3.3 Experimental Apparatus

The apparatus that surrounds the IC / microfluidic chips is described in this section. The apparatus consists of an interface to control the chip with a computer and an optical microscope with a video camera to observe what happens on the chip. A block diagram outlining the organization of the apparatus surrounding the chips is shown in Fig. 3.4a. Fluidics bring samples and reagents to the chip. The chip communicates to the outside world through electrical connections on a custom printed circuit board. The printed circuit board connects to a computer through a digital input / output (I/O) card. The computer can both write and read-out the state of the chip through custom control software. A fluorescence microscope images the contents of the chip. The images are sent to the computer through a digital camera. A graphical user interface (GUI) provides an intuitive platform for the user to interact with the chip. The overall system is aimed at being robust, easy, and flexible enough to use that new experiments can be quickly prototyped, with minimum setup and maintenance time.

### 3.3.1 Fluidics

A fluid cell is built directly on top of the IC with a silicone gasket (Invitrogen: p-24744) with a 1.2 mm hole that is cut with a hole punch, as is shown in Fig. 3.4c. A 3 x 3 mm$^2$ glass cover slip is placed on top of the fluid cell to seal it. The fluid cell can be filled with a pipette. Directly pipetting fluid onto the chip's surface, rather than setting up a microfluidic network, keeps the experimental apparatus flexible, allowing many experiments to be attempted in a short time.

48

The IC / microfluidic chip can be integrated as a component in a larger PDMS or glass based microfluidic system.  Passive microfluidics can couple the outside world, and its macroscopic fluid samples, to the chip in a role that is analogous to the role printed circuit boards play for ICs in computers.  The IC / microfluidic chip could behave as a programmable component to perform tasks such as sorting or combining samples and reagents.  In such a setup, the fluid output of the chip could be fed to output channels of the passive microfluidic device for further processing or collection.

*3.3.2 Electronics*

In this section the electronics surrounding the DEP chip are described. Electronically the chip is effectively a 32 kbit SRAM; As such, the electronics surrounding the chip are identical to the read/write electronics surrounding any SRAM array.  The IC / microfluidic chip is mounted on a standard 84 pin chip carrier as is shown in Fig. 3.4c.  The IC is mounted with silver paint to both electrically ground the substrate of the IC and to create a thermally conductive connection to a thermal reservoir.  Wire bonds connect the IC to the pins of the chip carrier.  In all the chip requires 24 wire bonds, including redundant power lines.  All of the wire bonds are on the same side of the IC to make it easier to protect them from the fluid. The wire bonds can be covered with epoxy to protect them further from the nearby fluid.  However most often the bonds are left unprotected, as the fluid cell is a sufficient barrier between the fluid and the wire bonds.

The chip carrier sits on a custom PCB which connects the IC to the computer, provides power, and connects the IC to an RF voltage source, as is shown in Fig. 3.4d. The PCB has RC filters on each of the inputs and outputs of the chip with a corner frequency $f_{3dB}$ = 100 MHz to protect the chip from voltage spikes. The digital lines connect from the PCB to the computer through a proprietary National Instruments cable (NI: SHC68-68-EPM) to the digital I/O card (NI: PCI-6254). The RF voltage is produced off of the chip and is brought onto the board with a BNC connector. The DEP chip has a power consumption of 0.5-2 W, depending on how many pixels are turned on and the frequency of the RF voltage.

### 3.3.4 Optics

The IC / microfluidic chip sits under a fluorescence microscope, as is shown in Fig. 3.4d. Fluorescence microscopy is a powerful and widely used tool to image biological and chemical systems. (Pawley, 2008) Coupling fluorescence microscopy with the chip enables access to a well developed technique to image the samples and reagents that the chip controls. The silicon substrate of the IC is not optically transparent and so the microscope operates by measuring reflected light. The IC is not fluorescent at optical frequencies and so behaves as a black background. The microscope views the samples through the glass cover slip of the fluid cell.

The microscope apparatus consists of a pillar mounted Olympus BX-52, hovering above the IC / microfluidic chip, as is shown in Fig. 3.4d. Long working distance objectives are used to give enough space for the fluid cell (Olympus: LMPLFL series). The light source is a 100 W mercury lamp. The device is monitored with an

50

Hamamatsu ORCA-ER cooled CCD camera. Images are taken with MicroSuite Basic

Edition (Olympus) and StreamPix digital video recording software (Norpix).

Future devices that utilize IC / microfluidic chips and hope to be portable surely can

not include a laboratory-sized fluorescence microscope. Recent work has shown

that fluorescence microscopy can be performed in microfluidic devices using small

LED light sources and photodiodes. (Psaltis *et al.,* 2006) More forward looking, a

CCD array could be flipped and bonded on top of the IC forming a fluid channel

between the two chips. (Cui *et al.*, 2008 and Henga *et al.,* 2006)

*3.3.5 Thermal Management*

Temperature control is essential for experiments on biological systems. The

temperature of the chip is controlled using heat-sinks. Typical ICs have operational

temperatures between 65°C and 85°C. (Lee *et al.,* 1998) For many biological and

chemical experiments that might be performed on the chip 65°C is far too hot. As

such, steps are taken to control the temperature of the chip.

In the first iteration of thermal management, the ceramic chip carrier sits on top of a

machined copper block with a thin layer of thermal grease (Arctic Silver Inc.: Arctic

Silver). Air is blown with a fan over the large surface area of the copper block's

bottom side. The temperature of the DEP chip's top surface with the chip turned on

is 40°C-50°C compared to 90°C when no heat sink is attached. The chip

temperature is measured with an infrared non-contact temperature sensor (Control

Company 4477).

The second iteration of the heat sink was designed for the HV-DEP / Magnetic

Chip (Chapter 5) and utilizes a water cooler. With water cooling the temperature of

the chip can be controlled by setting the flow rate and temperature of the water

bath. The water cooler is constructed with a machined copper piece that is

connected with a thermally conductive epoxy (Loctite 383 and 7387) to a

commercial CPU water cooler (Danger Den, MC). The top of the copper block is

polished and immediately covered with a thermally evaporated layer of

8 nm Ti / 100nm gold to keep copper oxide from growing. The chip carrier sits on

top of the machined copper block with a thin layer of thermal grease (Arctic Silver).

The water cooler is driven with a submersible pump (Becket Corp, Versa) with a

flow rate of 92 gallons/hour. The HV-DEP / Magnetic Chip (Chapter 5) has

temperature sensors integrated into the IC. The analog output of the sensors can be

placed into a feedback loop with the water-cooler to create a control system to

maintain the chip temperature.
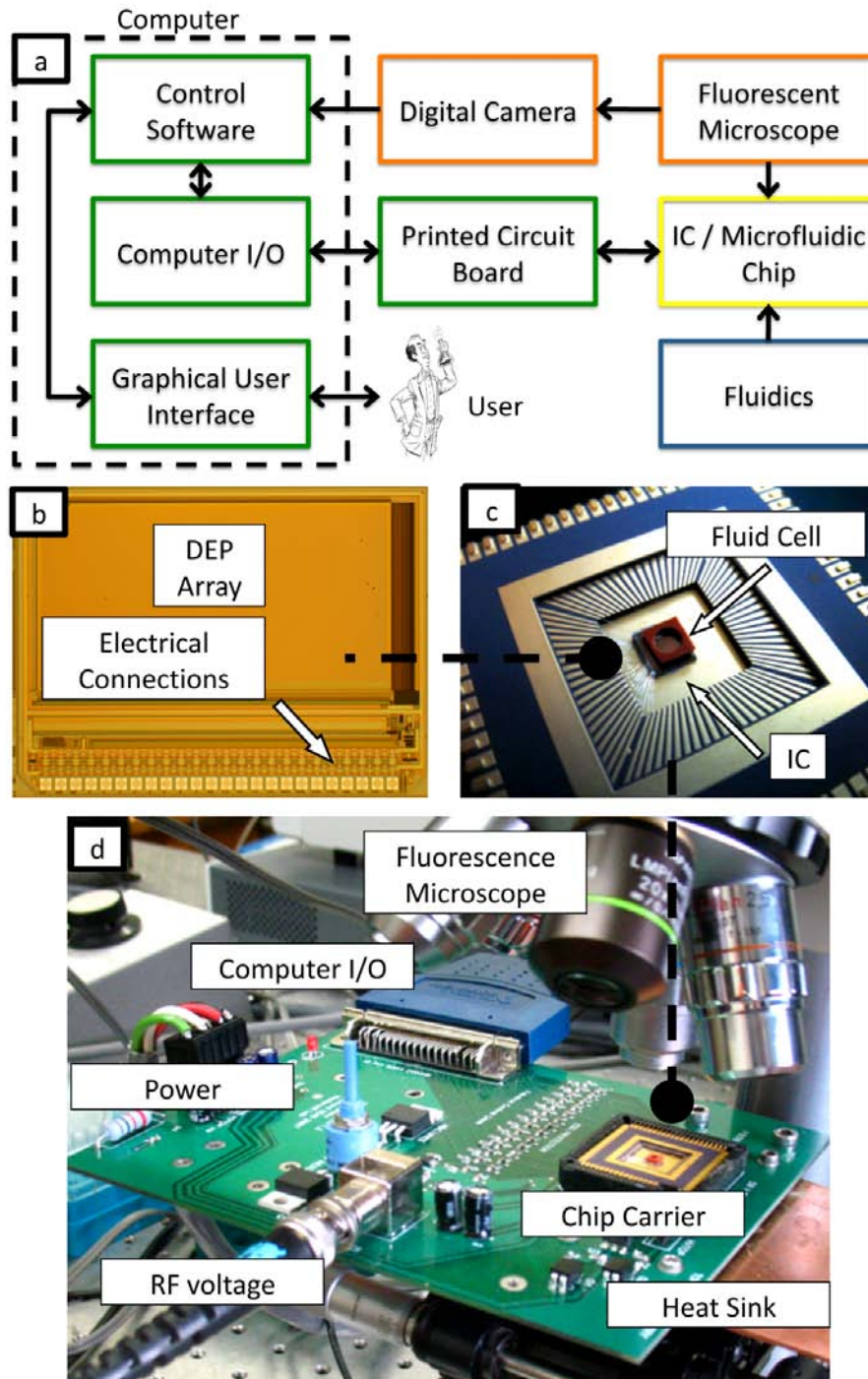
**Figure 3.4.** (a) A schematic of the experimental apparatus surrounding the IC/microfluidic chip. The green boxes represent components that are electrical, blue represent fluidic, orange represent optic, and yellow represents where the components come together, (b) an optical micrograph of the IC (b) 84 pin chip carrier holding the IC, on top of the IC is a red fluid cell, (c) a photograph of the experimental setup of the hybrid IC / microfluidic system.

*3.3.6 Computer Control*

Computer software is used to program and to interface the IC / microfluidic chip with a user. The computer communicates with the chip through a National Instruments PCI board (NI: PCI 6254). The PCI board is controlled with custom Lab View (NI) software. MATLAB (The Math Works) code is used on the front-end to interface with the user and to translate a user's input into the commands that will be sent to the chip. All MATLAB and Lab View code is included in Appendix C.

The GUI that we designed is shown in Fig. 3.5. In the GUI a user can draw objects onto a bit-map that corresponds to the DEP pixel array of the chip. Objects can be created, recognized by the computer, and moved around the screen with a cursor. Basic default shapes can automatically be drawn such as horizontal, vertical, and diagonal lines and checker-board patterns. In addition to the static drawings that can be drawn in the GUI, multi-frame movies, where each frame is a state of the chip, can be imported into a compiler and played on the chip. (Appendix C) To maximize the refresh rate, the code can send commands to write only word-lines in the SRAM array that have changed from frame to frame.

The digital camera on the microscope connects to the computer and is displayed with Streampix (Norpix). Currently, the coordinate system on the video-feed from the digital camera and the GUI is manually aligned by trapping and moving an object and then finding it on the microscope. The combination of image-recognition software and automated control of the microscope stage could be used to remove

the human from the control loop, and allow complex automated tasks such as

sorting to be done in a closed-loop.
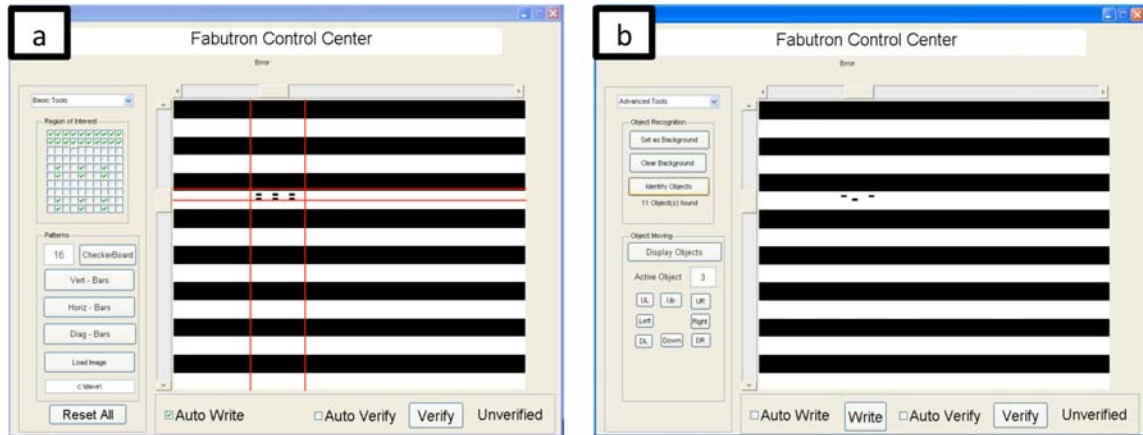


**Figure 3.5.** Screen shots of the GUI, (a) The main screen for the GUI where objects can be drawn on a bit map that represents the state of the chip. The black and white stripes are the arbitrary pattern that is being written to the chip in the screen-shot, (b) the "advanced mode" of the GUI where objects that are created in the main screen can be moved with a cursor.

# Chapter 4. A Hybrid Integrated Circuit / Microfluidic Platform to Control Living Cells and pL Biomimetic Containers

## 4.1 Overview

This chapter describes how the hybrid Dielectrophoresis (DEP) Chip, introduced in Chapter 3, can be used to perform biology and chemistry experiments. The DEP chip simultaneously controls many individual living cells and small volumes of fluid. The small volumes of fluid are contained in pL sized lipid vesicles which provide a stable container for aqueous solutions that can be suspended in water. The vesicles can be moved around the chip, fused together, and have their contents released into the solution. Living cells can also be moved around the chip and can be electroporated to allow substances from the solution to enter the cells. In addition, the chip can controllably mechanically deform the cells or vesicles. These basic functions, which are demonstrated in this chapter, can be strung together to perform complex biological and chemical laboratory tasks.

Previous work has been done to use hybrid integrated circuit (IC) / microfluidic chips for biology and chemistry experiments. Tom Hunt's thesis describes hybrid chips being used to trap and move drops of water suspended in oil. (Hunt, 2007) The DEP Chip can position the drops, splits the drops in two, and merges two drops together, demonstrating a potential platform for performing programmable chemistry experiments. (Hunt, 2007 and Hunt *et al.,* 2008) In these emulsion-based

systems, drops of water are suspended in oil and are stabilized using a surfactant, as is shown in Fig. 4.1. (Holtze *et al.,* 2008)  Drop based microfluidic chips have been shown to be important technology for performing high-throughput biological and chemical experiments.  (Koster *et al.,* 2008) A challenge for these systems, however, is that cells must also be encapsulated in drops because the oil-based continuous phase is not biocompatible.  In addition, molecules with hydrophobic tails can leak from inside the vesicles into the oil, thus limiting the chemistry that can be done in these systems. (Hunt, 2007 and Holtze *et al.,* 2008)

In this chapter a versatile platform is developed for biology and chemistry experiments on the DEP chip.  This platform can simultaneously control both living cells and small isolated volumes of fluid suspended in water.  In Section 4.2.1 the functionality and capabilities of the DEP Chip are reviewed.  To package small volumes of fluid, such that they can be suspended in water, inspiration is taken from cellular biology.  The preparation of the vesicles used in this chapter is described in Section 4.2.2.  Lipid vesicles, drops of water surrounded by a thin phospholipid bilayer membrane, are commonly used in cells to package substances for intercellular transport, to store enzymes, and to create isolated chemical reaction chambers. (Alberts *et al.,* 2007)  Artificially produced unilamellar vesicles mimic natural vesicles and provide robust pL containers that are impermeable and stable for a wide range of salinity, pH, and other environmental conditions. (Tresset *et al.,* 2007)  A schematic of a phospholipid vesicle is shown in Fig. 4.1.  This chapter demonstrates the use of unilamellar vesicles as a robust pL container for fluids on the DEP Chip.

The frequency dependence of the dielectric properties of vesicles and cells enable the dielectric phenomenon used in this chapter to be independently accessed with electric fields at different frequencies.  Voltages at MHz frequencies are used for DEP, to trap, position, and deform cells and vesicles as is described in Section 4.2.3.  Voltage pulses with ms pulse-widths are used for electroporation and electrofusion, to trigger the release of the contents of vesicles, fuse two vesicles together, and permeablize the membranes of cells as is described in Section 4.2.4.

The DEP Chip is used in this chapter demonstrate basic functions on living cells and unilamellar vesicles, which can be strung together to perform complex biological and chemical laboratory tasks.  In Section 4.3.1 the DEP Chip is used to simultaneously and independently trap and move many individual vesicles and living cells with dielectrophoresis (DEP).  In Section 4.3.2 voltages pulses created by the DEP Chip are used to selectively electroporate vesicles to release their contents, fuse two vesicles together, and permeabilize living cells.  In Section 4.3.3 vesicles are deformed by changing the shape of the DEP traps.  The platform demonstrated in this chapter can be used for a wide range of chemical and biological applications and is a step forward for the field of hybrid IC / microfluidics.
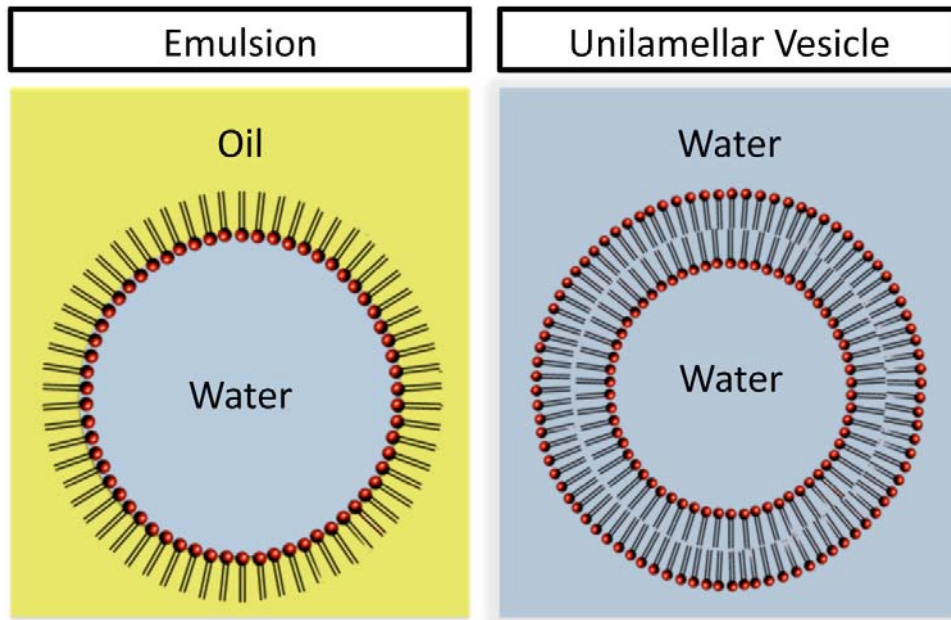
**Figure 4.1.** A schematic representation of a water drop in oil emulsion stabilized with surfactants is shown on the left. A schematic representation of a unilamellar vesicle is shown on the right. The phospholipid molecules that form the surfactant and the vesicle membrane are shown with red circles for the hydrophilic heads and black lines for the hydrophobic tails.

**4.2  Methods**

*4.2.1  The Hybrid Integrated Circuit / Microfluidic Platform*

In this section the DEP Chip, which is described fully in Chapter 3, is used to control living cells and small volumes of fluid using spatially patterned electric fields.  Here, the DEP chip and its capabilities are summarized.  The hybrid chip consists of a microfluidic chamber built directly on top of an IC.  The IC consists of an array of electrodes, each of which can be driven with an RF voltage to spatially pattern the electric field magnitude above the chip's surface.  Underneath each pixel is a static random access memory (SRAM) element.  The state of the SRAM element determines whether the pixel is driven by the external RF voltage source (the pixel turned 'off') or by the logical inverse of the RF voltage (the pixel turned 'on').  The array consists of 128 x 256 (32,568) 11 x 11 $\mu m^2$ pixels, each of which can be driven with an RF voltage with a bandwidth from DC – 11 MHz.  The entire array of pixels can be updated hundreds of times in a second. A micrograph of the IC / microfluidic chip is shown in Fig. 1.1b.

*4.2.2 Unilamellar Vesicles*

Lipid vesicles are drops of water encapsulated by a thin phospholipid bilayer membrane.  A schematic of the cross-section of a phosphlipid unilamellar vesicle is shown in Fig. 4.1. The phospholipid membrane consists of amphipathic phospholipids that self-assemble into bilayers such that their hydrophilic heads face the inside and outside of the vesicle, providing a robust container for aqueous

60

solutions. (Alberts *et al.,* 2007)  A unilamellar vesicle consists of a single bilayer membrane, as opposed to several as some vesicles do.

The vesicles are made through collaboration with Thomas Franke at University of Augsburg in Germany.  The vesicles are prepared with liposome electroformation using a modification of the Angelova Method. (Angelova *et al.,* 1986)  The recipe used to create the vesicles is as follows.  Briefly, a small amount of lipid in chlorophorm (ca. 20 microliter of a 5 mg/ml solution) is deposited onto two indium-tin-oxide coated glass slides. After evaporation of the organic solvent for at least 6 hours the slides are assembled in parallel with a separating 2 mm teflon spacer to form the preparation cell and incubated for one hour in a saturated water vapor at room temperature for prehydration.  Subsequently, the electroformation cell is filled with 200 mOsm aqueous solution (50 mM sodium chloride and sucrose) and a low frequency electric field of 500 Hz and amplitude 1 V/mm is applied to the ITO-slides.  After approximately 8 hours lipid vesicles of diameters larger the 20 μm are harvested.  The external salty solvent is removed by repeatedly washing with an iso-osmotic aqueous glucose solution and gentle centrifugation at low rotation frequencies. This procedure provides the dielectric contrast necessary for DEP actuation and still ensures the integrity of the vesicle containers.

### 4.2.3  Dielectrophoresis (DEP) of Vesicles Suspended in Water

The hybrid chip uses positive DEP to trap and move cells and vesicles suspended in water.  Any object that has a complex permittivity that is different than the surrounding medium can be controlled using DEP, (Jones, 1995) as is described in

detail in Chapter 2.  By shifting the location of the DEP Chip's pixels that are turned

on, the location of local electric field maxima are moved around the array.  In

Fig. 3.1a quasi-static finite element simulations (Ansoft: Maxwell 3D) are shown of

the electric field magnitude $\left|\vec{E}\right|$ 5 μm above the chip's surface. Two pixels are set to

5 V and the rest are set to 0 V.   A vesicle with a radius $a$ = 5 μm is shown being

pulled towards the maximum of the field.  The simulations show that a vesicle

experiences a maximum electric field strength $\left|\vec{E}\right| \approx 0.5 \ V/\mu m$.

The dielectrophoretic response of vesicles can be controlled by setting the salinity of

the solution inside the vesicle $\sigma_{int}$ relative to the conductivity of the solution on the

outside of the vesicle $\sigma_{sol}$, as is described in full detail in Chapter 2.  In Fig. 2.3b a

plot of the Clausius-Mosotti (CM) factor, a measure of the difference in permittivity

of the object and the medium, is shown *versus* the interior conductivity of an

$a$ = 5 μm vesicle suspended in a deionized solution with a conductivity of

$\sigma_{sol}$ = 10$^{-3}$ S/m.  If the conductivity inside the vesicle is greater than $\sigma_{int}$ > 10$^{-2}$ S/m

then the CM factor is positive, and the vesicle can be trapped and positioned with

positive DEP.

The dielectrophoretic response of cells and vesicles is a function of the frequency of

the applied electric field.  In Fig. 2.3c a plot of CM *versus* frequency is shown for a

vesicle with interior conductivity $\sigma_{int}$ = 50 mS/m.  Below a cut-off frequency of

$\omega_d$ = 50 MHz and above a cut-off frequency of $\omega_{mem}$ = 2 kHz, the CM factor is positive

and invariable to changes in frequency.  It is in this frequency band that positive

DEP is used in this chapter.  The high frequency cut-off is set by the dielectric

relaxation time $\tau_d = \varepsilon_p/\sigma_{int}$ of the solution inside the vesicle. The low frequency cut-off is set by the charging time of the membrane of the vesicle $\tau_{mem} = aC_{mem}(1/\sigma_{int}+1/\sigma_{sol})$.

### 4.2.4 Electroporation and Electrofusion

Voltage pulses created by the chip can be used to electroporate and electrofuse vesicles and cells, as is explained in full detail in Chapter 2. Electroporation generally occurs when there is a transmembrane voltage $V_{TM} > 1V$. (Sugar *et al.,* 1987) The maximum voltage induced across a membrane $V_{TM}$ of a spherical vesicle or cell in an external electric field is given by Eq. 2.8. The characteristic charging time of the membrane is given by the expression: (Jones, 1995)

$$\tau_{mem} = aC_{mem}(\frac{1}{\sigma_{int}} + \frac{1}{2\sigma_{sol}})$$

**4.1**

where $C_{mem} = 10^{-2}$ F/m$^2$ is the specific membrane capacitance of a unilamellar vesicle. (Jones, 1995) For a vesicle with a radius $a$ = 5 μm and internal conductivity $\sigma_{int}$ = 0.1 S/m in a solution with conductivity $\sigma_{sol}$ = $10^{-2}$ S/m, there is a membrane charging time $\tau_{mem}$ = 20 ms. Electric fields with frequencies $1/\omega < \tau_{mem}$ are used for DEP. At the $f$ = 1 MHz frequencies used for DEP the transmembrane voltage $V_{TM} \approx 10$ mV and no damage is caused to the membrane. (Alberts *et al.,* 2007 and Grosse *et al.,* 1992) Electric fields created with voltage pulses with a pulse width $\tau > \tau_{mem}$ create transmembrane voltages $V_{TM} \sim 1V$ and are used to electroporate and electrofuse vesicles and cells.

The ability to selectively electroporate vesicles enables the chip to locally release

substances into the solution. This local release of substances creates a gradient in

the concentration as a function of the distance $r$ from the center of the vesicle.

Consider a vesicle with a radius $a$ filled with a concentration n = $n_s$ of a substance

suspended in a solution that has none of the substance n = 0. The gradient in the

concentration is calculated by solving the diffusion equation in spherical

coordinates around the vesicle with the boundary conditions that the concentration

n = $n_s$ a distance r = $a$ from the center of the vesicle and n = 0 at a distance r = ∞.

(Dill and Bromberg, 2003) The solution to the diffusion equation is plotted for a

vesicle with radius $a$ = 5 μm in Fig. 4.2a and is given by the expression:

$$n(r) = \frac{n_S a}{r}.$$

4.2

When a cell or vesicle is electroporated, such that a reaction occurs at the

membrane's surface, a concentration gradient is also created. Consider a

reaction that occurs at the membrane surface with a reagent in the solution that

has a bulk concentration $n_\infty$. In this case, the concentration at the surface

disappears because it is consumed by the reaction, and the concentration at an

infinite distance away is that of the bulk concentration. The boundary conditions

are then that n = $n_\infty$ at a distance r = ∞ form the center of the vesicles and n = 0 at

a distance r = a. The solution to the diffusion equation is plotted for a vesicle

with radius $a$ = 5 μm in Fig. 4.2b and is given by the expression:

$$n(r) = n_\infty (1 - \frac{a}{r})$$

4.3

The concentration gradients depend only on the concentration of the substances, the radius of the vesicle, and the distance from the vesicle. The ability to create well-controlled concentration gradients in the solution is a tool that can be used for delivering reagents and samples to cells or to other reagents for chemistry and biology experiments on the chip.

The voltage pulses used for electroporation can be time-multiplexed with the voltages used for DEP. This is possible because during the duration of the ms voltage pulses, during which the DEP force is turned off, cells or vesicles do not diffuse a substantial amount. A particle suspended in a solution takes $\tau_{\text{diff}} = L^2/16D$ to diffuse the distance of half of a pixel length $L/2$, as is explained in Chapter 3. The time that it takes for a particle with a radius $a$ = 1 µm suspended in water to diffuse $L/2$ = 5 µm is $\tau_{\text{diff}} \approx 1$ sec, which is much longer than the time that the DEP trap is turned off. The diffusion time $\tau_{\text{diff}}$ is even larger for bigger particles.

Electric field pulses can also be used trigger the fusion of vesicles, as is explained in full detail in Chapter 2. The model for electrofusion is a multi step process. Two vesicles are brought into tight contact with DEP. Electric field pulses are then used to induce a transmembrane voltage across the contact area of the two vesicles. The transmembrane voltage causes electroporation on the contact-area, and if the pore density is large enough then the pores nucleate and the vesicles fuse. (Sugar *et al.,* 1987) On the chip, voltages at MHz frequency are used to hold the vesicles in contact with DEP while time-multiplexed electric field pulses are used to trigger the fusion.
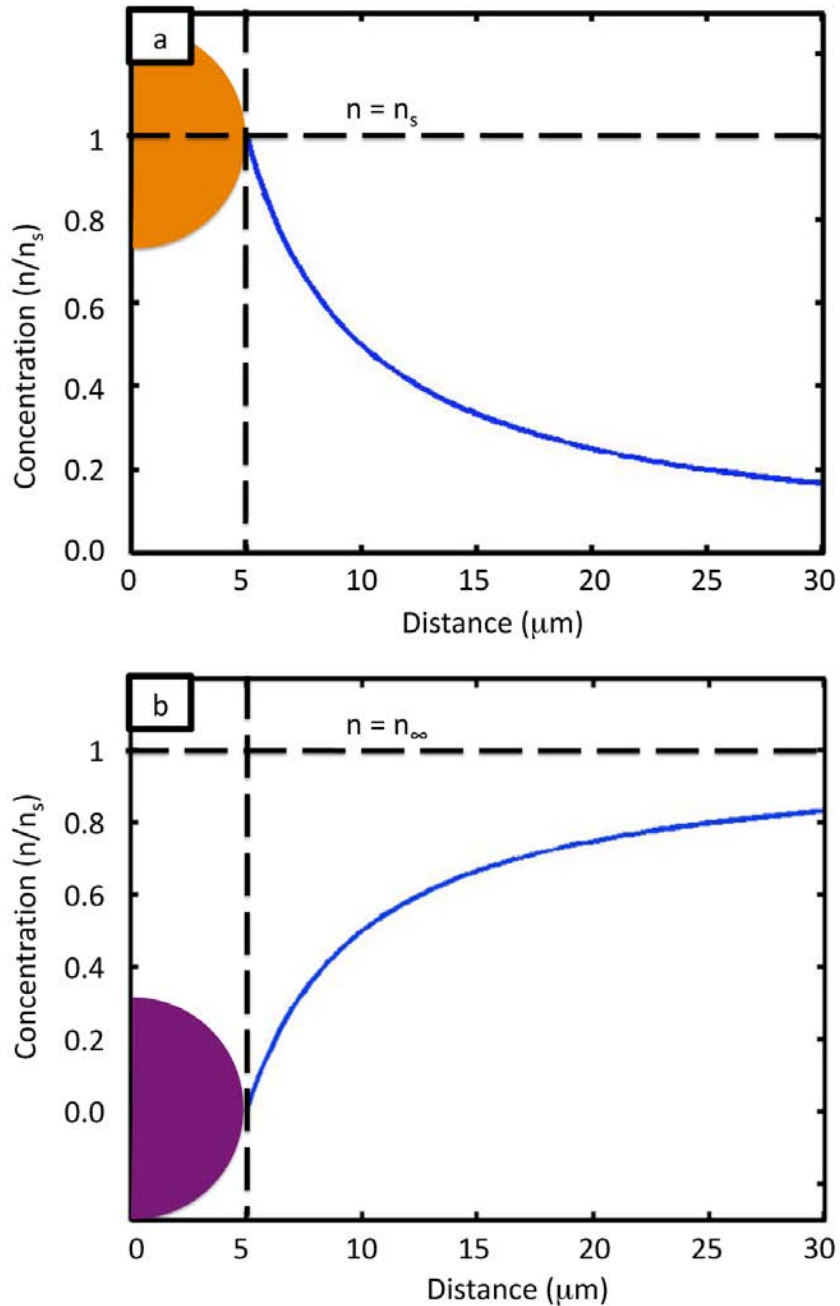
**Figure 4.2** (a) A plot of the concentration gradient created around a vesicle, shown as the orange circle, that is releasing a substance at its surface, (b) a plot of the concentration gradient created around a vesicle or cell, shown as the purple circle, that is reacting with a substance in the solution at its surface.

## 4.3 Demonstrations

### 4.3.1 Trapping and Moving

In this section it is shown how the hybrid IC / microfluidic chips can trap and move
individual vesicles and cells, both suspended in water, along arbitrary paths.
Figure 4.3a shows how individual vesicles can be independently trapped and moved
along independent paths. Figure 4.3a (i) shows three vesicles that are
independently trapped on the chip with DEP. In Fig. 4.3a (i-iii) the vesicle on the left
is brought between the two other vesicles at 70 μm/sec. In Fig 4.3a (iv-vi) the
vesicle on the bottom is moved upwards, positioning the vesicles into a triangle.
This demonstration shows that the DEP Chip can independently control several
objects at once, enabling complex experiments to be performed in parallel on the
hybrid chip.

Figure 4.3b shows how the hybrid IC / microfluidic chip can simultaneously trap
and move many vesicles. In Fig. 4.3b hundreds of vesicles are simultaneously
positioned into an 'H', demonstrating that the chip can control the position of many
vesicles at once. To accomplish this, many DEP pixels are turned 'on' to spell 'H' and
the vesicles sediment onto the interface of the pixels that are turned 'on' and those
that are turned 'off'. This demonstration shows that the DEP Chip is capable of
simultaneously controlling many individual objects.

Figure 4.3c shows how the hybrid IC / microfluidic chip can simultaneously trap and
move both vesicles and living cells that are suspended in water. Yeast cells are

cultured overnight in YPD broth (BD Inc.) at 37°C, and then resuspended in a 250 mM glucose solution.  Figure 4.3c shows a vesicle and a budding yeast cell trapped on the chip.   The fluorescence image of the rhodamine filled vesicle is superimposed onto the brightfield image of the yeast cells and is colored red.  In Fig. 4.3c (ii) the vesicle is moved upwards while the cell is trapped in place.  In Fig. 4.3c (iii) the yeast cell is moved to the left while the vesicle is held in place.  In Fig. 4.3c (iv) the yeast cell is moved downwards as the vesicle is simultaneously moved to the left.  This demonstration shows that the DEP Chip can simultaneously control cells and small volumes of fluid held in vesicles, both suspended in water.  This enables biological and chemical experiments to be performed on the hybrid chip that use both cells and small compartmentalized volumes of fluid.
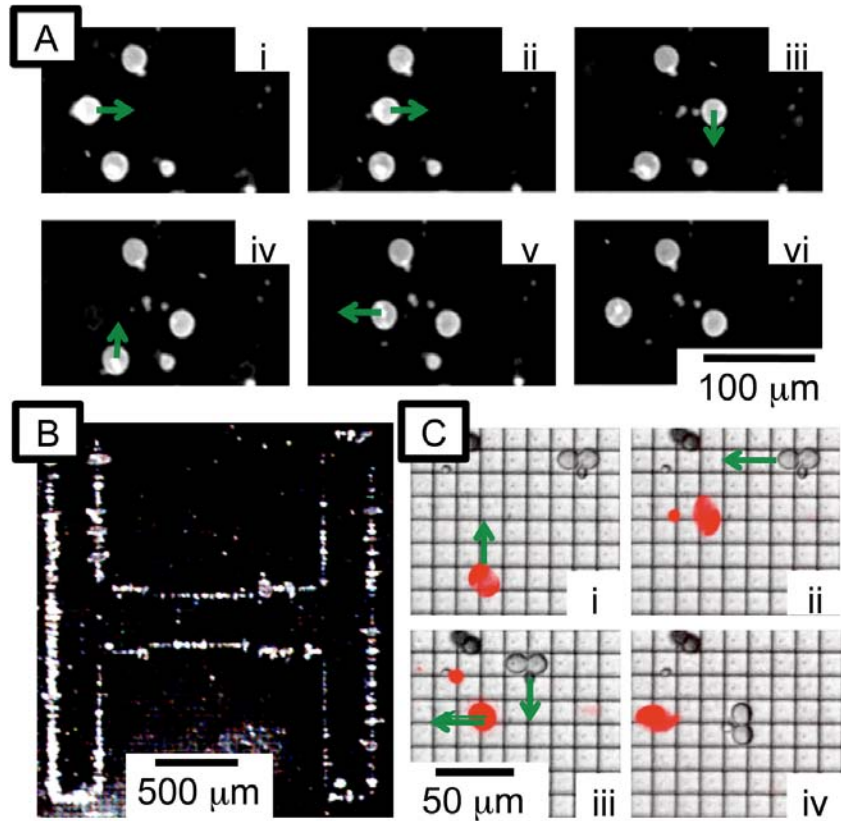
**Figure 4.3** (a) Time sequence of vesicles positioned with DEP. Pixels are turned on in sequence to trap and move the vesicles. The green line shows the direction that the chip moves the vesicle. The maximum speed of a vesicle is 70 µm/sec. Each frame is separated by ~1 sec, (b) a micrograph of hundreds of vesicles simultaneously positioned to spell an 'H,' (c) time sequence of vesicles and cells simultaneously trapped and moved on the chip. The fluorescence image of the vesicles is superimposed onto the brightfield image of the cells and is colored red. The green line shows the direction that the chip is moving the vesicles or cells. Each frame is separated by ~1 sec.

### 4.3.2 Triggered Release of the Contents of Vesicles

In this section it is demonstrated that the hybrid IC / microfluidic chips can controllably release the contents of vesicles. Figure 4.4a shows how the hybrid IC / microfluidic chip can controllably release the contents of a vesicle into the surrounding solution while holding it in place with a DEP trap. Figure 4.4a shows a vesicle filled with 4 mM NaCl solution suspended in a concentrated fluorescently self-quenched fluoroscein solution. A 1 ms electric field pulse, that is time multiplexed with the DEP fiel, and repeats every 5 ms, is turned on at time $t = 0$ sec. The vesicle is electroporated and the concentrated fluoroscein mixes with the solution in the vesicle causing the vesicle to fluoresce. After $\Delta t = 8$ sec the pulse sequence is turned off and the vesicle is held in a DEP trap for $\Delta t = 2$ minutes. The vesicle maintains its fluorescence, demonstrating that when the pulses are turned off the vesicle heals it self and stops mixing with the solution. After $\Delta t = 2$ minutes the pulse sequence is turned on until the concentration of fluoroscein inside the vesicle matches that of the solution and the vesicle ceases to fluoresce. This demonstration shows that the chip can use electroporation to controllably mix the contents of vesicles with the solution. Electroporation of vesicles can be used to form chemical gradients in the solution surrounding the vesicle or to allow substances in the solution to mix with the contents of the vesicle.

### 4.3.3 Electroporation of Cells

In this section it is demonstrated how the hybrid IC / microfluidic chips can permeabilize a cell's membrane, allowing substances in the solution to enter the cell.

Figure 4.4b shows an individual yeast cell held in place with DEP and selectively electroporated, allowing substances in the solution to enter the cell. Yeast cells are cultured overnight in YPD broth (BD Inc.) at 37 °C and resuspended in 250mM glucose solution. A 0.4% solution of the viability stain, Trypan Blue, is added to the suspended cells. When Trypan Blue enters a cell it stains it blue. In Fig. 4.4b a yeast cell is held in place with DEP. Because the cell is healthy, Trypan Blue does not enter the cell and the cell does not turn blue. A 1ms pulse that repeats every 5 ms, that is time multiplexed with the DEP field, is turned on at $t = 0$. After $\Delta t = 40$ sec the cell is observed to turn dark blue, as is shown in a grayscale image in Fig. 4.4b. The ability to electroporate cells on the chip enables substances in the solution to be controllably introduced into selected cells. This functionality could be used to introduce substances such as molecular probes, DNA, or drugs into select cells.

### 4.3.4 Triggered Fusion of Vesicles

In this section it is shown how the hybrid IC / microfluidic chip can fuse two vesicles together and mix their contents. Figure 4.4c shows two vesicles that are brought into contact with DEP and then fused together with electrofusion. In Fig. 4.4c (i) two vesicles are brought into contact with DEP. In Fig. 4.4c (ii) the vesicles are brought into tight contact with DEP, creating a large contact area between the two vesicles. In Fig. 4.4c (iii) a 1 ms pulse that repeats itself every 5 ms, multiplexed with the DEP field, is turned on for 0.5 sec causing the two vesicles to fuse into one. The vesicle is stretched into the shape of the DEP trap. In Fig. 4.4c (iv) the trap is turned off and the fused vesicle relaxes into a spherical shape.

The fusion of two vesicles allows pL volumes of samples to be controllably mixed. The voltage pulses used to fuse the vesicles do not lead to an appreciable mixing of the contents of the vesicle with the solution. The vesicles are observed to fuse after 0.5 sec of the pulse sequence. In the experiment shown in Fig. 4.4a, it takes ~4 sec for a similar vesicle to have appreciable mixing with the outside solution using the same pulse sequence. Therefore in the time that it takes to fuse the vesicles there should not be appreciable mixing of the vesicles with the solution. The ability to selectively fuse two vesicles together enables small isolated volumes of samples to be mixed on the chip, an important function for performing chemistry and biology experiments.
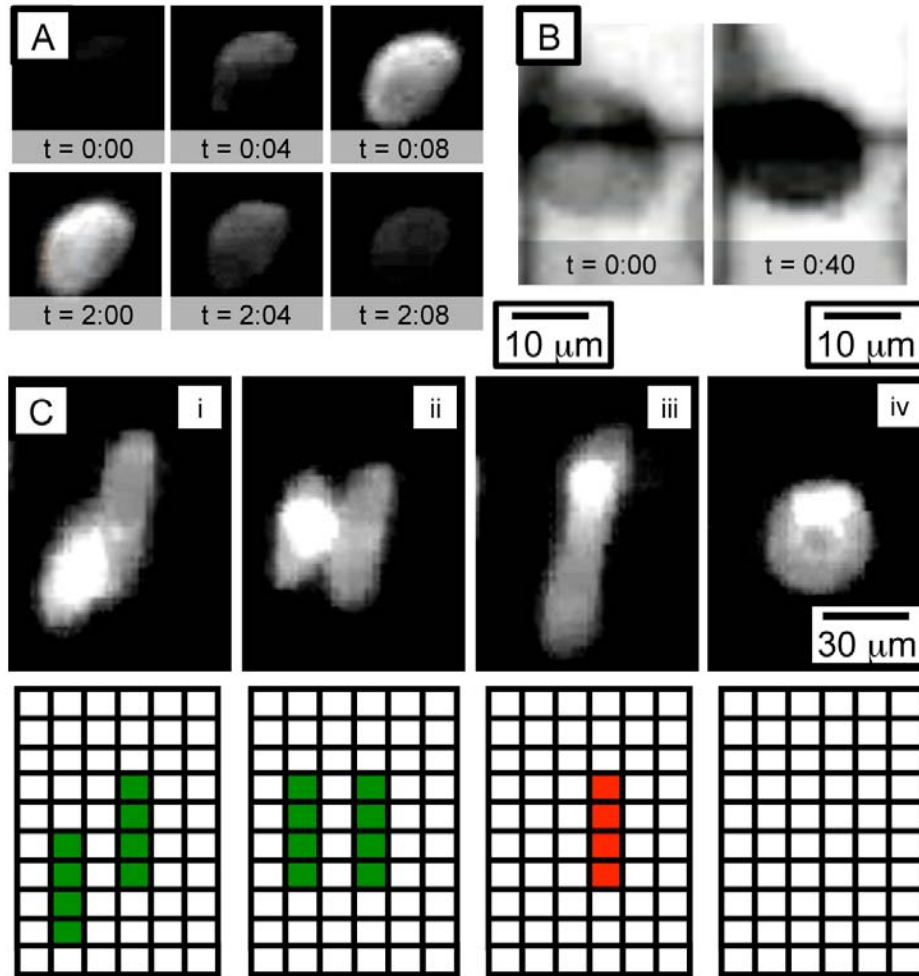
**Figure. 4.4** (a) Time sequence of a vesicle held in place with DEP fields while its contents are released into the solution with electroporation. The vesicle is suspended in a concentrated fluoroscein solution. The electroporation cause the vesicle to mix its contents with the solution, making the vesicle to fluoresce. In the first three frames, each separated by 4 seconds, the vesicle is electroporated. The vesicle is held in a DEP trap for 2 minutes. In the next three frames, separated by 4 seconds, the vesicle is electroporated until the contents of the vesicle fully mixes with the solution and the vesicle stops fluorescing, (b) a cell is held in place with DEP and electroplated in a solution containing Trypan Blue stain. The left and right frame show the cell before electroporation and after 40 sec. of electroporation, respectively, (c) two vesicles are brought into contact with DEP and then fused together with electrofusion. The schematic on the bottom show which pixels are turned on. A green pixel indicates a pixel that is turned on for DEP and a red pixel indicates a pixel that is turned on with voltage pulses multiplexed with the MHz frequency voltage.

*4.3.5  Deforming Vesicles with Dielectrophoresis*

In this section it is shown how the hybrid IC / microfluidic chip can controllably

deform objects.  Figure 4.5 shows how changing the shape of the DEP traps can

deform vesicles.  Several DEP pixels are turned on underneath a vesicle, causing the

vesicle to be deformed into the shape of the DEP trap.  The left column of Fig. 4.5

shows a map of which pixels on the chip are turned on.  The middle column shows

simulations (Ansoft: Maxwell) of the electric field generated 5 μm above the chip's

surface.  The right column shows micrographs of vesicles deformed in the DEP trap.

The same vesicle is used for each demonstration.  In Fig. 4.5a the vesicle is held in a

simple trap of 4 pixels and the vesicle's cross-section is circular.  In Fig. 4.5b the trap

is spread into two displaced bars, and the vesicle is pulled into an oblong shape.

More complicated pixel patterns lead to shapes such as diamonds in Fig. 4.5c,

hexagons in Fig. 4.5d, and squares in Fig. 4.5e.  The ability to deform vesicles using

DEP traps is an important proof-of-concept for performing rheology and for

controlling the mechanical environment of objects on the chip. (Riske *et al.,* 2006)

This technique could be especially useful in future chips, that have smaller pixel

sizes, for controlling the mechanical environment of living cells. (Wang *et al.,* 1994)
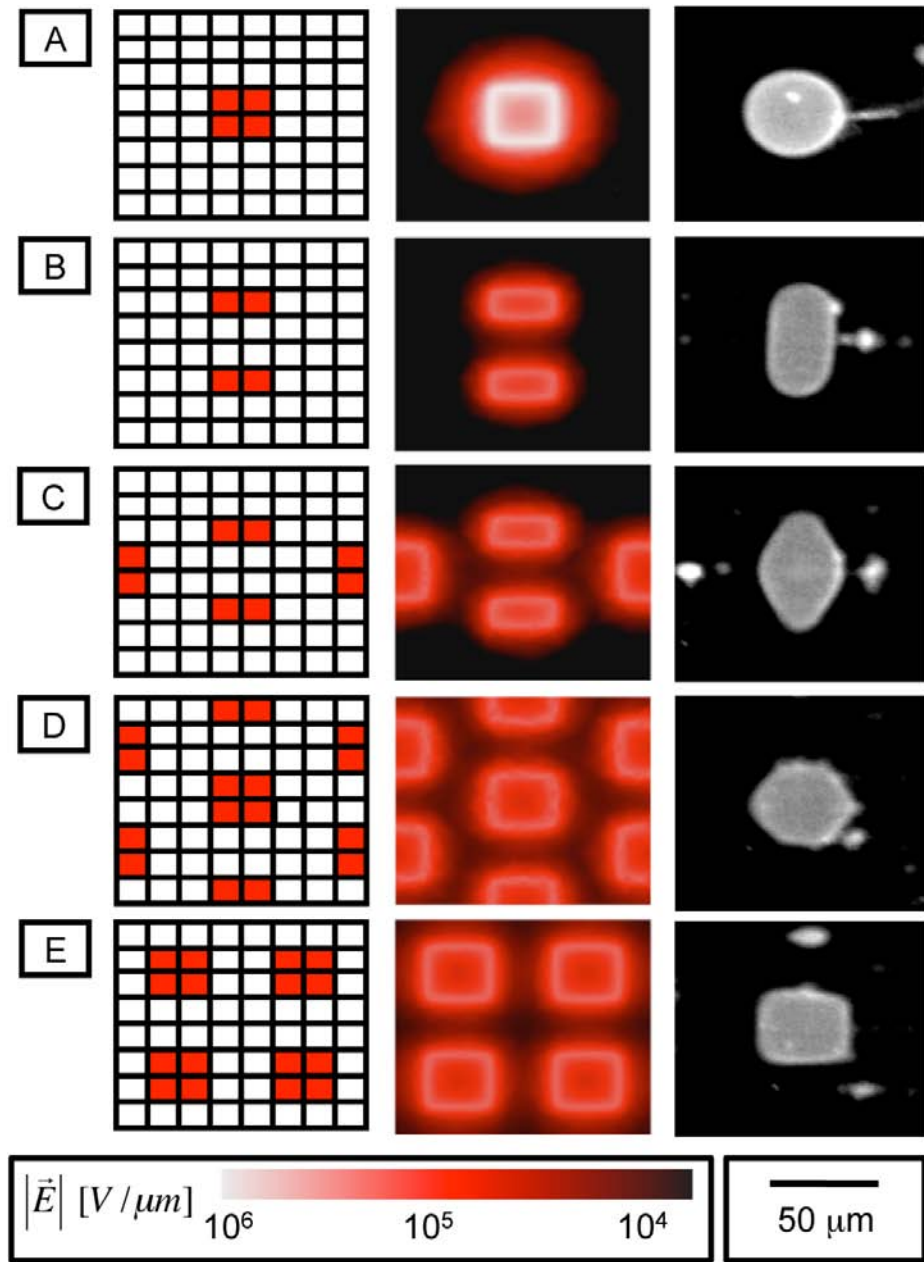
**Figure 4.5** Vesicles are deformed into a variety of shapes by changing the shape of the DEP trap. The schematics on the left show which pixels are turned on. Red and white pixels indicate pixels that are turned on or off, respectively. The center graphics are plots of the simulated electric field strength $|\vec{E}|$ 5 μm above the chip's surface. On the right are micrographs of the deformed vesicles.

## 4.4 Discussion

The platform that is presented in this chapter takes advantage of the capabilities of ICs and the properties of unilamellar vesicles to make a versatile platform for biological and chemical experiments on a chip. This chapter has demonstrated a platform that can trap, move, deform, fuse, and locally release the contents of pL volume vesicles suspended in water. On the same chip, at the same time and in the same solution, the platform can trap, move, and permeabilize living cells suspended in water. This platform provides an important step forward for performing biological and chemical experiments on a hybrid IC / microfluidic chip by demonstrating functions that are important building blocks for more complex tasks.

To move this laboratory-on-a-chip platform from the laboratory into a portable, inexpensive tool for biological and chemical testing, further functionality must be included. For instance, while the platform can perform complex operations on many vesicles and cells, the samples themselves are prepared on laboratory bench equipment and then pipetted onto the chip. Integrating the hybrid chip into a complex microfluidic network, where sample preparation could be performed, could solve this problem. Another hurdle for the hybrid chip is that it is connected to large, laboratory sized equipment, such as a fluorescence microscope and a desktop computer. Further integration of tasks into the hybrid chips such as local temperature control, (Issadore *et al.,* 2009) NMR sensors, (Lee *et al.,* 2008) measurement of eletrogenic cells, (DeBusschere *et al.,* 2001) and integrated

optics (Cui *et al.,* 2008) would open up more applications and lead to a more

versatile and self-sufficient platform. (Lee *et al.,* 2007)

# Chapter 5. Hybrid Magnetic and Dielectrophoretic IC / Microfluidic Chip

## 5.1 Overview

This chapter describes the development of a hybrid integrated circuit (IC) / microfluidic chip that uses both dielectrophoresis (DEP) and magnetic forces to control living cells and small volumes of fluid.  The chip that is presented is called the High Voltage Dielectrophoresis / Magnetic Chip (HV-DEP Chip, Fabutron 2.0). The hybrid chip is fabricated using a special high voltage IC process that enables DEP forces that are roughly 100x as strong as those demonstrated on the DEP Chip in Chapter 3.  A micrograph of the HV-DEP / Magnetic Chip is shown in Fig. 5.1a. The combination of both DEP and magnetic forces on the same chip expands the capabilities of hybrid IC / microfluidic technology, as is demonstrated in this chapter.

The HV-DEP / Magnetic Chip is similar to the DEP Chip described in Chapter 3, but includes additional functionality.  The IC includes an array of pixels that can each be addressed with a radio frequency (RF) voltage to locally apply DEP forces, a matrix of wires that runs underneath the DEP pixel array to apply local magnetic forces, and integrated sensors to locally report the temperature of the chip. The large array of DEP pixels, magnetic wires, and temperature sensors are controlled using static random access memory (SRAM) and logic that are built into the IC.  Figure 5.1a shows a micrograph of the IC.

Previous hybrid chips have been developed to control living cells and drops of fluid using electric or magnetic fields. Chips have been developed to simultaneously control the position of individual pL drops of fluid (Hunt *et al.,* 2008) and living cells (Manaresi *et al.,* 2003 and Hunt *et al.,* 2008) using dielectrophoresis (DEP) for biological and chemical experiments on a chip as is shown in Chapter 4. Chips have also been developed to create local, programmable magnetic fields using matrixes of wires (Lee *et al.,* 2004) and arrays of coils (Lee *et al.,* 2006) to control cells and biological objects implanted with magnetic nanoparticles. Magnetic actuation of nanoparticles has been used to apply precise mechanical stresses on cell membranes, (Berry *et al.,* 2003) manipulate and activate individual mechanically sensitive ion channels and surface receptors on specific cells, (Dobson *et al.,* 2008) and to trap and sort cells and other magnetically tagged objects. (Berry *et al.,* 2003)

This chapter demonstrates the HV-DEP / Magnetic Chip use its DEP pixel array to position pL volumes of fluid encapsulated in lipid vesicles in Section 5.3.1, use its magnetic matrix to position magnetic beads in Section 5.3.2, and use its DEP pixel array and magnetic matrix together to deform microscopic objects implanted with magnetic nanoparticles in Section 5.3.3. Unilamellar vesicles are used as biologically inspired pL containers for fluids that are impermeable and stable for a wide range of salinity, pH, and other environmental conditions, as is described in Chapter 4. (Chiu *et al.,* 1999 and Tresset *et al.,* 2007)

## 5.2 Description of the Chip

*5.2.1 Field Simulations*

The chip creates electric fields above its surface with a 60 x 61 pixel array of

30 x 38 $\mu m^2$ electrodes that can be individually addressed with 50 V peak-to-peak

voltages at frequencies from DC to 10 MHz. The pixels are separated from one

another by 0.8 $\mu m$.   In Fig. 5.1b the results of quasi-static finite element simulations

(Maxwell 3D, Ansoft) of the electric field are shown.  Two pixels are held at 50 V

relative to the surrounding pixels.  The electric field is plotted 5 $\mu m$ above the chip's

surface.  The maximum magnitude of the electric field is $\left|\vec{E}\right| = 3 \ V/\mu m$.

The chip uses electric fields to trap and move dielectric objects, such as cells or pL

volumes of fluid, with DEP. (Manaresi *et al.,* 2003 and Hunt *et al.,* 2008) A spherical

object in an electric field $\vec{E}$ will experience a force given by Eq. 2.3 (Jones *et al.,*

1995)  For an object with a radius $a$ = 5 $\mu m$ with the dielectric properties of a living

cell or vesicle suspended in deionized glucose solution, a $\left|\vec{F}\right| \approx 1 \ nN$ force pulls the

object towards the activated pixels from a location one pixel-length away.  A vesicle

filled with saline solution has dielectric properties similar to that of a living cell in

electric fields at MHz frequencies, and thus behaves similarly in the DEP field. (Chiu

*et al.,* 1999)

Beneath the DEP pixels is a magnetic grid that consists of 60 wires that run

horizontally and 60 wires that run vertically across the chip, which are used to form

a magnetic field above the IC's surface. The wires can be individually sourced with

±120 mA or 0 mA.  Fig. 5.1c shows the results of quasi-static simulations 5 $\mu m$ above

the chip's surface. Two wires that run in perpendicular directions across the chip are driven with120 mA and all other wires are not driven with current. The maximum magnitude of the magnetic field is $\left|\vec{B}\right|$ = 6 mT.

The chip uses magnetic fields to trap and move objects with magnetic susceptibility different than the surrounding medium. A spherical object in a magnetic field $\vec{B}$ will experience a force given by Eq. 2.12. On the chip an iron oxide bead with a radius $a$ = 1 μm (Bioclone: FF102) will experience a 10 pN towards the maximum of the magnetic field, which exists where the two activated wires intersect. Objects can be trapped and moved along arbitrary paths by changing the location where the activated wires cross. Current can be driven through several wires in the array simultaneously to create more than one field maximum, allowing the chip to trap and move many magnetic objects independently. (Lee *et al.,* 2004)
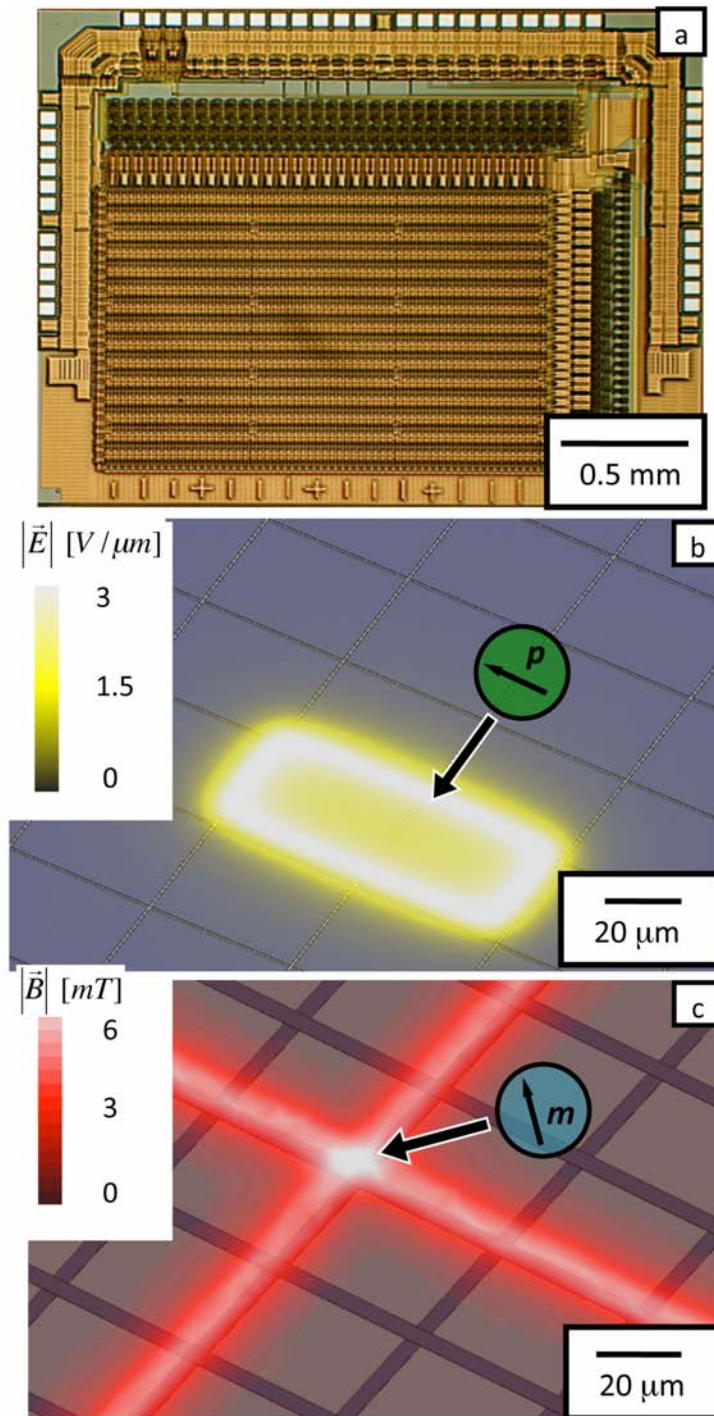
**Figure 5.1**. (a) A micrograph of the integrated circuit, (b) the magnitude of the electric field $|\vec{E}|$, from a quasi-static electric field simulation, plotted 5 μm above the chip surface. The pixels are shown as blue tiles that cover the surface of the chip. Two pixels are held at 50 V relative to the surrounding pixels, (c) the magnitude of the magnetic field $|\vec{B}|$, from simulation, plotted 5 μm above the chip's surface. The wires are shown as blue stripes running across the surface of the chip. Two wires are sourced with 120 mA and all surrounding wires set to 0 mA.

*5.2.2 Chip Architecture*

The chip's large array of 60 x 61 (3,660) DEP pixels, 60 horizontal and 60

vertical (120) magnetic wires, and 16 temperature sensors are addressed with logic

and memory built into the IC, such that only 6 data lines (not including two clocks

and the 4 control lines) are required to update the entire chip.  Figure 5.2a shows a

micrograph of a section of the chip that shows the DEP pixel array, the current

drivers for the magnetic matrix, and the digital logic that is used to update and read

from the array.  The state of the chip is stored in an integrated SRAM memory that

controls the DEP pixels, magnetic wires, and the temperature sensors.

The SRAM memory is organized into 32 words that have 128 bits.  There is an SRAM

memory element underneath each DEP pixel, temperature sensor, and current

driver for the magnetic wires. The memory array is updated by selecting a word-line

and then loading its state using a 128 bit shift register. The shift register uses a two-

phase clocking scheme.  Word selection is done with a standard 5 bit row decoder.

The entire SRAM array can be updated at a rate of ~50Hz and individual words in

the SRAM can be updated at a rate of ~1.5 kHz.  The logic, memory, and surrounding

electronics that are used to update the chip are similar to that used for the DEP chip

described in Chapter 3.

A schematic for the circuit underneath each DEP pixel is shown in Fig. 5.2b.  The

state of the SRAM memory element controls the 2:1 multiplexer (MUX) that directs

either the RF signal or its logical inverse to the voltage driving circuit that connects

to the pixel.  A schematic for each magnetic line is shown in Fig. 5.2c. The magnetic

lines have driving circuitry on both ends. By setting the memory elements on either side of the wire a current of ±120 mA or 0 mA flows through the wire. Interspersed throughout the array are 16 distributed temperature sensors that can be individually addressed to be routed to an analog voltage output.

The hybrid chip is constructed by building a simple fluid cell directly on top of the IC with a silicone gasket. The fluid cell is prepared by cutting a 1.2 mm hole out of Press-to-Seal™ 0.5 mm thick silicone sheets from Invitrogen (Invitrogen: p-24744) with a hole-punch. The silicone gasket is placed onto the IC under a stereoscope with tweezers. A 3 x 3 mm$^2$ glass cover slip seals the fluid cell. The integrated circuit was designed at Harvard using Cadence Design Software (Cadence) and fabricated in a commercial foundry on a high voltage 0.6 μm process (X-Fab – XC06 MIDOX).

The experimental setup surrounding the hybrid IC / microfluidic chip is similar to that of the DEP Chip described in Chapter 3. The device sits on a chip carrier on a custom printed circuit board (PCB) connected to a computer through a PCI card (National Instruments: PCI-6254). The patterns sent to the chip are created using a GUI written in MATLAB (The MathWorks) and sent to the PCI card with a custom Labview (National Instruments) program. The device sits under an Olympus fluorescence microscope with an Orca-ER (Hammamatsu) digital camera that connects to the computer.
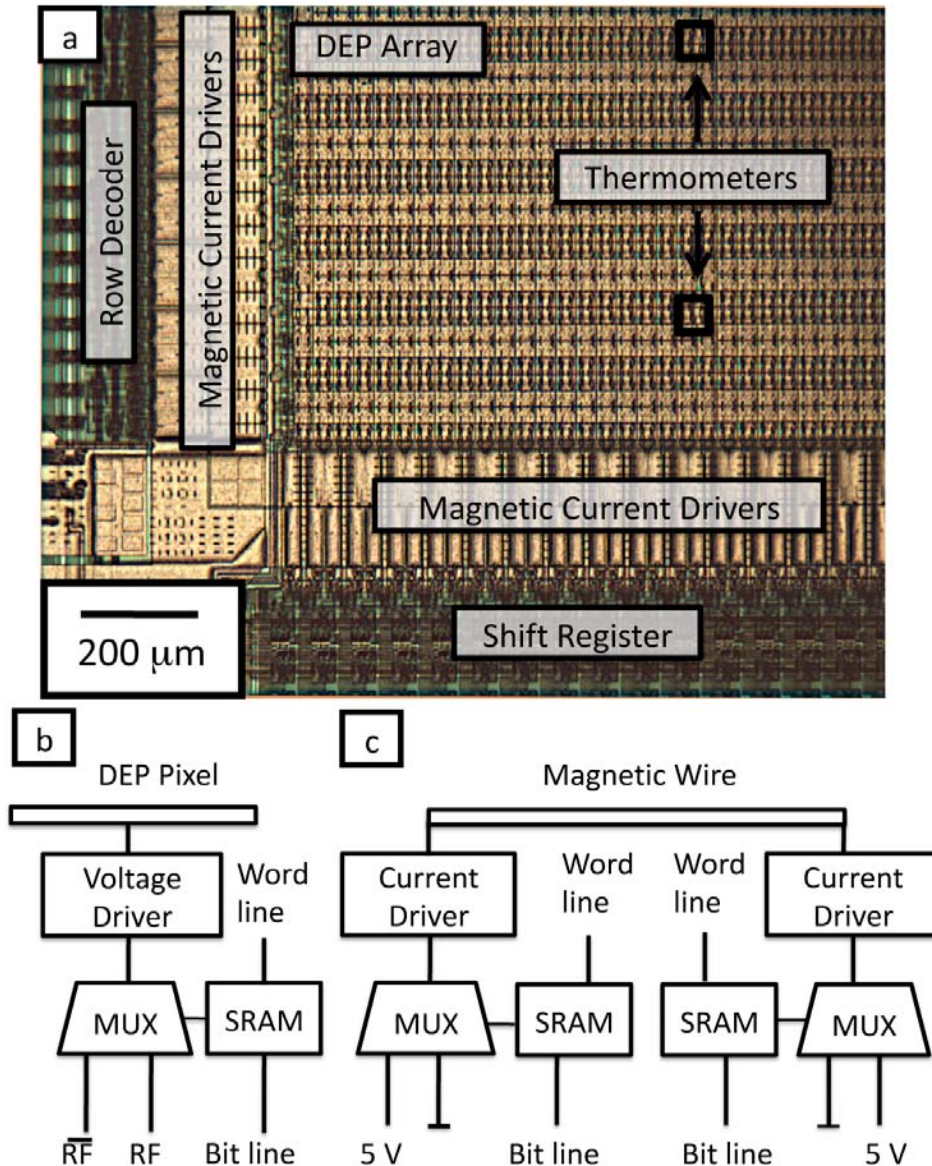
**Figure 5.2.** (a) A micrograph of a part of the integrated circuit showing the DEP array, the magnetic current drivers, and the logic and memory used to update the SRAM array, (b) a schematic of the circuitry underneath each DEP pixel, showing the SRAM memory element, a multiplexer (MUX) that directs either the RF signal or its logical inverse to a voltage driver that connects to the electrode, (c) a schematic of the circuitry for each magnetic wire in the matrix, showing the SRAM memory elements, and the MUXs that connect to the current drivers to drive the wires with either ±120 mA or 0 mA.

**5.3 Demonstrations**

This section demonstrates the HV-DEP/Magnetic chip using DEP to trap and move dielectric objects, magnetic forces to trap and move magnetically tagged objects, and magnetic and DEP forces used together to deform objects implanted with magnetic nanoparticles. Section 5.3.1 shows how the hybrid chip can be used to trap and move objects along programmable paths with DEP. Section 5.3.2 shows how objects that are tagged with magnetic beads can be trapped and moved along programmable paths using the magnetic matrix. Section 5.3.3 demonstrates the utility of having both electric and magnetic forces on the same chip by holding a unilamellar vesicle embedded with iron oxide nanoparticle in place with DEP and controllably pulling a thin tether from the vesicle's membrane using the magnetic matrix.

The vesicles are prepared with liposome electroformation using a modification of the Angelova Method, as is described in detail in Chapter 4. (Angelova *et al.,* 1986) The unilamellar vesicles are loaded with 4mM NaCl and suspended in a glucose solution with matched osmolarity, which provides contrast in the complex dielectric response to facilitate DEP forces. (Hunt *et al.,* 2008) The vesicles' membranes are stained with rhodamine such that the vesicles are easily observable under a fluorescence microscope.

*5.3.1 Dielectrophoresis: Trapping and Positioning Vesicles*

This section demonstrates how the HV-DEP/Magnetic Chip simultaneously and independently controls the position of objects with DEP. Figure 5.3 shows

unilamellar vesicles that are trapped and moved along programmed paths using the DEP pixel array. Figure 5.3a shows two vesicles that are independently trapped on the chip with two sets of DEP pixels. In Fig. 5.3 (a-d) the vesicles are moved at speeds up to 80 μm/sec by sequentially changing the pixels that are turned on. In Fig. 5.3a the vesicle on the right is independently moved downwards while the vesicle on the left is held in place. In Fig. 5.3b both the left and right vesicle are moved downwards simultaneously. In Fig. 5.3c the vesicle on the left is simultaneously moved to the right while the vesicle to the right is moved to the left. The chip has 3,660 pixels and the entire array can be refreshed at ~50 Hz, enabling many individual vesicles to be controlled simultaneously. The ability to trap and move objects with DEP is a useful tool to control the position of pL volumes of fluid and living cells that are not tagged or modified.
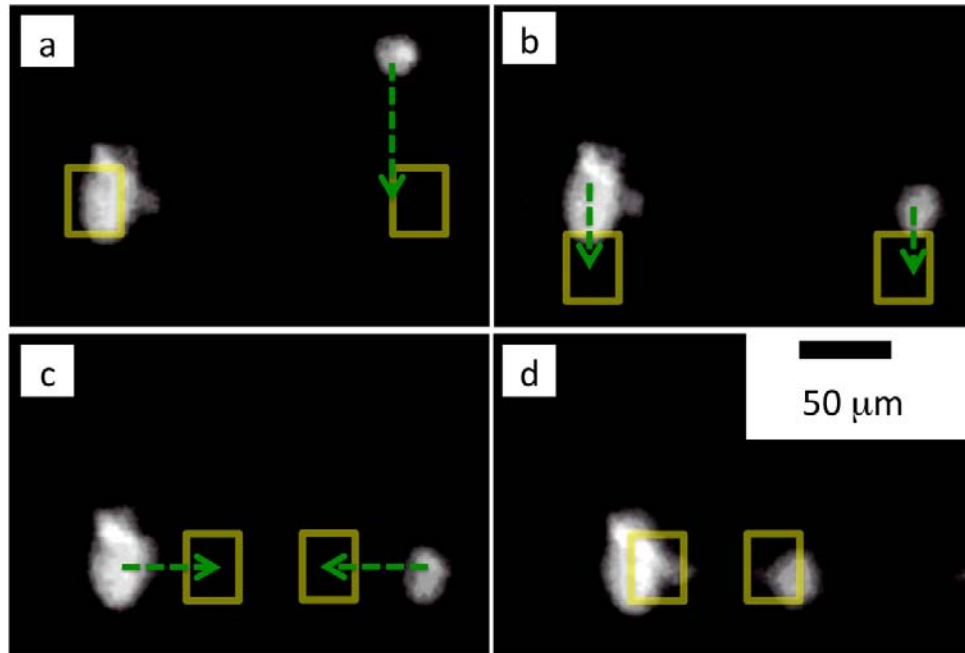
**Figure 5.3** A time sequence of the DEP positioning of vesicles. The frames (a-d) are fluorescence images of the rhodamine stained membranes of the vesicles. The DEP pixels are turned on in sequence to position the vesicles. The dashed green line shows the direction that the chip is moving the vesicles, the yellow square shows the DEP pixel that is activated. The maximum speed of a vesicle is 80 µm/sec. Each frame is separated by roughly 1 sec.

*5.3.2 Magnetophoresis:  Trapping and Positioning Magnetic Beads*

This section demonstrates how the HV-DEP/Magnetic Chip can control the position

of objects with magnetophoresis.  The ability to trap and move magnetic objects

along programmed paths is a useful tool to control the position of samples that

cannot be trapped with DEP forces, but which can be tagged with magnetic

particles. (Lee *et al.,* 2007)  Figure 5.4 shows the magnetic matrix trapping and

moving an iron oxide bead with a radius $a$ = 1 µm (Bioclone: FF102) along an

arbitrary path.  In Fig. 5.4a two perpindicular wires are driven with 120 mA, such

that the bead is trapped at the field maximum that occurs at the wire's intersection.

In Fig. 5.4(b-d) different intersecting wires are turned on to move the bead along a

programmed path at speeds of 2 µm/s.  The magnetic force is not as localized as the

DEP force.  Along the length of each intersecting wire, particles are attracted to the

activated wire.
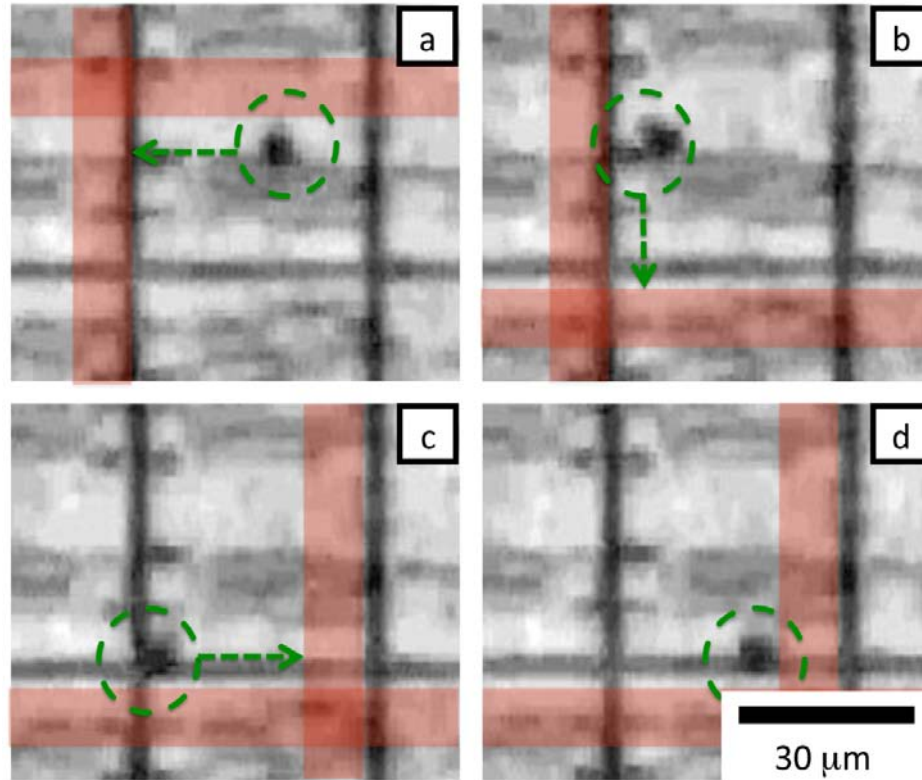
**Figure 5.4** Time sequence of magnetic trapping and positioning of a magnetic bead. Magnetic wires in the matrix are turned on in sequence to position the bead. The position of the particle is marked with a green circle. The direction that the bead is being pulled is marked with a green arrow. The red lines shows which magnetic wires in the matrix have been turned on, the actual wires are buried under the DEP pixels and are not visible. Each frame (a-d) is separated by roughly 2 sec.

*5.3.3 Dielectrophoresis and Magnetophoresis: Deforming Vesicles*

This section demonstrates how the HV-DEP/Magnetic Chip can use magnetic and DEP forces together. Figure 5.5 show the chip holding a vesicle, that is implanted with iron oxide nanoparticles, in place with DEP body forces while pulling a thin tether from the vesicle's membrane by applying point forces on the magnetic nanoparticles with magnetophoresis. This demonsration shows that DEP and Magnetophoresis can be used together to apply point forces with nm resolution to micrometer sized objects. (Waugh *et al.,* 1992) In Fig. 5.5a a vesicle is positioned with DEP pixels. Two magnetic wires that cross near the DEP pixel are sourced with 120 mA and the iron oxide nanoparticles inside the vesicle are pulled towards the magnetic field maximum. The vesicle's membrane is locally deformed into a thin tether, as vesicles have been shown to do in the presence of a point force. (Waugh *et al.,* 1992) In the proceeding frames Fig. 5.5(b-f) the magnetic field is turned off and tension in the membrane pulls the tether back into the vesicle. (Waugh *et al.,* 1992) The ability to locally deform microscopic objects using DEP as a body force and magnetophoresis as a point force is a useful tool to apply precise mechanical stresses on vesicles and living cells. (Berry *et al.,* 2003 , Dobson *et al.,* 2008, and Tresset *et al.,* 2007)
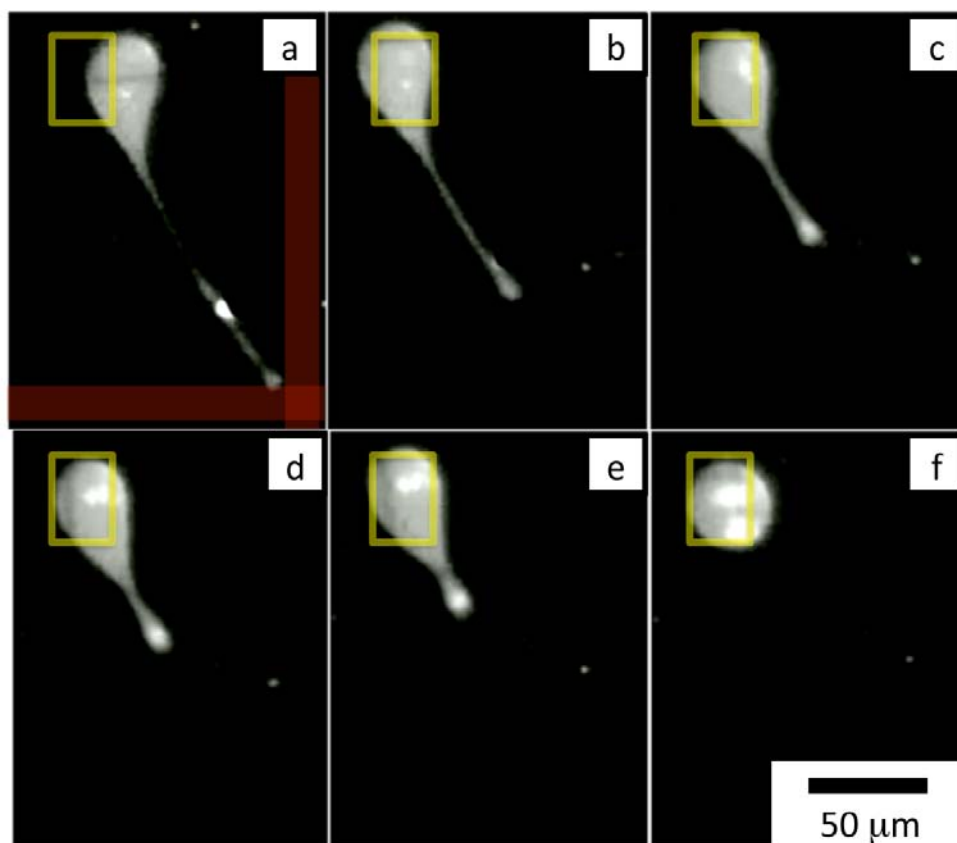
**Figure 5.5** A vesicle is held in place with a DEP pixel while a tether is pulled using the magnetic matrix. The yellow square shows the DEP pixel that is activated, and the red lines show the magnetic wires that are turned on. The vesicle is implanted with iron oxide nanoparticles. After the first frame (a) the magnetic field is turned off and the tether is pulled back into the vesicle. Each frame (a-f) is separated by 0.2 seconds.

**5.4 Discussion**

Hybrid IC / microfluidic chips provide a versatile platform to control small volumes of fluid and living cells. The combination of both magnetic (Lee *et al.,* 2004 and Lee *et al.,* 2007) and DEP forces (Manaresi *et al.,* 2003 and Hunt *et al.,* 2008) onto a single chip further expands the capabilities and generality of the platform. Dielectrophoresis can be used to trap and position untagged living cells and drops of fluid and magnetic forces can be used to trap and position objects tagged with magnetic nanoparticles. Dielectrophoresis and magnetophoresis can be used together to apply precise nm-resolution point forces to micrometer-sized objects.

Magnetic actuation of nanoparticles embedded in cells or vesicles has many exciting scientific applications. The technique demonstrated in this chapter, pulling a thin tether from a unilamellar vesicle and observing the vesicle pull the tether back into itself, can be used as a tool to study the complex mechanical properties of lipid bilayers. (Waugh *et al.,* 1992) A number of exciting applications exist for magnetically actuating cells tagged with magnetic nanoparticles, such as applying precise mechanical stresses on cell membranes (Berry *et al.,* 2003) or manipulating and activating individual ion channels and surface receptors on specific cells. (Dobson *et al.,* 2008)

The techniques demonstrated in this chapter can be combined with the 'laboratory-on-a-chip' functions demonstrated in Chapter 4, to create a general-purpose platform for biology and chemistry experiments on individual living cells. The techniques demonstrated in Chapter 4 can be used to mix small volumes of reagents

and samples together and to control the chemical environment of individual cells. The magnetic actuation of nanoparticles, demonstrated in this chapter, can be used to control cells embedded with magnetic nanoparticles to activate or deactivate specific surface receptors or ion channels. The hybrid chips can simultaneously perform many of these experiments in parallel, allowing a statistical number of independently controlled single-cell experiments to be carried out.

# Chapter 6. Microwave Dielectric Heating of Drops in Microfluidic Devices

## 6.1 Overview

In this chapter a technique is presented to locally and rapidly heat drops of water with microwave dielectric heating.  This technique adds a key functionality to the list of functions that are demonstrated in Chapters 3, 4, and 5, the ability to control temperature. Water absorbs microwave power more efficiently than polymers, glass, silicon, or oils, due to its permanent molecular dipole moment that has a large dielectric loss at GHz frequencies.  This selective absorption of microwave power by water allows thermal energy to be directly inserted into small volumes of fluid in a microfluidic device without significantly heating the surroundings.  The relevant heat capacity of such a system is that of a single thermally isolated picoliter-scale drop of water, enabling very fast thermal cycling.

In this chapter microwave dielectric heating is demonstrated in a microfluidic device that integrates a flow-focusing drop maker, drop splitters, and metal electrodes to locally deliver microwave power from an inexpensive, commercially available 3.0 GHz source and amplifier.   The temperature change of the drops is measured by observing the temperature dependent fluorescence intensity of cadmium selenide nanocrystals suspended in the water drops.  Characteristic heating times are demonstrated that are as short as 15 ms to steady-state temperature changes as large as 30°C above the base temperature of the

microfluidic device.  Many common biological and chemical applications require rapid and local control of temperature and can benefit from this new technique.

Microwave dielectric heating is well suited to be integrated with the hybrid integrated circuit (IC) / microfluidic chips described in Chapters 3, 4, and 5.  Using modern IC technology and designing the circuits with appropriate radio frequency design principals, pixels can be driven with GHz frequency voltages.  A hybrid IC / microfluidic chip with electrodes that can be driven with voltages at GHz frequencies, could individually control the temperature of thermally isolated, small volumes of fluid using the technique outlined in this chapter.

A growing library of elements for microfluidic chips have been developed in recent years for tasks such as the mixing of reagents, detecting and counting cells, sorting cells, genetic analysis, and protein detection. (Whitesides *et al.,* 2001, Stone *et al.,* 2004, Tabeling *et al.,* 2005, Yager *et al.,* 2006, Martinez *et al.,* 2008, Lee *et al.,* 2007, Hunt *et al.,* 2008, Maltezos *et al.,* 2005) There is one function, however, that is crucial to many applications and which has remained a challenge: the local control of temperature. The large surface area to volume ratios found in micrometer-scale channels and the close proximity of microfluidic elements make temperature control in such systems a unique challenge. (Maltezos *et al.,* 2005, Lee *et al.,* 2005)

Much work has been done in the last decade to improve local temperature control in microfluidic systems.  The most common technique uses Joule heated metal wires and thin films to conduct heat into fluid channels. (Nakano *et al.,* 1994, Lagally *et al.,* 2000, Liu *et al.,* 2002, Khandurina *et al.,* 2000) The thermal conductivity of

microfluidic devices control the localization of the temperature change and tends to be on the order of centimeters. (Nakano *et al.,* 1994 and Khandurina *et al.,* 2000) Temporal control is limited by the heat capacity and thermal coupling of the microfluidic device to the environment and thermal relaxation times tend to be on the order of seconds. (Nakano *et al.,* 1994 and Khandurina *et al.,* 2000) Alternative techniques to improve the localization and response time have been developed, such as those that use non-contact infrared heating of water in glass microfluidic systems (Oda *et al.,* 1998) and integrated micrometer size Peltier Junctions to transfer heat between two channels containing fluid at different temperatures. (Maltezos *et al.,* 2005) Fluids have also been cooled on millisecond time scales with evaporative cooling by pumping gasses into the fluid channels. (Maltezos *et al.,* 2006)

The focus of the research described in this thesis is to integrate electronics with microfluidics to bring new capabilities to lab-on-a-chip systems. This chapter presents a technique to locally and rapidly heat water in drop based microfluidic systems with microwave dielectric heating. The devices are fabricated using soft lithography and are connected to inexpensive commercially available microwave electronics. This work builds on previous work in which microwaves have been used to heat liquid in microfluidic devices(Shah *et al.,* 2007, Sundaresan *et al.,* 2005, Sklavounos *et al.,* 2006, and Geist *et al.,* 2007) by achieving significantly faster thermal response times and a greater temperature range. In our device, drops of water are thermally isolated from the bulk of the device and this allows exceptionally fast heating and cooling times $\tau_s$ = 15 ms to be attained and the drops'

97

temperature to be increased by 30°C.  The coupling of microwave electronics with microfluidics technology offers an inexpensive and easily integrated technique to locally and rapidly control temperature.

## 6.2 Model of Dielectric Heating of Drops

Due to water's large dielectric loss at GHz frequencies, microwave power is absorbed much more strongly by water rather than PDMS or glass.  The device described in this chapter operates at 3.0 GHz, a frequency very close to that of commercial microwave ovens (2.45 GHz), that is below the frequency associated with the relaxation time of water but where water still readily absorbs power. It is inexpensive to engineer electronics to produce and deliver 3.0 GHz frequencies because it is near the well-developed frequencies of the telecommunications industry.

Two independent figures of merit describe the heater, the steady-state change in temperature $\Delta T_{ss}$ that the drops attain and the characteristic time $\tau_s$ that it takes to change the temperature.  The steady-state temperature occurs when the microwave power entering the drop equals the rate that heat leaves the drop into the thermal bath.  The thermal relaxation time depends only on the geometry and the thermal properties of the drops and the channel and is independent of the microwave power.

To describe the heater a simplified model is used in which the temperature of the channel walls do not change.  The thermal conductivity of the glass and PDMS channel walls is much larger than that of the fluorocarbon (FC) oil in which the

drops are suspended, which allow the glass and PDMS mold to act as a large thermal reservoir that keep the channel walls pinned to the base temperature.

The drop is modeled as having a heat capacity that connects to the thermal reservoir through a thermal resistance. The drop has a heat capacity $C = VC_w$ that connects to the thermal reservoir with a thermal resistance $R = L_D/Ak_{oil}$, where V is the volume and A is the surface area of the drop, $C_w$ is the heat capacity per volume of water, $L_D$ is the characteristic length between the drop and the channel wall, and $k_{oil}$ is the thermal conductivity of the oil surrounding the drop. A steady-state temperature $\Delta T_{ss}$ is reached when the microwave power PV entering the drop is equal to the power leaving the drop $\Delta T_{ss}k_{oil}A/L_D$. The steady-state temperature $\Delta T_{ss} = PVR$ is:

$$\Delta T_{SS} = \frac{V}{A}\frac{L_D}{k_{oil}}P$$

     **6.1**

The system has a characteristic time scale $\tau_s = RC$ that describes the thermal response time of the system,

$$\tau_S = \frac{V}{A}\frac{L_D}{k_{oil}}C_W$$

     **6.2**

The characteristic time scale $\tau_s$ describes the thermal relaxation time, the time it takes for the drop to reach an equilibrium temperature when the microwave power is turned on and the time that it takes for the drop to return to the base temperature of the device when the microwaves are turned off.

This simplified model describes several key features of the microwave heater. The steady-state temperature is linearly proportional to the microwave power, whereas the characteristic thermal relaxation time is independent of the microwave power. The characteristic time and the steady-state temperature are both proportional to the volume to surface ratio of the drops. A trade-off relation exists between the rate of heating $1/\tau_s$ and the steady-state temperature, whereby a larger volume to surface ratio reduces the thermal relaxation time of the heater but decreases its steady-state temperature for a given microwave power, and vice versa. Similarly an increase in the ratio of the characteristic length between the drop and the channel wall and the thermal conductivity of the oil $L_D/k_{oil}$ increases the thermal relaxation time and increases the steady-state temperature.

## 6.3 The Microfluidic Device

The devices are fabricated using poly(dimethylsiloxane) (PDMS)-on-glass drop-based microfluidics. Microwave power is locally delivered via metal electrodes that are directly integrated into the microfluidic device and that run parallel to the fluid channel, as is shown in Fig. 6.1a. The drops are thermally insulated from the bulk by being suspended in low thermal conductivity oil. A schematic of the device is shown in Fig. 6.2a. Syringe pumps provide the oil and water at constant flow rates to the microfluidic device. A drop maker and two drop splitters in series create drops that are properly sized for the microwave heater. The microwave power is created off chip using inexpensive commercial components.

Drops are created using a flow-focusing geometry (Anna *et al.,* 2003) as is shown in

Fig. 6.2b. A fluorocarbon oil (Fluorinert FC-40, 3M) is used as the continuous phase

and the resulting drops contain 0.1 µM of carboxyl coated CdSe nanocrystal

(Invitrogen) suspended in a phosphate buffered saline (PBS)  solution.  A surfactant

comprised of a polyethyleneglycol (PEG) head group and a fluorocarbon tail

(RainDance Technologies) is used to stabilize the drops. (Holtze *et al.,* 2008) The

walls of the microfluidic channels are coated with Aquapel® (PPG Industries) to

ensure that they are preferentially wet by the fluorocarbon oil.  Fluid flow is

controlled via syringe pumps.
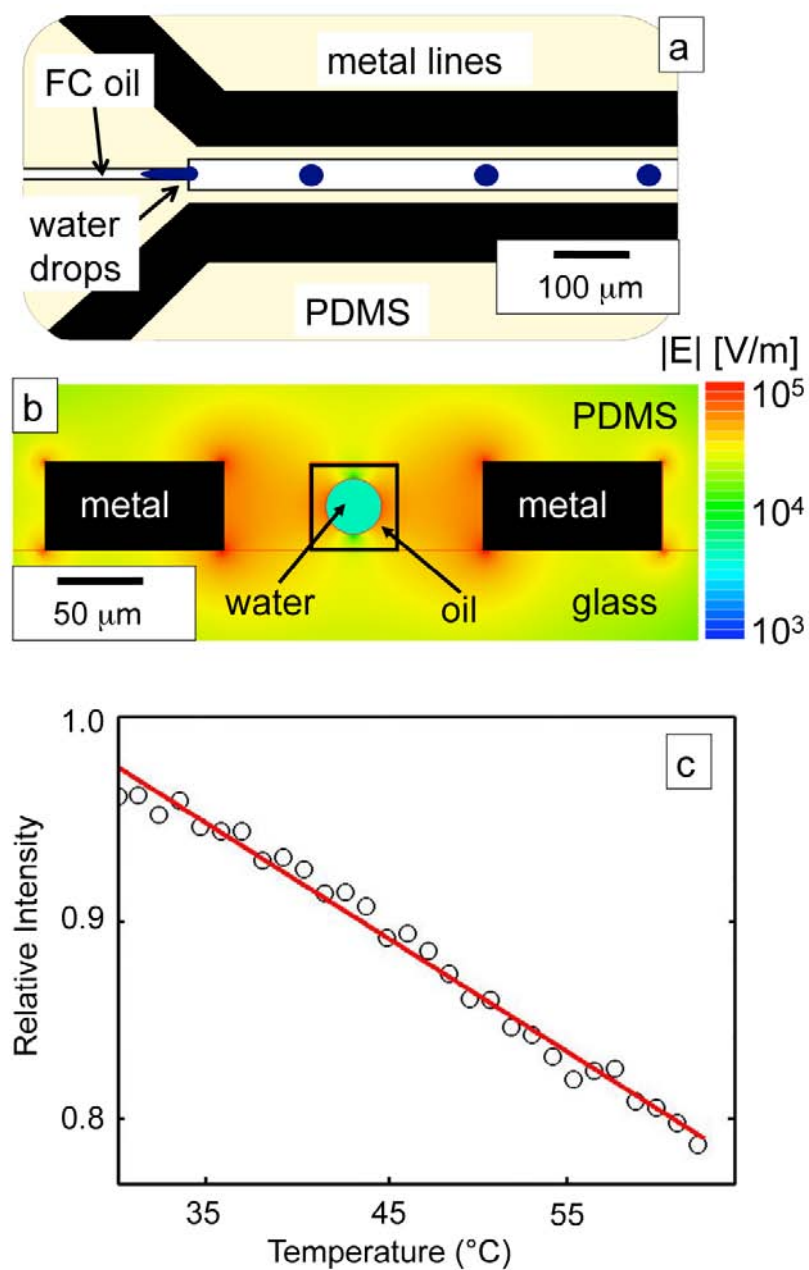
**Figure 6.1** (a) A schematic of the microwave heater. The black lines represent the metal lines which are connected to the microwave source, the center fluid channel carries drops of water immersed in fluorocarbon (FC) oil, (b) a cross section of the microwave heater with a quasi-static electric field simulation superimposed is shown, the electric field is plotted in log scale, (c) the calibration curve of the CdSe nanoparticles which are used as temperature sensors, where the circles are data points and the red line is the fit.

To make drops smaller than the channel height, and thus separated from the walls of the channel to ensure adequate thermal isolation, drop splitters are used (Link *et al.,* 2004) as is shown in Fig. 6.2c. The drop splitters are designed to break each drop into two drops of equal volume. Passing a spherical drop through two drop splitters in series decreases the radius of a drop by a factor of $(½)^{2/3} = 0.63$. Drop splitters allow the device to be made in a single fabrication step, because they remove the necessity of making the drop maker with a channel height smaller than the rest of the device. (Anna *et al.,* 2003)

The metal electrodes are directly integrated into the PDMS device using a low-melt solder fill technique. (Siegel *et al.,* 2006) The masks for the soft lithography process are designed to include channels for fluid flow and a set to be filled with metal to form electrodes. After inlet holes have been punched into the PDMS and the PDMS is bonded to a glass slide, the microfluidic device is placed on a hot plate set to 80°C. A 0.02 inch diameter indium alloy wire (Indalloy 19; 52% Indium, 32.5% Bismuth, 16.5% Tin from Indium Corporation) is inserted into the electrode channel inlet holes and, as the wire melts, the electrode channels fill with metal via capillary action. The resulting electrode channels run along either side of the fluid as is shown in Fig. 6.2d. To keep the drops from heating from the fringe electric fields before the drop enters the heater the fluid channel is constricted to press the drops against the PDMS wall, which keeps the drops at the same temperature as the base temperature of the microfluidic device.

The electronics that create the microwave power are assembled using inexpensive modules. The microwaves are generated with a voltage controlled oscillator (ZX95-3146-S+, Mini-Circuits) and amplified to a maximum of 11.7 V peak-to-peak with a maximum power of 26 dBm with a power amplifier (ZRL-3500+, Mini-Circuits). The microwave amplifier connects with a cable to a sub miniature assembly (SMA) connector mounted next to the microwave device as is shown in Fig. 6.2e. Copper wires approximately 2 mm in length connect the SMA connector to the metal electrodes in the PDMS device. Our electronics operate at 3.0 GHz where water's microwave power absorption is roughly 1/3 as efficient as at the frequency associated with water's relaxation time (~18 GHz) but where electronics are inexpensive and commercially available. The electronics used in our system costs less than $US200 and are easy to setup.

Finite element simulations are performed to determine the electric field strength in the microwave heater which is used to calculate the microwave power absorbed by the drops. Figure 6.1b shows a schematic cross-section of the microfluidic device where the drops pass between the metal electrodes. The channel cross-section has dimensions 50 x 50 $\mu m^2$. Parallel to and 20 $\mu$m away from each side of the fluid channel are metal lines that are 100 $\mu$m wide and 50 $\mu$m high. Superimposed on the schematic in Fig. 6.1b is a quasi-static electric field simulation of the electric field (Maxwell, Ansoft). For a 12 V peak-to-peak signal across the metal lines, the RMS electric field within a drop with a 15 $\mu$m radius suspended in fluorocarbon oil is $|E| \sim 8 \times 10^3$ V/m. The electric field linearly scales with the voltage across the metal lines which allows us to calculate the field within the drop for any voltage. The

simulated electric field is combined with Eq. 2.1 and Eq. 2.2 to calculate the microwave power that enters the drops which may be combined with Eq. 6.1 to predict steady-state temperature changes.

The temperature change of the drops is measured remotely by observing the temperature-dependent fluorescence of CdSe nanocrystals suspended in the drops. (Mao *et al.,* 2002)  To calibrate this thermometer, the microwave power is turned off and a hot plate is used to set the temperature of the microfluidic device. The fluid channel is filled with CdSe nanocrystals suspended in water and the temperature of the hot plate is slowly increased from 25°C to 58°C while the fluorescence intensity of the CdSe quantum dots is measured. The measured fluorescence intensity is plotted as a function of temperature in Fig. 6.1c.  A line is fit with a slope 0.69 %/°C ± 0.03 %/°C to the data and this slope is used to convert fluorescence measurements into measurements of the change in temperature.  A line is fit to the data using a least-squares technique and the error is the uncertainty in the coefficient of the fit.  A calibration curve is taken immediately before an experiment.  There is no evidence that the CdSe nanoparticles leak from the drops into the oil or precipitate onto the microfluidic channel.  The microfluidic channel and the oil in the waste line are checked after the experiments and there is no measured fluorescence signal.  The device is monitored with an Hamamatsu ORCA-ER cooled CCD camera attached to a BX-52 Olympus microscope.  Images are taken with MicroSuite Basic Edition by Olympus and analyzed in MATLAB (The MathWorks, Inc.).  The microfluidic device is connected with an SMA to the

microwave amplifier and sits on top of a hot plate underneath the microscope as is shown in Fig. 6.2d.

The devices are tested by measuring the temperature change of water drops as they travel through the microwave heater. A long-exposure fluorescence image of many drops traveling through the microwave heater shows the ensemble average of the temperature change of drops at each point in the channel. A plot of the drop heating in time may be extracted from this image using the measured flow rate of the drops through the microfluidic system. An experiment is performed with the constant volumetric flow rate of the water at 15 µL/hr and the oil at 165 µL/hr. A bright field, short shutter speed image is taken of the drops traveling through the microwave heater and the drops' average diameter is measured to be 35 µm. The microwave heater is turned on with a frequency of 3.0 GHz and a peak to peak voltage of 11 V. A long exposure (2 seconds) fluorescence image is taken of the microwave heater that is normalized against images taken with the microwaves turned off to remove artifacts that arise from irregularities in the geometry of the channel, the light source, and the camera.
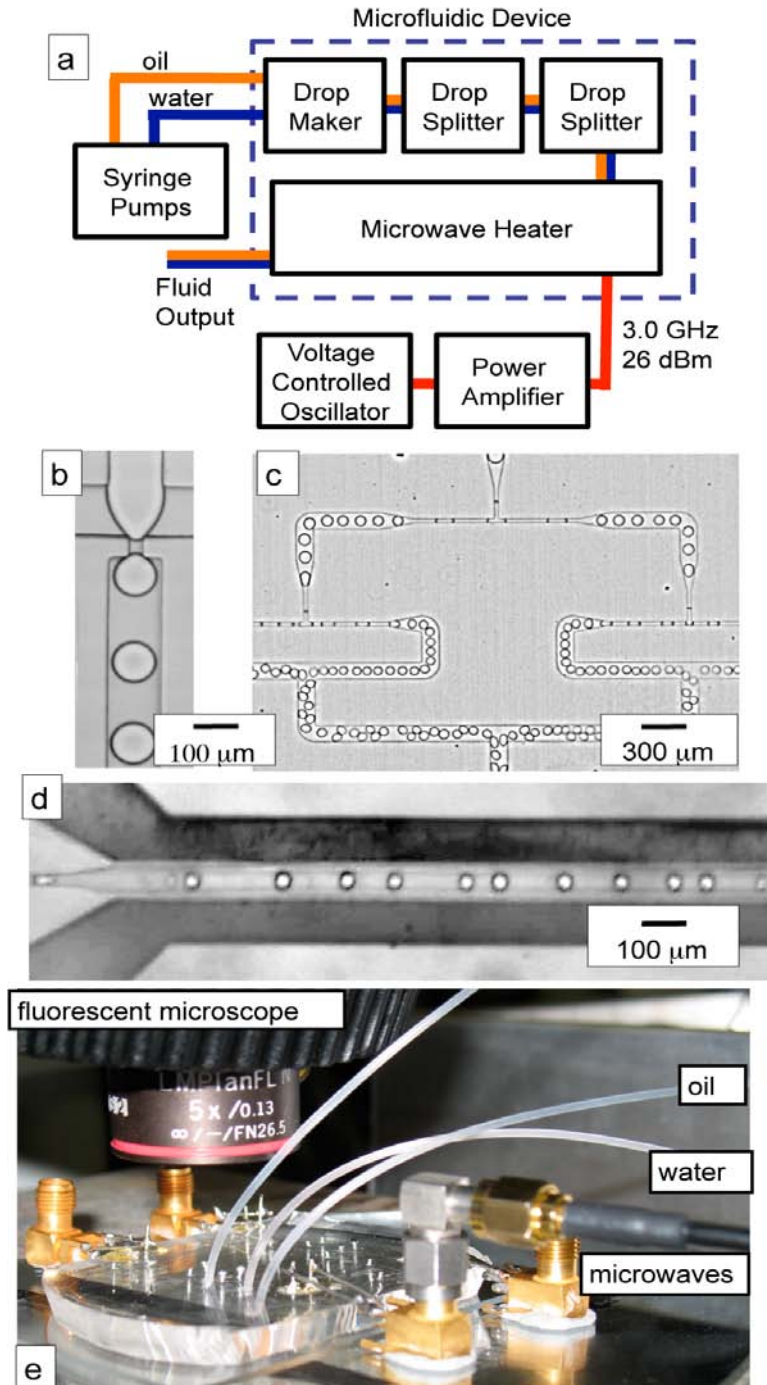
**Figure 6.2** (a) A schematic of the microwave heating device, showing the oil in orange, the water in blue, and the electronic connections in red, (b) a micrograph of the flow-focusing drop maker, (c) the two sets of drop splitters in series, (d) a micrograph of the microwave heater, the dark regions that run parallel to the fluid channel are the metal lines, (e) a photograph of the microfluidic device, connected to the microwave amplifier with a cable with an SMA connector, on top of a hot plate, underneath the fluorescence microscope.

## 6.4 Demonstration

The drops are heated to a steady-state temperature change $\Delta T_{ss}$ as they pass through the microwave heater. Figure 6.3a shows the normalized fluorescence intensity of the drops as they enter the microwave heater superimposed onto a bright-field image of the device. It can be seen that as the drops enter the channel their average fluorescence intensity drops which shows that they are being heated. A line average of the normalized image is taken in the direction perpendicular to the fluid flow and is plotted against the length of the channel, as in Fig. 6.3b. As the drops are heated the average fluorescence intensity of the drops falls exponentially with distance to 85% of its initial intensity after a path length of 300 μm. The fluorescence intensity measures the temperature change of the drops, and so the drops are heated in a characteristic length of 300 μm.

The drops are heated to steady-state temperature changes $\Delta T_{ss}$ as large as 30°C above the base temperature of the microfluidic device in only $\tau_s$ = 15 ms. The average temperature change of the drops as a function of time and distance traveled is plotted in Fig. 6.3c. For this heating power, the temperature rises to a steady-state value of 26°C above the base temperature of 21°C in 15ms. The curve in Fig. 6.3c is arrived at by using the calibration curve of the CdSe nanocrystals, Fig. 6.1c, to convert the fluorescence intensity in Fig. 6.3b into a change in temperature $\Delta T$. The sum of the flow rates of the oil and water are used to calculate the speed of the drops through the channel, which may be used to transform the

108

length in Fig. 6.3a into the time that the drops have spent in the heater.  Each data

point consists of the average of 20 independently taken 2 sec exposures.
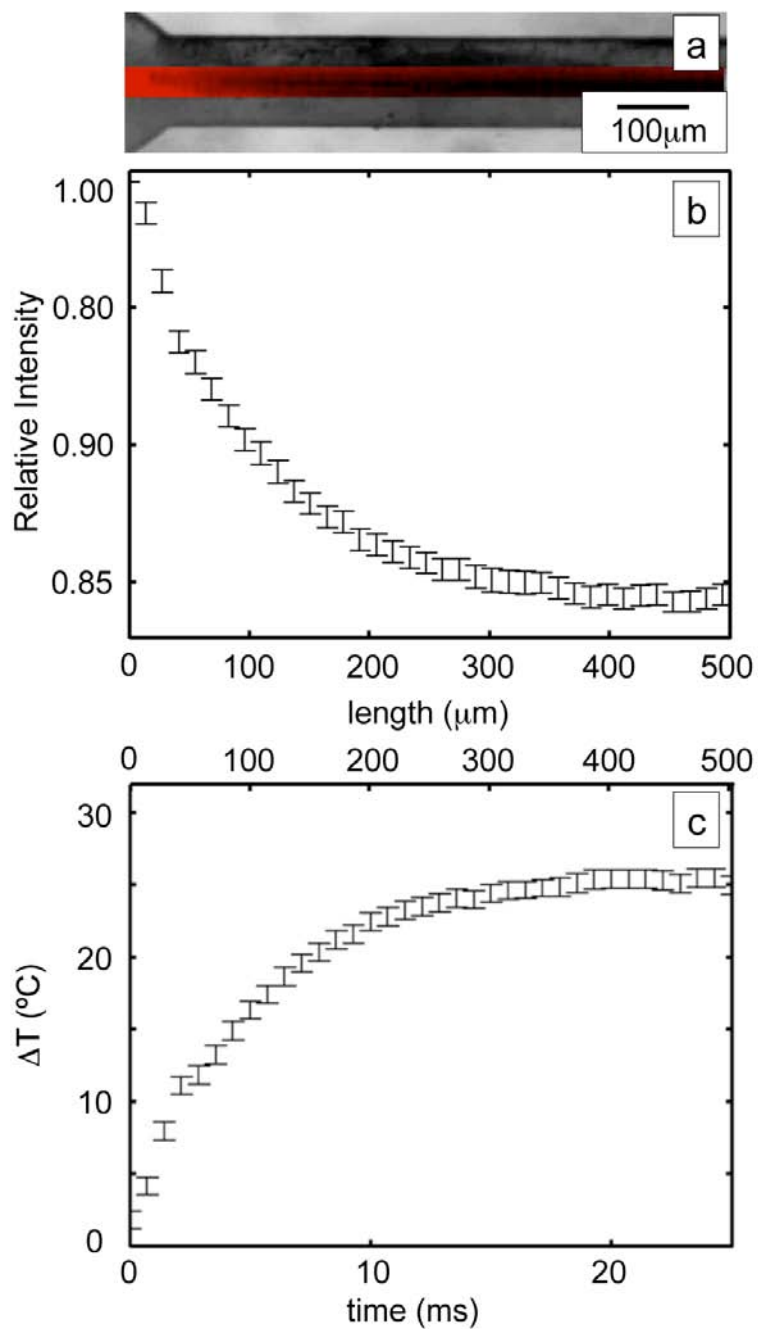
**Figure 6.3** (a) A 2 second exposure of the fluorescence signal normalized to an image taken with the microwave source turned off superimposed onto a bright field image of the device, (b) the line average of the normalized intensity plotted versus distance down the channel, (c) the temperature change ΔT plotted versus time and versus the distance the drops have traveled down the channel.

The combined statistical error of the measurement of the heating is also plotted in Fig. 6.3c. The average error is ~1.4°C. The statistical error in the steady-state temperature is found to come primarily from variations in the size of the drops. The steady-state temperature change of each drop is linearly related to the volume-to-area ratio of the drop and to the distance of the drop to the channel walls, as is described in Eq. 6.1. By observing the drops exit the microwave heating region of the chip, the drops are found to cool with a characteristic time similar to the heating time. In addition, by narrowing the channel at the exit of the microwave heater, the drops are brought closer to the channel wall and the drops return to the base temperature of the oil in less than 1 ms.

The steady-state temperature change $\Delta T_{ss}$ of the drops may be set from 0°C to 30°C by varying the applied microwave power as is described in Eq. 6.1. The microwave power is controlled by experimentally varying the peak-to-peak voltage of the applied microwave voltage which varies the strength of the electric field inside the drops as is described by our simulations. A series of plots of the change in temperature versus time for different applied powers is shown in the inset of Fig. 6.4a, and shows steady-state temperature changes ranging from 2.8°C to 30.1°C, with an average error of 1.5°C. It is noteworthy that all of the heating curves have an exponential form and have the same characteristic rise time $\tau_s$ = 15 ms.

Good agreement is found between the steady-state temperature changes observed in Fig. 6.4a for different applied microwave powers and the model of microwave heating outlined in the beginning of this chapter. The steady-state temperature

111

change is plotted versus the microwave power density in Fig. 6.4a and is fit with a line. As is expected from Eq. 6.1 the steady-state temperature change rises linearly with applied microwave power. The microwave power density is calculated using the electric field values determined from simulations (Fig. 6.1b). The only variable in Eq. 6.1 that is not measured or that is not a material property is the characteristic length scale between the drop and the channel wall $L_D$. This characteristic length $L_D = 28$ µm is estimated using the measured steady-state temperature change (Fig. 6.4a) and the known material properties, using Eq. 6.1.

Good agreement is found between the observation that the temperature change approaches steady-state exponentially in time in Fig. 6.4b and the model for microwave heating outlined in the beginning of this chapter. To compare the model's prediction that the drops approach equilibrium exponentially in time with a single relaxation time constant (Eq. 6.2) with our observations, the change in temperature $\Delta T$ subtracted from the steady-state change in temperature $\Delta T_{ss}$ is plotted *versus* time on a semi-log plot and fit with a line. As is predicted by the model the drops approach equilibrium exponentially with a single time constant. The thermal relaxation time constant is measured to be $\tau_s = 14.7 \pm 0.6$ ms. The only variable in Eq. 6.2 that is not measured is the characteristic length $L_D$ between the drop and the channel wall. This characteristic length $L_D = 35$ µm is estimated using the measured characteristic time constant and the known material properties, using Eq. 6.2. The independent measurements of the thermal relaxation time and the steady- state temperature change versus power give two independent measures of the length $L_D$ that are within 20% of each other. The difference in the two

predictions of $L_D$ can be at least partially explained by noting that the heat capacity in Eq. 6.2 is larger than is calculated , due to the fact that the channel walls are not a perfect heat sink as the model assumes.  The agreement between the two independent measurements supports the simple model for microwave heating of drops outlined in the beginning of this chapter.
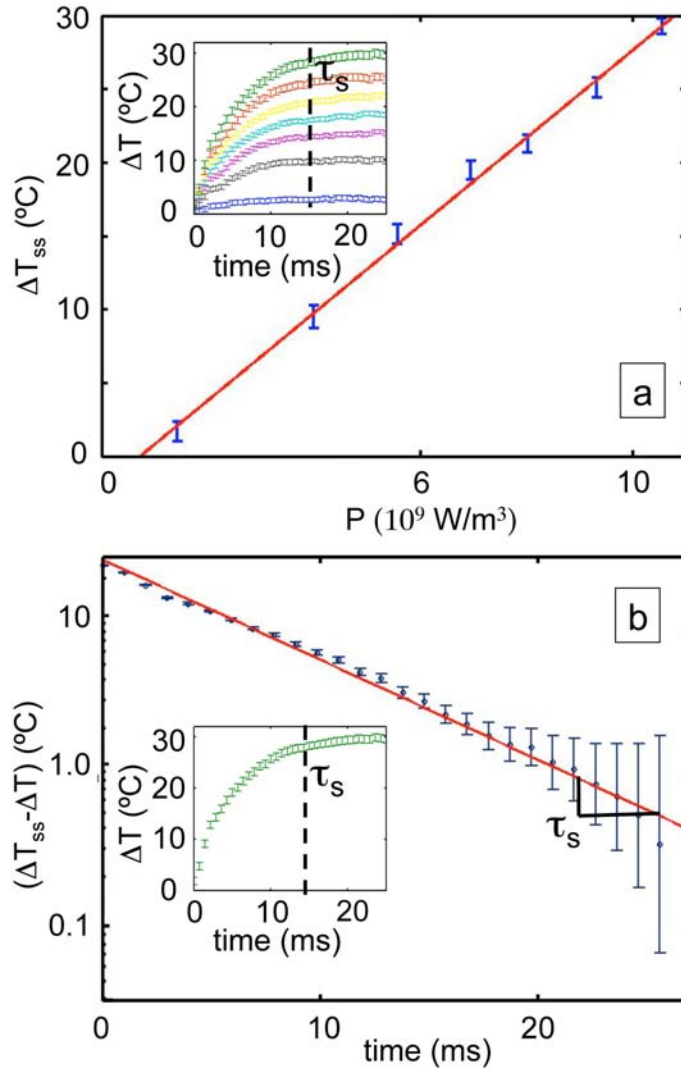
**Figure 6.4** (a) The steady-state temperature change of the drops is controlled by varying the amplitude of the microwave voltage. In the inset the green curve shows the drop heating versus time for microwaves with an amplitude of 11.7 V, the red 11.0 V, the yellow 10.3 V, the light blue 9.3 V, the purple 8.5 V, the grey 7.5 V, and the blue 4.5 V. The steady-state temperature change is plotted versus the power density, as calculated by Eq. 2.1, in the main plot, (b) the magnitude of the change in temperature $\Delta T$ subtracted from the maximum change in temperature $\Delta T_{SS}$ versus time is plotted on a log-linear scale. The temperature rises as a single exponential with a characteristic time, $\tau_s = 14.7 \pm 0.56$ ms. The inset shows the temperature versus time plot from which the log-linear plot is taken.

114

## 6.5 Discussion

In this chapter an integrated microfluidic microwave dielectric heater is demonstrated that locally and rapidly increases the temperature of drops of water suspended in oil. The large absorption of microwave power by water relative to oil, glass, and PDMS allows local and rapid heating in microfluidic devices without difficult fabrication. Both improving the insulation of drops from the channel walls and increasing the volume to surface area ratio of the drops would allow for larger temperature changes. The statistical error in the steady-state temperature of the drops can be improved by reducing variations in the drop size that arise from fluctuations in the flow from the syringe pumps.

Microwave dielectric heating of drops is well suited for integration with the hybrid integrated circuit (IC) / microfluidic chips described in Chapters 3, 4, and 5. (Lee *et al.,* 2007) If electrodes on the chip are driven with voltages at GHz frequencies, then one can use the chip to locally heat small volumes of fluid using dielectric heating. The addition of locally addressable temperature control to the lab-on-a-chip functions demonstrated in Chapters 3, 4, and 5 would further expand the capabilities of the hybrid chip platform and would be a valuable tool for a number of applications, including DNA analysis. (Lee *et al.,* 2007)

Microwave dielectric heating has many exciting scientific and technological applications. One noteworthy potential application for rapid, localized heating in microfluidic devices is PCR. (Lagally *et al.,* 2000, Liu *et al.,* 2002, Khandurina *et al.,* 2000, Oda *et al.,* 1998, Maltezos *et al.,* 2005, Maltezos *et al.,* 2006) The microwave

microfluidic heater can raise the temperature of drops up to 30°C above the base

temperature of the oil in which the drops are suspended.  By setting the base

temperature of the oil in our device to 65°C and appropriately setting the

microwave power, a 30°C change in temperature could cycle the temperature from

65°C to 95°C as required for PCR.  Drop-based PCR, which would be especially well

suited for this technique, allows for the rapid analysis of large populations of genes

and enzymes.  The microwave heating technique might also be used to set

temperatures rapidly and controllably in biological and chemical assays, such as for

protein denaturing studies (Arata *et al.,* 2008) and enzyme optimization assays

(Robertson *et al.,* 2004), where observations of thermal responses are made on the
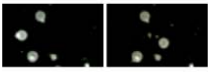
millisecond time scale.
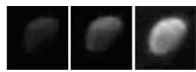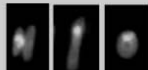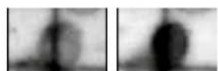
# Chapter 7. Conclusions

## 7.1 Summary

This thesis describes the development of a versatile platform for performing biology and chemistry experiments on a chip, using the integrated circuit (IC) technology of the commercial electronics industry. This work is an important step towards developing automated, portable, and inexpensive devices to perform complex chemical and biological tasks. Such a device would revolutionize the way that biological and chemical information is collected for applications such as medical diagnostics, environmental testing, and scientific research. (Ahn *et al.,* 2004, Chin *et al.,* 2007, and Martinez *et al.,* 2008)

The hybrid IC / microfluidic chips developed in this thesis control living cells and small volumes of fluid. Taking inspiration from cellular biology, phospholipid bilayer vesicles are used to package pL volumes of fluid on these chips. Table 7.1 summarizes the basic lab-on-a-chip functions that the hybrid chips can perform on the living cells and vesicles. The chips can be programmed to trap and position, deform, set the temperature of, electroporate, and electrofuse living cells and vesicles. These basic functions can be strung together to perform complex chemical and biological tasks. The fast electronics and complex circuitry of ICs enable thousands of living cells and vesicles to be simultaneously controlled, allowing many parallel, well-controlled biological and chemical operations to be performed in parallel.

**Table 7.1** A list of the lab-on-a-chip functions performed in this thesis using hybrid IC / microfluidic chips.

| Function | Method | | Chapter | Demonstration |
|---|---|---|---|---|
| Contain | Unilamellar Vesicles | pL | 4,5 |  |
| Position | Dielectrophoresis | MHz | 4,5 |  |
| | Magnetophoresis | DC | 5 |  |
| Deform | Dielectrophoresis | MHz | 4 |  |
| | Magnetophoresis | DC | 5 |  |
| Release | Electroporation | kHz | 4 |  |
| Fuse | Electrofusion | kHz | 4 |  |
| Permeabilize | Electroporation | kHz | 4 |  |
| Heat | Dielectric Heating | GHz | 6 | |

## 7.1 Future Directions

This thesis develops hybrid IC / microfluidic chips and demonstrates that they can perform basic functions that are necessary building blocks for biological and chemical experiments on a chip. However, the goal of a portable device that can perform biological and chemical tasks remains a challenge. For this goal to be fully realized, a more self-sufficient platform must be developed. Although a hybrid IC / microfluidic chip can be packaged into a portable device, the current chip requires a laboratory-sized fluorescence microscope, light source, and computer to fully function. To completely realize the potential of hybrid IC / microfluidic chips, additional functions must be added to the chips such that the large, external components are not required.

The hybrid chips described in this thesis could be made more self-sufficient by integrating sensors onto the ICs. A hybrid IC / microfluidic chip that included both sensors and the functionality demonstrated in this thesis could perform complex biological and chemical experiments and measure the results. These experiments could include multiple steps such as: mixing a library of cells with a library of chemicals, measuring the outcome of the experiments with sensors built into the chip, analyzing the results of the experiment, and designing the next set of experiments based on the results of the first, and repeat, until finally reporting the results. This sort of automated lab-on-a-chip platform could perform the complex, multi-step experiments that are currently performed in laboratories by trained staff using large and expensive equipment.

Several sensors have previously been developed using hybrid IC / microfluidic chips. Some examples of these sensors are NMR sensors for chemical detection, (Lee *et al.,* 2008) capacitive sensors for measuring eletrogenic cells, (DeBusschere *et al.,* 2001) electrical sensors for DNA detection, (Thewes *et al.,* 2002) and charge coupled devices (CCD) for optical imaging. (Cui *et al.,* 2008) These sensors are built using standard commercial IC processes, similar to the processes used to create the chips described in this thesis. A single IC could be built, using a commercial foundry, that includes the functionality demonstrated in this thesis and that of the sensors described above. Sensors that require specialized IC processes or that are made with e-beam lithography can also be included using flip-chip bonding. (Lee *et al.,* 2007)

A hybrid IC / microfluidic chip that controls, performs experiments on, and measures many living cells and small volumes of fluid would have a big impact. Tasks such as the detection and counting of cells, sorting cells, genetic analysis, protein detection, and combinatorial chemistry could be performed on these low-cost, automated devices. (Whitesides *et al.,* 2001, Stone *et al.,* 2004, Tabeling *et al.,* 2005, Yager *et al.,* 2006, Martinez *et al.,* 2008, Lee *et al.,* 2007, Hunt *et al.,* 2008, Maltezos *et al.,* 2005) The chips could be programmed to perform complex, multi-step tasks, and react to the results of experiments in real-time. The devices could be used for applications such as point-of-care disease detection or detecting toxic substances or parasites in drinking water. Such a device would realize the initial goal of microfluidics, to bring complex biological and chemical tests from laboratories out into the clinic and the field. (Whitesides, 2001)

# Works Cited

Ahn C. H., Choi J. W., Beaucage G., Nevin J., Lee B. J., Puntambekar A., and Lee J. Y. (2004) *Proceedings – IEEE*, **92**, 154.

Alberts B., Johnson A., Lewis J., Raff M., Walter P., and Roberts K. (2007) *Molecular Biology of The Cell,* Taylor & Francis Group.

Anna S. L., Bontoux N., and Stone H. A. (2003) *Appl. Phys Lett.,* **82**, 364.

Angelova M. I. and Dimitrov D. S. (1986) *Faraday Discuss. Chem. Soc.*, **81**, 303.

Arata H. F., Gillot F., Nojima T., Fujii T., and Fujita H. (2008) *Lab Chip*, **8**, 1436.

Bean C. P. and Livingston J. D. (1959), *J. Appl. Phys.,* **30**, S120.

Bengtsson N. E., Ohlsson T. (1974) *Proc. IEEE*, **62**, 44.

Berry C. and Curtis A. S. G. (2003) *J. Phys. D*, 2003, **36**, 198.

Chin C. D., Linder V., and Sia S. K. (2007) *Lab Chip*, **7**, 41.

Chiu D. T., Wilson C. F., Ryttsén F., Strömberg A., Farre C., Karlsson A., Nordholm S., Gaggar A., Modi B. P., Moscho A., Garza-López R. A., Orwar O., and Zare R. N. (1999) *Science*, **283**, 5409.

Cui X., Lee L. M., Heng X., Zhong W., Sternberg P. W., Psaltis D., Yang C. (2008) *Proc Natl Acad Sci*, **105**, 10670.

Curtis A. S. G. and Varde M. (1964) *J. Natl Cancer Res. Int.*, **33**, 15.

DeBusschere B. D., and Kovacs G. T. A. (2001) *Biosensors & Bioelectronics*, **16**, 543.

Dill K. A. and Bromberg S. (2003) *Molecular Driving Forces*, Taylor and Francis.

Dittrich P. S. and Manz A. (2006) *Nature reviews. Drug discovery*, **5**, 210.

Dobson J. (2008) *Nature Nanotechnology*, **3**, 139.

Eltoukhy H., Salama K., Gamal A. E. (2006) *Solid-State Circuits, IEEE,* **41**, 3.

Erickson D. and Li D. (2004) *Analytica Chimica Acta*, **507**, 11.

Eversmann B., Jenkner M., Hofmann F., Paulus C., Brederlow R., Holzapfl B., Fromherz P., Merz M., Brenner M., Schreiter M., Gabl R., Plehnert K., Steinhauser M., Eckstein G., Schmitt-Landsiedel D., and Thewes R. (2003) *J. Solid-State Circuits*, **38**, 2306.

Figeys D. and Pinto D. (2000) *Anal. Chem.*, **72**, 330.

Gascoyne P. R. C., Vykoukal J. V., Schwartz J. A., Anderson T. J., Vykoukal D. M., Current K. W., McConaghy C., Becker J. A., and Andrews C. (2004) *Lab Chip*, **4**, 299.

Geist J., Shah J. J., Rao M. V., and Gaitan M. (2007) *J. Res. Natl. Inst. Stand. Technol.*, **112**, 177.

Grant E. H., Shephard R. J., and South G. P. (1978) *Dielectric Behavior of Biological Molecules in Solution*, Oxford Univ. Press, Oxford.

Grosse C. and Schwan H. (1992) *Biophysical J.*, **63**,1632.

Heng X., Erickson D., Baugh L. R., Yaqoob Z., Sternberg P. W., Psaltis D., and Yang C. (2006) *Lab Chip*, **6**, 1274.

Holtze C., Rowat A. C., Agresti J. J., Hutchison J. B., Angile F. E., Schmitz, S. Koester, Duan H., Humphry K. J., Scanga R. A., Johnson J. S., Pisigano D., and Weitz D. A. (2008) *Lab Chip*, **8**, 1632.

Hunt T. (2007) *Integrated Circuit / Microfluidic Chips for Dielectric Manipulation*, PhD Dissertation, Harvard University.

Hunt T., Issadore D., Westervelt R. M. (2008) *Lab Chip*, **81**, 7.

Isambert H. (1998) *Phys. Rev. Lett.*, **80**, 15.

Issadore D., Humphry K. J., Brown K. A., Sandberg L., Weitz D. A., Westervelt R. M., *Lab Chip*, 2009, DOI: 10.1039/B822357B.

Jones T. B. (1995) *Electromechanics* of *Particles,* Cambridge University Press, Cambridge.

Keehan, S., Sisko A., Truffer C., Smith S.,Cowan C., Poisal J., Clemens M. K. and The National Health Expenditure Accounts Projections Team (2008) *Health Affairs*, doi: 10.1377.

Khandurina J., McKnight T. E., Jacobson S. C., Waters L. C., Foote R. S., and Ramsey J. M. (2000), *Anal. Chem.*, **72**, 2995.

Kilby J. S. (1976)*, Electron Devices, IEEE Trans.,* **23**, 7.

Koster S., Angilè F. E., Duan H., Agresti J. J., Wintner A., Schmitz C., Rowat A. C., Merten C. A., Pisignano D., Griffiths A. D., and Weitz D. A. (2008) *Lab Chip*, **8**, 1110.

Lagally E. T., Simpson P. C., Mathies R. A. (2000) *Sens. Actuators*, **B63**, 138.

Lee H. (2005) *Microelectronic / Microdluidic Hybrid System for the Manipulation of Biological Cells*, PhD dissertation, Harvard University.

Lee H., Ham D. and Westervelt R. M. eds. (2007) *CMOS Biotechnology*, Springer, New York.

Lee H., Liu Y., Alsberg E., Ingber D. E., Westervelt R. M., Ham D. (2005) I*SSCC*, 580-586.

Lee H., Liu Y., Westervelt R. M., and Ham D. (2006) *IEEE J. Solid-State Circuits*, **41**, 1471.

Lee H., Purdon A. M., and Westervelt R. M. (2004) *Appl. Phys. Lett.,* **85**, 1063.

Lee H., Sun E., Ham D., and Weissleder R. (2008) *Nature Medicine*, **14**, 869.

Lee J., Moon H., Fowler J., Schoellhammer T., and Kim C. J. (2002), *Sens. Actuators A*, **95**, 259.

Lee J. and Mudawar I. (2005) *Int. J. Heat Mass Transfer*, **48**, 928.

Lee T. (1998) *The Design of CMOS Radio-Frequency Integrated Circuits, Second Edition*, Cambridge University Press, Cambridge.

Lee W. G., Demirci U., and Khademhosseini A. (2009), *Integr. Biol.,* **1**, 242.

Link D. R., Anna S. L., Weitz D. A., and Stone H. A. (2004), *Phys. Rev. Lett.*, **92**, 54503.

Liu J., Enzelberger M., and Quake S. R. (2002) *Electrophoresis,* **23**, 1531.

Lopez M., Cabrera A., Agullo-Rueda M. (1970*) Electrooptics : Phenomena, Materials and Applications*, Academic Press.

Maltezos G., Johnston M., and Scherer A. (2005) *Appl. Phys. Lett.,* **87**, 154105.

Maltezos G., Rajagopal A., and Scherer A. (2006) *Appl. Phys. Lett.,* **89**, 074107.

Manaresi N., Romani A., Medoro G., Altomare L., Leonardi A., Tartagni M., and Guerrieri R. (2003), *IEEE J. Solid- State Circuits*, **38**, 2297.

Mao H., Yang T., and Cremer P. S. (2002) *J. Am. Chem. Soc.*, **124**, 4432.

Martinez A. W., Phillips S. T., Wiley B. J., Gupta M., and Whitesides G. M. (2008) *Lab Chip*, **8**, 2146.

Murrell J. N. and Jenkins A. D. (1994), *Properties of Liquids and Solutions*, 2nd Ed. John Wiley & Sons, Chichester, England.

Nakano H., Matsuda K., Yohda M., Nagmune T., Endo I., and Yamane T. (1994), *Biosci. Biotechnol. Biochem.,* **58**, 349.

Nyholm L. (2005) *Analyst*, **130**, 599.

Oda R. P., Strausbauch M. A., Huhmer A. F. R., Borson N., Jurrens S. R., Craighead J., Wettstein P. J., Eckloff B., Kline B., and Landers J. P. (1998), *Anal. Chem.*, **70**, 4361.

Olofsson J., Nolkrantz K., Ryttsén F., Lambie B., Weber S. G., and Orwar O. (2003) *Curr. Opin. Biotechnol.,* **14**, 29.

Pawley J. B. (2008) *J. Biomed. Opt.*, **13**, 029902.

Pollack M. G., Fair R. B., and Shenderov A. D. (2000), *Appl. Phys. Lett.*, **77,** 11.

Pollack M. G., Shendorov A. D., and Fair R. B. (2002), *Lab Chip*, **2**, 96.

Psaltis D., Quake S. R., and Yang C. (2006) *Nature*, **442**, 381.

Riske K. A. and Dimova R. (2006), *Biophysical J.*, **91**, 1778.

Robertson D. E. and Steer B. A. (2004), *Current Opinion in Chemical Biology*, **8**, 141.

Seifritz. W. (1924) *Brit. J. Exper. Biol.*, **2**, 1.

Shah J. J., Sundaresan S. G., Geist J., Reyes D. R., Booth J. C., Rao M. V., and Gaitan M. (2007) *J. Micromech. Microeng.,* **17**, 2224.

Siegel A. C., Shevkoplyas S. S., Weibel D. B., Bruzewicz D. A., Martinez A. W., and Whitesides G. M. (2006) *Angew. Chem.*, **45**, 6877.

Sklavounos A., Marchiarullo D. J., Barker S. L. R., Landers J. P., and Barker N. S. (2006) *Proc. Micro Total Anal. Syst.,* **2**, 1238.

Stone H. A., Stroock A. D., and Ajdari A. (2004) *Annual Reviews of Fluid Mechanics*, **36**, 381, and references therein.

Sugar P., Forster W., and Neumann E. (1987) *Biophysical Chem.*, **26**, 321.

Sundaresan S. G., Polk B. J., Reyes D. R., Rao M. V., and Gaitan M. (2005) *Proc. Micro Total Anal. Syst.,* **1**, 657.

Tabeling P. (2005) *Introduction to Microfluidics*, Oxford University Press.

Thewes R., Hofmann F., Frey A., Holzapfl B., Schienle M., Paulus C., Schindler P., Eckstein G., Kassel C., Stanzel M., Hintsche R., Nebling E., Albers J., Hassman J., Schulein J., Goemann W., and Gumbrecht W. (2002) *IEEE Int. Conf. Solid-State Circuits: Digest of Technical Papers*, **1**, 350.

Tresset G. and Iliescu C. (2007) *Appl. Phys. Lett.*, **90**, 173901.

Tudos A. J., G. A. J. Besselink, and R. B. M. Schasfoort (2001) *Lab Chip*, **1**, 83.

Unger M. A., Chou H. P., Thorsen T., Scherer A., Quake S. R. (2000) *Science*, **288**, 113.

United States Department of Health and Human Services (2007) *National Health Expenditure Fact Sheet.* <http://www.cms.hhs.gov/>.

Urdea M., Penny L. A., Olmsted S. S., Giovanni M. Y., Kaspar P., Shepherd A., Wilson P., Dahl C. A., Buchsbaum S., Moeller G., and Burgess D. C. H (2006) *Nature,* **444**, 73.

Varmus H., Klausner R., Zerhouni E., Acharya T., Daar A. S., and Singer P. A. (2003) *Science*, **302**, 398.

Vykoukal J., Schwartz A., F. F. Becker, and Gascoyne P. R. C. (2001) *Micro Total Analysis Systems*, **1,** 72.

Vyawahare S., Sitaula S., Martin S., Adalian D., and Scherer A. (2008) *Lab Chip*, **8**, 1530.

Wang N. and Ingber D. (1994) *Biophysical Journal*, **66**, 2181.

Waugh R. E., Song J., Svetina S. and Zeks B. (1992) *Biophysical Journal*, **61**, 974.

Wheeler A. R., Throndset W. R., Whelan R. J., Leach A. M., Zare R. N, Liao Y. H., Farrell K., Manger I. D., and Daridon A. (2003) *Anal Chem.*, **14**, 3581.

Whitesides G. M., Ostuni E., Takayama S., Jiang X., and Ingber D. (2001) *Annual Review of Biomedical Engineering*, **3**, 335.

Yager P., Edwards T., Fu E., Helton K., Nelson K., Tam M. R., Weig B. H. (2006) *Nature*, **442**, 412.

# Appendix A. Data Sheet for the Dielectrophoresis Chip (DEP Chip)

We document the specifications for the Fabutron 1.0, show the pin layout and detail the read / write protocol such that any user who reads this document should have all of the information necessary to make the Fabutron 1.0 work in their experiment.

**Summary of the Fabutron 1.0**

The Fabutron 1.0 is a custom integrated circuit designed in the Westervelt lab. The chip consists of an array of 128x256 pixels, 11x11 $\mu m^2$ in size, controlled by built-in SRAM memory; each pixel can be individually addressed with a radio frequency (RF) voltage up to 5 Vpp, with frequencies from DC-11 MHz. The IC was built in a commercial foundry and the microfluidic chamber was fabricated on its top surface at Harvard.

**Table A1** Specifications for the DEP chip

| Feature | Description |
| --- | --- |
| Bandwidth | DC-11 MHz |
| Process | 0.35 µm, CMOS MOSIS TSMC |
| Pixels | 128 x 256 (32,768)<br>11 x 11 $\mu m^2$ |
| Chip Size | 2.32 x 3.27 $mm^2$ |
| Addressing | 8-bit word line decoder<br>128 bit shift register, two phase clocked |
| Data Line Bandwidth | DC-20 MHz |
| Pixel Voltage | $V_{p-p}$ = 3-5 V |
| Pixel Bandwidth | DC – 5 MHz |
| Operating Voltage | 5 V |
| Operating Current | 30 mA – 300 mA |

**Table A2.** A list of the pins for the DEP Chip

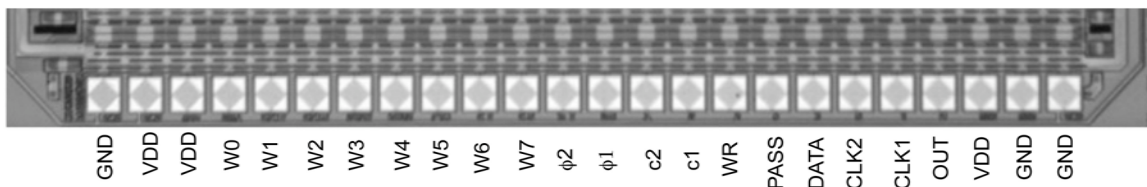| Pin | Description |
|---|---|
| GND | Ground |
| VDD | Operating Voltage (5V) |
| W(0:7)** | Word Address Decoder Lines |
| $\phi 1$ | Pixel Voltage 1 |
| $\phi 2$ | Pixel Voltage 2 |
| c2 | (0) decouples SRAM elements from the bitline, (1) connects SRAM elements on activated row to the bitline |
| c1 | (0)Precharge the bit lines, (1) disconnect precharge |
| WR | Control Line: (1) enables the shift register to write its value to the bitlines, (0) disables shift register from writing to bitlines |
| PASS | Control line: (1) Shift register elements looks to previous register for input, (0) registers look to bitline for input |
| DATA | Data input line for shift registers |
| CLK2 | Clock for shift register |
| CLK1 | Clock for shift register |
| OUT | Data output for shift register |



**Figure A1** Pin layout for the DEP chip

## Protocols
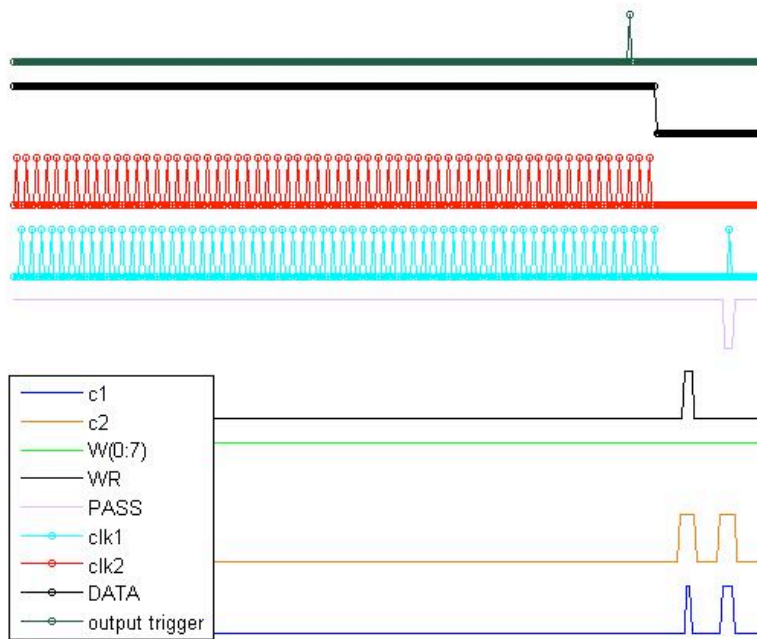


**Figure A2.** Load Data Into Shift Register and Write to Array.
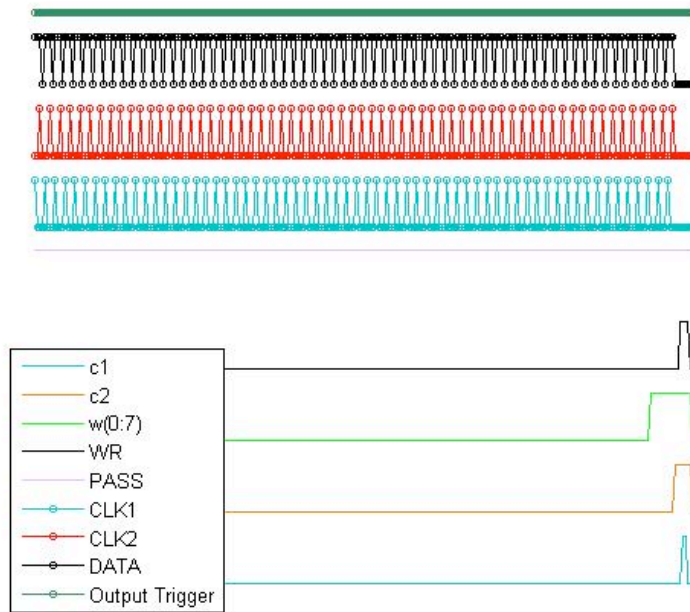
**Figure A3.** Read Data from SRAM Array into Shift Register and Read Out Array.

**Word Address Decoder Lines are incorrectly labeled on the chip. Note that going from MSB to LSB the correct ordering is: w3, w2, w1, w0, w7, w6, w5**

***Also note that there was an error in the design of the shift register and it actually functions as a 64 bit shift register, with neighboring registers tied together.  The full 128 bits are accessible by loading in 64 bits of data at a time, and use clock 1 to shift the data into the proper position.***

# Appendix B. Data Sheet for the High Voltage Dielectrophoresis / Magnetic Chip (HV-DEP / Magnetic Chip)

We document the specifications for the Fabutron 2.0, show the pin layout, and detail

the read / write protocol such that any user who reads this document should have

all of the information necessary to make the Fabutron 2.0 work in their experiment.

**Summary of the Fabutron 2.0**

The Fabutron 2.0 is a custom integrated circuit designed in the Westervelt lab.  The

chip consists of an array of 60 x 61 pixels, 30 x 38 $\mu m^2$ in size, controlled by built-in

SRAM memory; each pixel can be individually addressed with a radio

frequency (RF) voltage up to 50 Vpp, with frequencies from DC-10 MHz.  Interlaced

with the DEP pixels are a matrix of 60 x 61 wires that may be addressably sourced

with 100mA to apply forces on magnetically polarizable objects.    The IC was built

in a commercial foundry and the microfluidic chamber was fabricated on its top

surface at Harvard.   The chip suffers from local heating problems due to the

magnetic wires.  An improved version would switch to pulsed currents to minimize

heating.  The chip also has issues with the magnetic power lines and the digital

power lines being coupled, which leads to power line issues on the chip.  An updated

version would take extra care to make sure that power lines are decoupled.

**Table B1.** Specifications for the DEP chip

| Feature | Description |
|---------|-------------|
| Bandwidth | DC-10MHz |
| Process | 0.6 µm, CMOS XFAB XC06 |
| Pixels | 60 x 61 (3,660) |

|  | 30 x 38 μm² |
| --- | --- |
| Chip Size | 3.4 x 3.7 mm² |
| Addressing | 5-bit word line decoder<br>128 bit shift register, two phase clocked |
| Data Line Bandwidth | DC-20 MHz |
| Pixel Voltage | $V_{p-p}$= 20-50 V |
| Pixel Bandwidth | DC – 1 MHz |
| Operating Voltage (Logic) | 5 V |
| Operating Current (logic) | 20 mA |
| Operating Magnetic Wire Voltage | 5 V |
| Operating Magnetic Wire Current | 0 – 800 mA* |
| Operating High Voltage | 50 V |
| Operating High Voltage Current | 20-60 mA** |

**Table B2.** A list of the pins for the DEP Chip

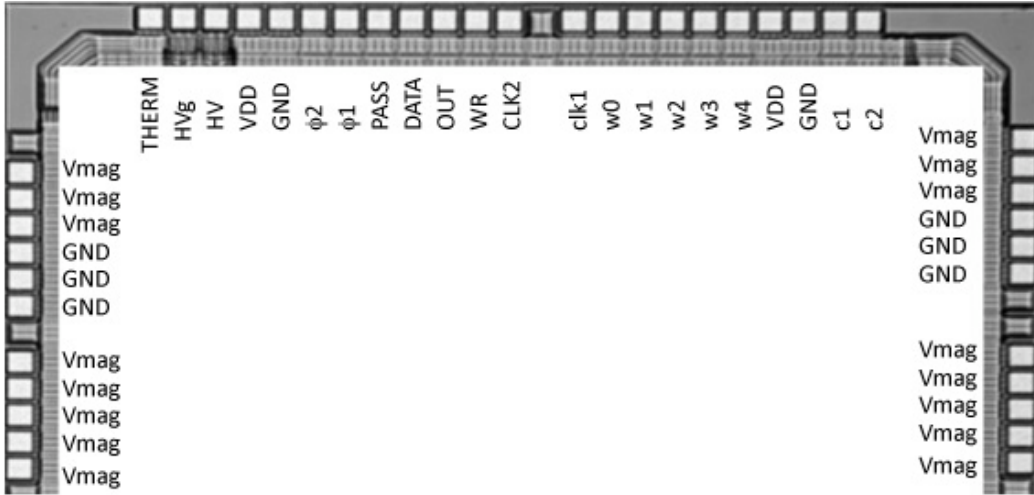| Pin | Description |
| --- | --- |
| GND | Ground |
| VDD | Operating Voltage (5 V) |
| HV | High Voltage (50 V) |
| HVg | High Voltage Gate (45-50V), controls the active impedance in the RF voltage driving circuit  underneath each circuit |
| Vmag | Power Supply for the Magnetic Lines (5 V) |
| W(0:5) | Word Address Decoder Lines |
| THERM | Analog Output for the Thermometer (0-5 V) |
| φ1 | Pixel Voltage 1 |
| φ2 | Pixel Voltage 2 |
| c2 | (0) decouples SRAM elements from the bitline, (1) connects SRAM elements on activated row to the bitline |
| c1 | (0)Precharge the bit lines, (1) disconnect precharge |
| WR | Control Line: (1) enables the shift register to write its value to the bitlines, (0) disables shift register from writing to bitlines |
| PASS | Control line: (1) Shift register elements looks to previous register for input, (0) registers look to bitline for input |
| DATA | Data input line for shift registers |
| CLK2 | Clock for shift register |
| CLK1 | Clock for shift register |
| OUT | Data output for shift register |

**Figure B1**  Pin layout for the DEP chip

**Protocols**

The protocol to update the SRAM array is identical as for the Fabutron 1.0

The SRAM addresses of the DEP pixels, magnetic wires, and thermometers are as

follows:

**Table B3.** A map of the features of the 50 V / magnetic chip on the SRAM array

| Array | SRAM Address (word, bit) |
|---|---|
| DEP Array (1:60,1:161) | SRAM (3:32, 5:126)*** |
| Magnetic Matrix X direction (1:2,1:122) | SRAM (1:2,5:126)*** |
| Magnetic Matrix Y direction (1:2, 1:122) | SRAM (1:30,1:4)*** |
| Thermometers (1:16) | SRAM (1:8,127:128)*** |

* Note that special care must be taken when the chip is first turned on.  The SRAM

will be set to a random state and more than a few magnetic lines will be turned on.

It is advantageous to leave the $V_{mag}$ turned off until the states of the wires can be set

such that none or few of the wires are turned on.

** Note that a special fuse and voltage conditioning / current limiting circuitry must be built into the PCB that houses the IC. Spikes in the HV line can destroy the chip.

*** For more detail on how the SRAM array maps onto the DEP and Magnetic array please see line the attached MATLAB code where the detailed mapping is laid out.

# Appendix C. Fabutron Control Software

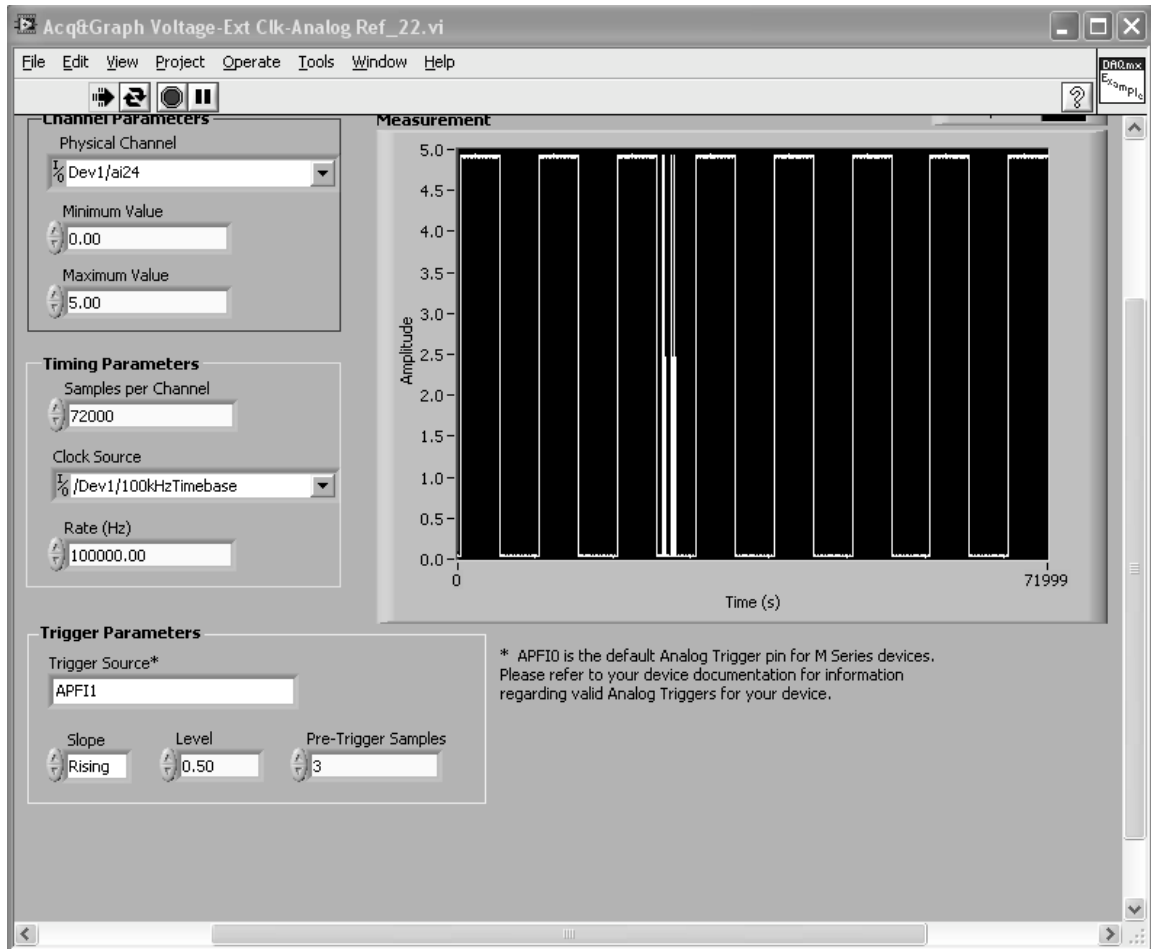**Labview Programs used to Communicate with the Chips**



**Figure C1**.  Labview code used to read data coming from the chips.
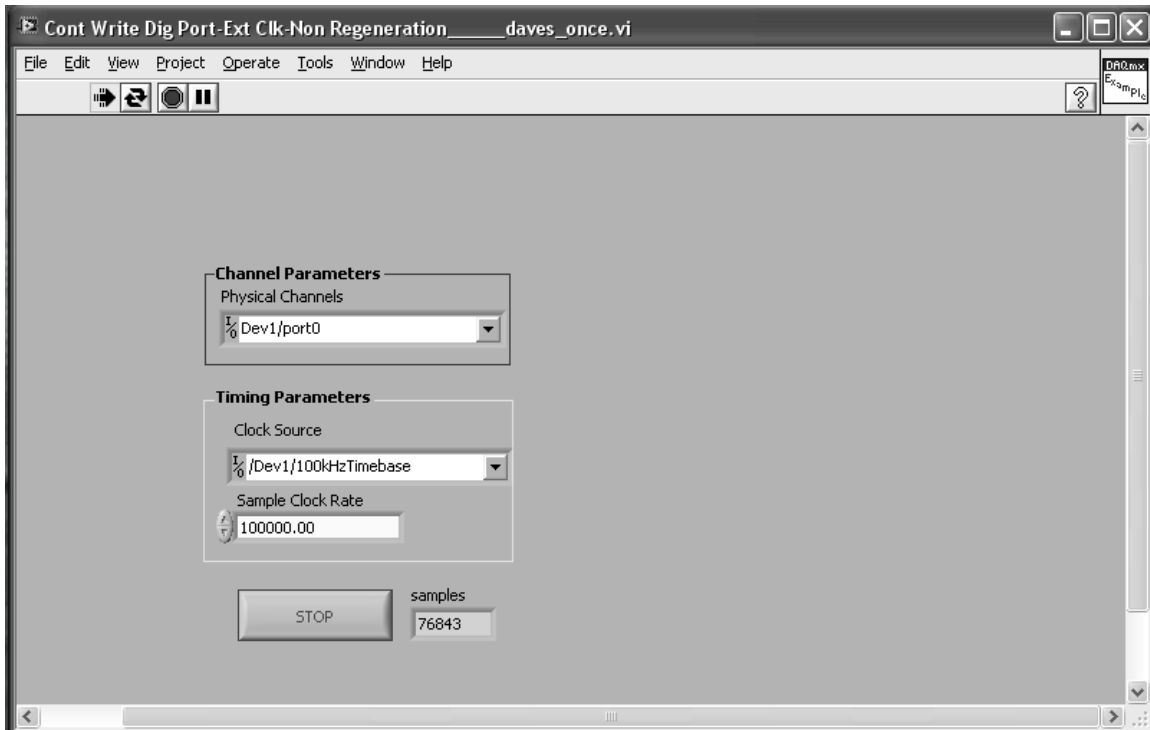
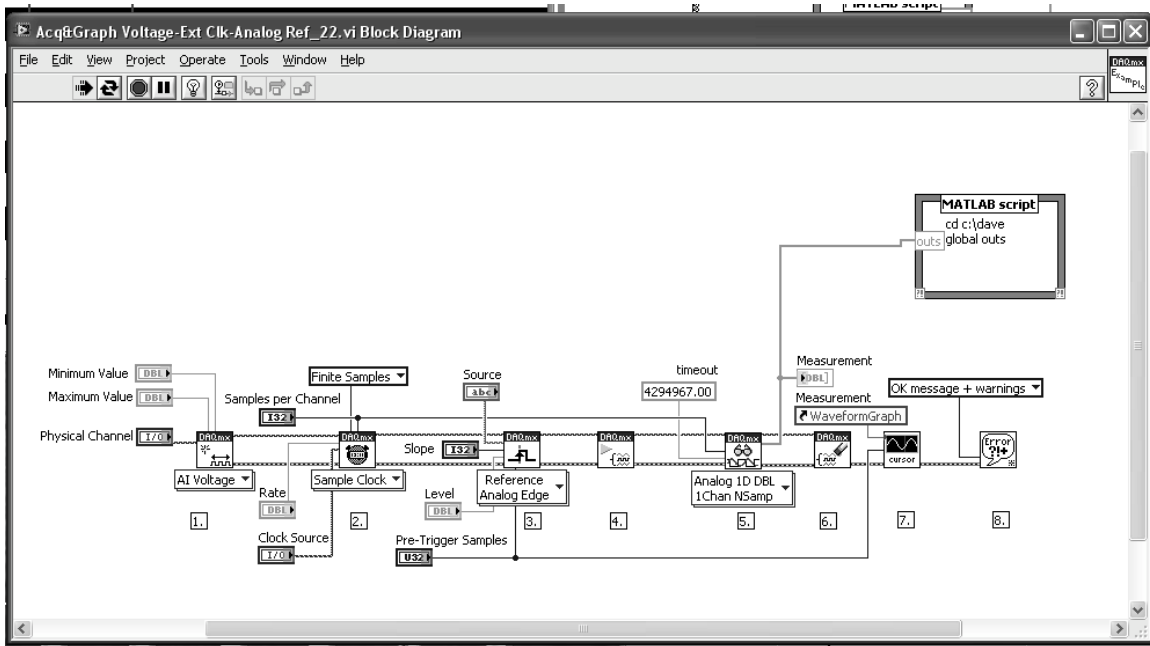**Figure C2.** Labview code used to write data to the chips



**Figure C3.** Block diagram of Labview code used to read data from the chips
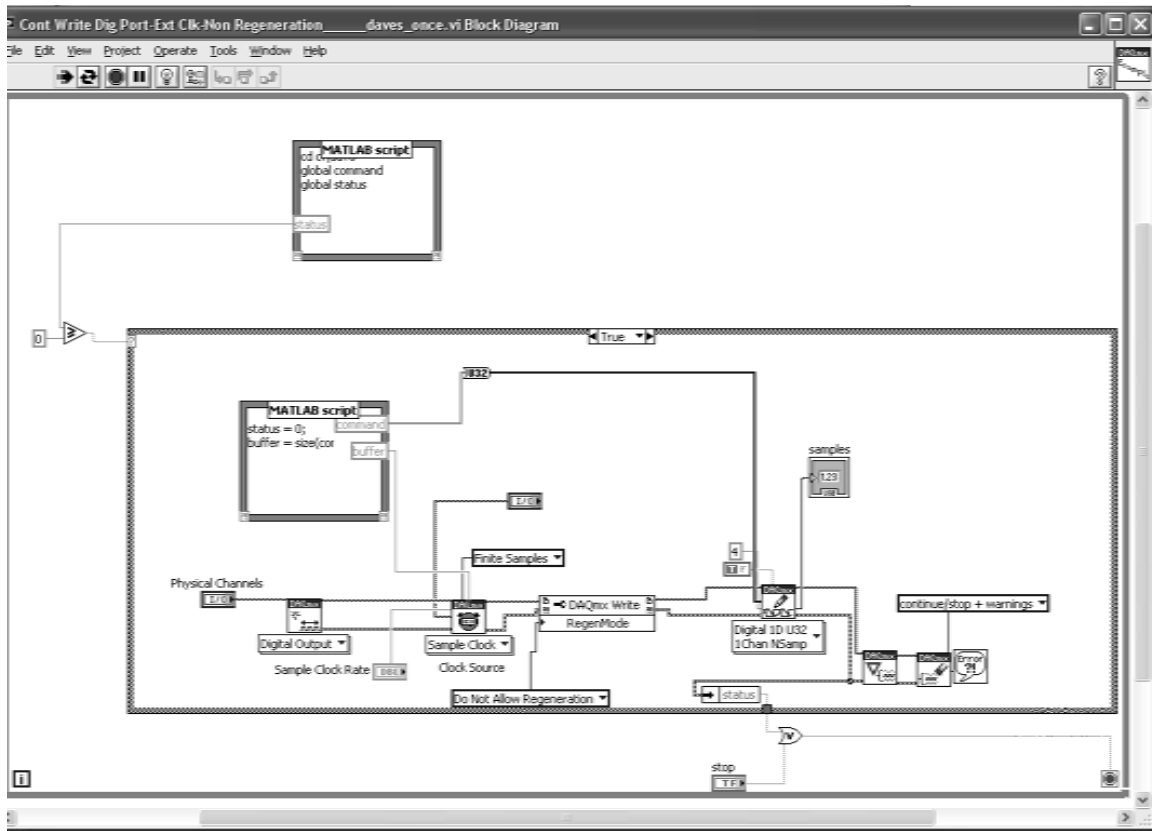
**Figure C4.** Block diagram of Labview code used to write to the chip

## Matlab Code used to Generate and Read Patterns to the Chip

## Program to write data from a matrix created in the GUI and package it into a line of commands sent to the chip with the Labview program

```matlab
function fabwrite(image,protocol)

%function fabwrite(image,protocol)
%
%1.30.2008
%
%Create a Text file that LabView can read which directs it to write a file
%to the Fabutron and read from it at the same time. the output file z.txt
%Written by David Issadore and Keith Brown
%
%Changed on 2.4.2008 to also work with 5 and 50 volt fabutrons
%Changed on 2.24.2008 to accomidate multiple layer images
%changed on 8-15-08 to switch clock1 and clock2 on line 90
%
% %%
% %added by dave to rearrange the data for the 50V chip.  for now we will
% %just concern ourselves with the DEP array and not magnetic lines or
% %thermometers
if protocol == 50
   %image=arrange50V(image);
end

%% Setup Variables
frames = size(image,3);
bits_per_row=size(image,2);
rows = size(image,1);
```

137

*ecorr = 10;*

*bcorr = 10;*

*icorr = 10;*

*command_lines=13+bcorr+ecorr+icorr;*

*cycles_per_bit=4;*


*commands_per_row = command_lines + bits_per_row*cycles_per_bit;*


*%% Define Row Write Command*



*%Loads data from data port or memory into shift register*

*clock1 = zeros(1,commands_per_row);*

*clock1(linspace(2,commands_per_row-command_lines-2,bits_per_row))=ones(1,bits_per_row);*

*%clock1(bits_per_row*cycles_per_bit+12)=1;*


*%Advances the shift register*

*clock2 = zeros(1,commands_per_row);*

*clock2(linspace(4,commands_per_row-command_lines,bits_per_row))=ones(1,bits_per_row);*

*clock2(bits_per_row*cycles_per_bit+10+bcorr+icorr)=1;*


*%Modulates the data image so that it has the right form*

*data = zeros(commands_per_row,bits_per_row);*

*for i=0:bits_per_row-1*

*  data(i*cycles_per_bit+1:(i+1)*cycles_per_bit,i+1)=[1;1;1;1];*

*end*

*%Write enables data to be written into memory from the shift register*

*write = zeros(1,commands_per_row);*

*write(bits_per_row\*cycles_per_bit+2+bcorr:bits_per_row\*cycles_per_bit+5+bcorr) = ones(1,4);*

*%Pass tells it when to look at the previos register/data(1) and when to*

*%look at memory(0)*

*pass = ones(1,commands_per_row);*

*pass(bits_per_row\*cycles_per_bit+8+bcorr+icorr:bits_per_row\*cycles_per_bit+11+bcorr+icorr) =zeros(1,4);*

*%Tells when the word lines should be enegaged*

*% words = zeros(1,commands_per_row);*

*% words(bits_per_row\*cycles_per_bit-10:commands_per_row-1) = ones(1,command_lines+10);*

*words = ones(1,commands_per_row);*

*%Clock_C1 Loads data to/from memory to/from the bit line*

*clock_c1 = zeros(1,commands_per_row);*

*clock_c1(bits_per_row\*cycles_per_bit+3+bcorr:bits_per_row\*cycles_per_bit+4+bcorr) = ones(1,2);*

*clock_c1(bits_per_row\*cycles_per_bit+7+bcorr+icorr:bits_per_row\*cycles_per_bit+11+bcorr+icorr) = ones(1,5);*

*%clock_c1(bits_per_row\*cycles_per_bit+3:bits_per_row\*cycles_per_bit+11) = ones(1,9);*

*%Clock_C2 Turns off pre-charging of pull-up circuitry*

*clock_c2 = zeros(1,commands_per_row);*

*clock_c2(bits_per_row\*cycles_per_bit+bcorr:bits_per_row\*cycles_per_bit+6+bcorr) = ones(1,7);*

*clock_c2(bits_per_row\*cycles_per_bit+6+bcorr+icorr:bits_per_row\*cycles_per_bit+12+bcorr+icorr) = ones(1,7);*

```matlab
%output trigger tells the code when to start recording
output_trigger = zeros(1,commands_per_row);
output_trigger(bits_per_row*cycles_per_bit-10)=1;
%output_trigger(1)=1;

%%
temp=clock1;
clock1=clock2;
clock2=temp;
%%

% plot the control singals to make sure they look ok
% Test code to be removed
%
% figure
% plot(clock_c1-1.5,'b-')
% hold on
% plot(clock_c2+0,'r-')
% plot(words+1.5,'g-')
% plot(write+3,'k')
% plot(pass+4.5,'y')
% plot(clock1+6,'b-o','MarkerSize',3)
% plot(clock2+7.5,'r-o','MarkerSize',3)
% plot(data*ones(bits_per_row,1)+9,'k-o','MarkerSize',3);
% plot(output_trigger+10.5,'g-o','MarkerSize',3);
% legend('clock c1','clock c2','word lines','write','pass','clock1','clock2','data','output trigger');
%% Build Command
```

```matlab
temp = [];

for cf=1:frames

if protocol==5

    k=linspace(0,255,256);

    k=dec2bin(k,8);

%This is the order that we originally suspected

     %changed 6-27-08, found in Tom's binder.

    w0=str2num(k(:,4));

    w1=str2num(k(:,3));

    w2=str2num(k(:,2));

    w3=str2num(k(:,1));

    w4=str2num(k(:,8));

    w5=str2num(k(:,7));

    w6=str2num(k(:,6));

    w7=str2num(k(:,5));

   %This is the order that is the opposite of the one that we

   %orignially suspected. pshaw.

%      w0=str2num(k(:,1));

%      w1=str2num(k(:,2));

%      w2=str2num(k(:,3));

%      w3=str2num(k(:,4));

%      w4=str2num(k(:,5));

%      w5=str2num(k(:,6));

%      w6=str2num(k(:,7));

%      w7=str2num(k(:,8));


    %% build bit map

   bit_map = zeros(32,(rows+1).*commands_per_row);
```

```
for i=0:rows-1

    %0.1-0.8 not set

    %0.9 <-> CLK1

    bit_map(9,i*commands_per_row+1:(i+1)*commands_per_row) = clock1;

    %0.10-0.13 not set

    %0.14 <-> CLK2

    bit_map(14,i*commands_per_row+1:(i+1)*commands_per_row) = clock2;

    %0.15 <-> OUT_TRIGGER - not set in this loop

    %0.16 <-> DATA

    %bit_map(16,i*commands_per_row+1:(i+1)*commands_per_row) = 0;

     bit_map(16,i*commands_per_row+1:(i+1)*commands_per_row) =
(data*image(i+1,:,cf)')';

    %0.17 <-> PASS

    bit_map(17,i*commands_per_row+1:(i+1)*commands_per_row) = pass;

    %0.18 not set

    %0.19 <-> W0

    bit_map(19,i*commands_per_row+1:(i+1)*commands_per_row) = words.*w0(i+1);

    %0.20 <-> W1

    bit_map(20,i*commands_per_row+1:(i+1)*commands_per_row) = words.*w1(i+1);

    %0.21 <-> WR

    bit_map(21,i*commands_per_row+1:(i+1)*commands_per_row) = write;

    %0.22 <-> C1

    bit_map(22,i*commands_per_row+1:(i+1)*commands_per_row) = clock_c1;

    %0.23 <-> W4

    bit_map(23,i*commands_per_row+1:(i+1)*commands_per_row) = words.*w4(i+1);

    %0.24 <-> W5

    bit_map(24,i*commands_per_row+1:(i+1)*commands_per_row) = words.*w5(i+1);

    %0.25 <-> C2

    bit_map(25,i*commands_per_row+1:(i+1)*commands_per_row) = clock_c2;
```

142

*%0.26-0.27 not set*

*%0.28 <-> W6*

*bit_map(28,i\*commands_per_row+1:(i+1)\*commands_per_row) = words.\*w6(i+1);*

*%0.29 <-> W2*

*bit_map(29,i\*commands_per_row+1:(i+1)\*commands_per_row) = words.\*w2(i+1);*

*%0.30 <-> W7*

*bit_map(30,i\*commands_per_row+1:(i+1)\*commands_per_row) = words.\*w7(i+1);*

*%0.31 <-> W3*

*bit_map(31,i\*commands_per_row+1:(i+1)\*commands_per_row) = words.\*w3(i+1);*

*%0.32 not set*

*end*


*%Set the output trigger to go off only once*

*bit_map(15,1:commands_per_row) = output_trigger;*


*%Set clock1, clock2 and pass for the final data out*

*bit_map(9,rows\*commands_per_row+1:(rows+1)\*commands_per_row) = clock1;*

*bit_map(14,rows\*commands_per_row+1:(rows+1)\*commands_per_row) = clock2;*

*bit_map(17,rows\*commands_per_row+1:(rows+1)\*commands_per_row) = pass;*

*elseif protocol==50*

*%% prepare word lines*

*%prepare word lines*

*k=1:32;*

*k=dec2bin(k,5);*


*w0=str2num(k(:,5));*

*w1=str2num(k(:,4));*

*w2=str2num(k(:,3));*

```matlab
w3=str2num(k(:,2));
w4=str2num(k(:,1));


%% build bit map
bit_map = zeros(32,(rows+1).*commands_per_row);
for i=0:rows-1
    %0.1-0.16 not set
    %0.17 <-> PASS
    bit_map(17,i*commands_per_row+1:(i+1)*commands_per_row) = pass;
    %0.18 <-> C1
    bit_map(18,i*commands_per_row+1:(i+1)*commands_per_row) = clock_c1;
    %0.19 <-> C2
    bit_map(19,i*commands_per_row+1:(i+1)*commands_per_row) = clock_c2;
    %0.20 <-> W4
    bit_map(20,i*commands_per_row+1:(i+1)*commands_per_row) = words.*w4(i+1);
    %0.21 <-> DATA
    bit_map(21,i*commands_per_row+1:(i+1)*commands_per_row) = (data*image(i+1,:)')';
    %0.22 <-> OUT
    %0.23 <-> W1
    bit_map(23,i*commands_per_row+1:(i+1)*commands_per_row) = words.*w1(i+1);
    %0.24 <-> W0
    bit_map(24,i*commands_per_row+1:(i+1)*commands_per_row) = words.*w0(i+1);
    %0.25 <-> WR
    bit_map(25,i*commands_per_row+1:(i+1)*commands_per_row) = write;
    %0.26 and 0.27 not set
    %0.28 <-> CLK1
    bit_map(28,i*commands_per_row+1:(i+1)*commands_per_row) = clock1;
    %0.29 <-> W3
```

*bit_map(29,i\*commands_per_row+1:(i+1)\*commands_per_row) = words.\*w3(i+1);*

*%0.30 <-> CLK2*

*bit_map(30,i\*commands_per_row+1:(i+1)\*commands_per_row) = clock2;*

*%0.31 <-> W2*

*bit_map(31,i\*commands_per_row+1:(i+1)\*commands_per_row) = words.\*w2(i+1);*

*end*

*%Set the output trigger to go off only once*

*bit_map(15,1:commands_per_row) = output_trigger;*

*%Set clock1, clock2 and pass for the final data out*

*bit_map(28,rows\*commands_per_row+1:(rows+1)\*commands_per_row) = clock1;*

*bit_map(30,rows\*commands_per_row+1:(rows+1)\*commands_per_row) = clock2;*

*bit_map(17,rows\*commands_per_row+1:(rows+1)\*commands_per_row) = pass;*

*end*

*% convert to 32-bit number*

*exponent = (1:32)'\*ones(1,size(bit_map,2));*

*temp = [temp ,sum(bit_map.\*2.^exponent,1)];*

*end*

*global command;*

*command = temp;*

*%tell it to write*

*global status;*

*status = 1;*

**Program to read data from the chip and repackage it as a matrix**

*Function [pixel_array] = fabload(sizes,protocol)*

*%function [pixel_array] = fabload(sizes)*

*%Created by Keith Brown 1.30.2008 to read files created by the LabView*

*%script that reads the fabutron*

*%2.12.2008 Works with 5V chip*

```matlab
%commented out by david issadore to let labview pass the data without
%saving to the hard drive
%[header data]=hdrload('out.txt');
%%
global outs
data=outs;
size(data)
%%
if protocol == 5
    %fabwrite
    icorr=10;
    bcorr=10;
    ecorr=10;
    overhead_per_row=13+icorr+bcorr+ecorr;
    offset = 26+icorr+bcorr+ecorr;
%    %fabverify
%    icorr=0;
%    bcorr=0;
%    ecorr=0;
%    overhead_per_row=13+icorr+bcorr+ecorr;
%    offset = 21+icorr+bcorr+ecorr;
    pixel_array=zeros(sizes(1),sizes(2));
    bits_per_row = 4.*sizes(2)+overhead_per_row;
temp = zeros(sizes(1),sizes(2)*4);
    for j = 1:sizes(1);
    temp(j,:)= data(offset+bits_per_row*(j-1):offset+bits_per_row*(j-1)+sizes(2)*4-1);
    end
pixel_array=temp(:,4*(1:sizes(2))-1); elseif protocol == 50
```

```matlab
  icorr=20;

  bcorr=20;

  ecorr=20;

  overhead_per_row=(15+icorr+bcorr+ecorr).*1;

  pixel_array=zeros(sizes(1),sizes(2));

  bits_per_row = 8.*sizes(2)+overhead_per_row;

  %bits_per_row = 4.*sizes(2)+overhead_per_row;

  %offset=45

  offset = -11 +icorr+bcorr+ecorr ;
temp = zeros(sizes(1)./2,sizes(2)*8)';
%  temp = zeros(sizes(1),sizes(2)*4);
 size(temp)
  for j = 1:sizes(1)./2;
 % for j = 1:sizes(1);
temp(:,j)= data(offset+bits_per_row*(j-1):offset+bits_per_row*(j-1)+sizes(2)*8-1);
%temp(j,:)= data(offset+bits_per_row*(j-1):offset+bits_per_row*(j-1)+sizes(2)*4-1);
  end
%pixels(1:60,1:30)=DEP_array(1:60,1:30)
%pixels(61:120,1:30)=DEP_array(1:60,31:60);

pixel_array(1:60,1:30)=temp(4*(1:60)-3,1:30);
pixel_array(1:60,31:60)=temp(4*(61:120)-3,1:30);
%pixel_array=temp(:,4*(1:sizes(2))-1);
  size(pixel_array)
end
```